Title
Engineering of Synthetic Reverse Glyoxylate Shunt Module for enhanced carbon incorporation in cyanobacteria

Author
Li, Xiaoqian

Publication Date
2016

Peer reviewed|Thesis/dissertation

UNIVERSITY OF CALIFORNIA

Los Angeles

Engineering of Synthetic Reverse Glyoxylate Shunt Module for enhanced carbon incorporation in cyanobacteria

A dissertation submitted in partial satisfaction of the requirements for the degree Doctor of Philosophy in Chemical Engineering

by

Xiaoqian Li

2016

ABSTRACT OF THE DISSERTATION

Engineering of Synthetic Reverse Glyoxylate Shunt Module

for enhanced carbon incorporation in cyanobacteria

By

Xiaoqian Li

Doctor of Philosophy in Chemical Engineering

University of California, Los Angeles, 2016

Professor James C. Liao, Chair

Synthetic Biology and Metabolic engineering research aim to elucidate the underlying principle of biological systems and enable a predicable cellular behavior through artificial design. In this work, the discipline of synthetic biology was applied to photosynthetic organism to improve carbon intake efficiency.

After survey and analysis of existing carbon fixation metabolic pathways, the design of a synthetic Reverse Glyoxylate Shunt (rGS) core module was invented. This core module could potentially pair with multiple metabolic routes to generate various synthetic carbon incorporation/fixation pathways. The design of **rGS-Glycerate** pathway, which could

theoretically double the Acetyl-CoA yields from C3 metabolites, was reduced to practice at first due to its technical feasibility simulated through computation. The performance of rGS-Glycerate pathway reached its theoretical value *in vitro*. The pathway was further proved to be functional in *E.coli* through growth auxotroph test. Finally, rGS-Glycerate pathway was implemented into a model photosynthetic microorganism, *Synechococcus elongatus* PCC7942, after iterative "Design-Build-Test" engineering cycles. The higher Acetyl-CoA yield was characterized in terms of higher production of ketoisocaproate (KIC) that required Acetyl-CoA as its precursor in cyanobacteria. Further metabolomics analysis found out that one of the most abundant fatty acids, Oleic acids, reached to 2.5 folds of its content in WT. Another rGS core module contained pathway, **rGS-Serine** pathway, was also constructed in *Synechococcus elongatus* PCC7942. Similar level of KIC production was detected in those rGS-Serine strains as well.

In sum, this work is the initial demonstration that the rGS core module contained pathways were compatible with photosynthetic machinery and could potentially lead to enhanced carbon incorporation in photosynthetic organisms.

The dissertation of Xiaoqian Li is approved.

Yi Tang

James W. Gober

James C. Liao, Committee Chair

University of California, Los Angeles

2016

DEDICATION

This work is dedicated to my parents, Gang Li and Wencun Li for their unconditional love and understanding. Without them, this would not have been possible.

TABLE OF CONTENTS

Chapter I. Review 1

1.1 Challenge of Synthetic Metabolic Pathway Design and Metabolic Engineering 1

1.2 Synthetic Biology for improving carbon intake efficiency 3

1.3 Cyanobacteria as a host for novel metabolic pathway design 4

1.4 Figures 5

1.5 Reference 6

Chapter II Design and demonstration of reverse glyoxylate shunt pathway *in vitro* and in *E.coli* 8

2.1 Introduction 8

2.1.1 Problems of initial design of reverse glyoxylate shunt 8

2.1.2 Design of reverse glyoxylate shunt-glycerate pathway 9

2.2 Materials and Methods 12

2.2.1 Protein expression and purification 12

2.2.2 Pathway assay conditions and detection methods *in vitro* 12

2.2.3 *In vitro* enzyme assay condition 13

2.2.4 *E.coli* strain construction and test condition 15

2.3 Results and discussion 16

2.3.1 rGS-Glycerate cycle analysis by EMRA and thermodynamics 16

2.3.2 reverse glyoxylate shunt pathway individual enzyme activity characterization 16

2.3.3 *In vitro* demonstration of reverse glyoxylate shunt pathway at theoretical yield 17

2.3.4 *In vivo* demonstration of reverse glyoxylate shunt-citrate pathway in *E.coli* 18

2.4 Figures 20

2.5 Tables 31

2.6 Reference 35

Chapter III. Engineering a reverse glyoxylate shunt facilitated carbon fixation cycle in cyanobacteria for enhanced acetyl-CoA derived metabolites production . 36

3.1 Introduction 36

3.1.1 Insufficient photosynthesis by RuBisCO and alternative carbon fixation/incorporation cycles evaluations 36

3.1.2 Design of rGS core module 37

3.1.3 Design of carbon fixation/incorporation into Acetyl-CoA pathway with rGS module 39
3.2 Materials and Methods 41
3.2.1 Strain culturing 41
3.2.2 Plasmids and strain construction 42
3.2.3 Enzyme assay measurement 42
3.2.4 Organic acids detection 43
3.2.5 GC/MS measurement methods 44
3.2.6 Metabolomics conditions 44
3.3 Results and discussion 46
3.3.1 Production of ketoisocaproate through rGS-Glycerate Pathway after iterative Engineering of *Synechococcus PCC 7942* 46
3.3.2 Inverse relationship between GCL activity and MTK/MCL activity as result of natural evolution to avoid intermediate toxicity 49
3.3.3 *LeuA* overexpression led to higher KIC production in cyanobacteria 50
3.3.4 Metabolomics profile of rGS-glycerate pathways in *Synechococcus elongatus PCC7942* 51
3.3.5 Photosynthetic production of KIC through rGS-Serine pathway 52
3.4 Figures 54
3.5 Tables 84
3.6 Reference 87

Chapter IV Isobutanol production as an alternative metabolic sink to rescue the growth deficiency of the glycogen mutant of Synechococcuselongatus PCC 7942 89

4.1 Abstract 89
4.2 Main text 90
4.2.1 Introduction 90
4.2.2 Materials and methods 91
4.2.3 Results 99
4.2.4 Discussion 104
4.3 Figures 107
4.4 Tables 113
4.5 Supplementary Figures 115
4.6 Supplementary Tables 122
4.7 Reference 126

LIST OF FIGURES

Figure 1- 1 Energy loss associated with biofuel production 5
Figure 2- 1 Initial demonstration of reverse glyoxylate shunt pathway in E.coli20
Figure 2- 2 reverse glyoxylate shunt-citrate design and EMRA simulation.....21
Figure 2- 3 Design of different pathways of recycling glyoxylate into reverse glyoxylate shunt pathway 23
Figure 2- 4 EM Robustness Analysis of rGS-glycerate pathway 24
Figure 2- 5 His-tag purification of individual enzymes.....25
Figure 2- 6 Test of functions of sub-pathway of rGS-Glycerate cycle *in vitro* ...27
Figure 2- 7 *In vitro* demonstration of full rGS-citrate pathway.....28
Figure 2- 8 *in vivo* demonstration of rGS-citrate cycle in *E.coli* 30
Figure 3- 1 Schematic presentation of metabolic pathway design with rGS core module.....57
Figure 3- 2 Design of rGS core module contained Carbon fixation/incorporation pathway 59
Figure 3- 3 Carbon fixation into acetyl-CoA cycle rGS-Glycerate 60
Figure 3- 4 Enzyme Activity improvement for rGS-Glycerate Pathway 62
Figure 3- 5 Unknown peak from rGS-citrate full pathway strain.....63
Figure 3- 6 GC-MS confirmation of ketoisocaproate 64
Figure 3- 7 Schematic presentation of KIC production from rGS-glycerate pathway 65
Figure 3- 8 KIC production from rGS-glycerate pathway.....67
Figure 3- 9 Enzyme activity evolution due to intermediate toxicity 70
Figure 3- 10 KIC production with *leuA* overexpression.....71
Figure 3- 11 Metabolomics Study of rGS-glycerate pathway in cyanobacteria..77
Figure 3- 12 Metabolic pathway design of KIC production with rGS-Glycine/Serine pathway 78
Figure 3- 13 Growth Curve and KIC production of rGS-Serine pathway.....82
Figure 3- 14 rGS-Serine pathway with cyanobacteial Glycine Cleavage system83
Figure 4-1 Competing carbon sinks between glycogen and isobutanol in cyanobacteria. 107
Figure 4-2 Confirmation of *glgC* mutant strains.....108
Figure 4-3 Induction effect of isobutanol pathway on glgC mutant strains under constant light conditions (150 μE $s^{-1}m^{-2}$).....110
Figure 4-4 Effects of glycogen deficiency on productions. 111
Figure 4-5 Carbon flux distribution between cell mass and alcohols.....112
Figure S4-1 Quantification standard curves with Genomic DNA. 116
Figure S4-2 Quantification of amplified products. 119
Figure S4-3 Chlorophyll *a* contents in various strains.....120
Figure S4-4 $NaH^{14}CO_3$ scintillation reading conversion standard curve.....121

LIST OF TABLES

Table 2- 1 Thermodynamic calculation of reverse glyoxylate shunt Pathway Gibbs free Energy 31
Table 2- 2 Specific activity characterization of individual enzymes of reverse glyoxylate shunt–glycerate cycle 33
Table 2- 3 Plasmids used in E.coli growth rescue 34
Table 3- 1 Energy and reducing power consumption for Acetyl-CoA carbon fixation cycle 84
Table 3- 2 Plasmids used in this research 85
Table 3- 3 Strains used in this research 86
Table 4-1 Strains and plasmids used in this research 113
Table 4-2 Improvement in per cell productivity of isobutanol in *glgC* mutant at different stages 114
Table S4-1 C(t) determined by quantitative PCR 122
Table S4-2 Extraction efficiency test with non-incorporated $NaH^{14}CO_3$ 123
Table S4-3 Isobutanol and 3-Melthy-1-Butanol Extraction efficiency test. 124
Table S4-4 Normalized carbon flux distribution ratios among various mutants125

ACKNOWLEDGEMENT

My way to reach a Ph.D. degree is a long journey with a lot of surprises. Thanks to my doctoral advisor, Dr. James C. Liao, his influence over me is much more beyond scientific. I realize what is like to live as a passionate person and how much pain, efforts and responsibilities need to be taken in order to pursue the passion that could light up our lives. I am glad for myself that I start to make progress in finding my own passion. The fruitful feelings in my heart are going to lead me to seek for the true purpose of life. I would also appreciate my other committee members Dr. Tang Yi, Dr. Tatiana Segura and Dr. James W. Gober for their valuable opinions towards my Ph.D. research.

I would like to thank for my colleagues for their generous help for me to complete this journey. Thanks to Dr. Hong Yu, I gained a lot of strength and knowledge through discussions with him especially at the final stage of my Ph.D. Thanks to Dr. Yixin Huo, his advice and support helped me go through the most difficult time of my Ph.D. Thanks Dr. Wendy Higashide, Dr. Shota Atsumi, Dr.Tung-Yun Wu, Dr. Hao Luo, Dr. Claire Shen and Dr. Hidevaldo Machado for teaching me very important concepts and techniques of scientific research.

The work described here won't be possible without the efforts of other rGS team members. Thanks for Dr. Hong Yu, Dr. Samuel Mainguet, Dr. Luisa Gronnenberg and Dr. Avinash Srivastava for presenting me different perspectives of this project. Thanks for my collaborator, Fukusaki lab in Osaka University in Japan, for providing metabolomics data analysis to complement our understanding of rGS pathways. Thanks for the amazing research associates that

I have worked with, Reem Elteriefi, Hans Sebastian and Hannah Park for their technical assistance.

Thanks to all my fellow students in Liao lab, I can't believe that lab life can be *Joie de vivre* with all of you everyday. Thanks for all my friends for making my stay in Los Angeles the most memorable experience so far.

Thanks for DOE APRA-E PETRO grant for financial support.

VITA

EDUCATION

2009	M.E, Biochemical Engineering, School of Chemical Engineering Tianjin University, Tianjin, China
2007	B.E, Bioengineering, School of Chemical Engineering Tianjin University, Tianjin, China

PUBLICATIONS

X Li,, CR Shen, JC Liao Isobutanol production as an alternative metabolic sink to rescue the growth deficiency of the glycogen mutant of *Synechococcus* PCC 7942, Photosynthesis Research, 2014 Jun; 120 (3):301-10.

X Li, H Yu, JC.Liao Engineering reverse glyoxylate shunt cycle for enhanced carbon incorporation towards Acetyl-CoA derived chemicals in *Synechococcus PCC 7942*, in preparation

H Yu, X Li, JC, Liao Rewiring *E.coli* central metabolism with reverse glyoxylate shunt pathway for carbon conservation, in preparation

SELECTED PRESENTATIONS

A Srivastava, H Yu, X Li, F Duchoud, R Elteriefi, Metabolic engineering of CO2 fixation pathway for food and fuel production in plants, Poster, DOE ARPA-E Annual Summit, Washington DC, Feb 2015

S Mainguet, L Gronenberg, X Li, F Duchoud, R Elteriefi High Efficiency Photosynthetic Organism, Poster, Poster, DOE ARPA-E Annual meeting, Washington DC, Feb 2014

X Li, CR Shen, JC Liao Isobutanol production as metabolic sink to rescue the glycogen synthesis mutant, Oral presentation, 2013 Annual meeting of American Institute of Chemical Engineers, San Francisco, CA, Nov 2013

PATENTS

JC Liao, X Li, H Yu, A Srivastava, F Duchoud, SS Wong " Transgenic plants and microorganisms having an alternative CO2 fixing pathway. UCLA Case No. 2015-118, provisional patent application in progress.

Chapter I. Review

1.1 Challenge of Synthetic Metabolic Pathway Design and Metabolic Engineering

Synthetic Biology and Metabolic engineering research aim to elucidate the underlying principle of biological systems and enable a predicable cellular behavior through artificial design (J. Nielsen et al., 2014). While synthetic design capacity already reached the level of *de novo* genome reconstruction (Hutchison et al., 2016) and certain biological product already become commercial viable (Jullesson, David, Pfleger, & Nielsen, 2015), however, the newly established Synthetic Biology Standards Consortium still come to the consensus that "Synthetic organisms assembled from generic components don't always have predictable properties-at least not yet" (Hayden E. Nature. 2015)

When comes to large scale of metabolic pathway design, the iterative rounds of " Design-Build-Test-Learn" are the prerequisites for successfully implementation. With the advancement of sequencing technology, extensive genome DNA resources are yet to explore (Smanski et al., 2016). *De novo* rearrangement or reconfiguration of discovered metabolic pathways as well as facile mutagenesis provide numerous approaches to generate "microbe diversity". One problem that most metabolic engineers encountered in the lab is that the capacity of build and test can't keep pace with design. Insufficient build and test naturally lead to inconclusive evaluation of "first design " and thus very limited feedback could be extracted from completed experiments to instruct next round of the design. Another challenge for metabolic engineering is the lack of development of efficient phonotypical read out or diagnosis system for novel biological pathways. Due to our fundamentally insufficient understanding of existing biological systems,

not all of the engineering efforts may lead to identifiable or targeted phenotype. Therefore, comprehensively genetically modified strain may still appear as a black box for designers. “Unsatisfactory activity” of enzymes or the obvious metabolic burden that the synthetic pathway could bring about is often easily concluded. However, those speculations and assumption don’t necessarily help to dissect the problem. “Design more” strategy seems to be the only solution to overcome the ignorance (Church, Elowitz, Smolke, Voigt, & Weiss, 2014) . Third, compromised performance of designed biological system due to instability or irreproducibility complicates the design process. Since engineered pathways are not co-evolved with native metabolic networks, toxic intermediate or/and final product were often introduced and those pathway may facing robust issue itself or lack of feedback control (Way, Collins, Keasling, & Silver, 2016), the artificial feature could be easily looped out or mutated by the strains.

The magnitude of build and test and the speed of establishing links between iterative designs are the keys to overcome the intricacy lies in the nature of metabolic networks. High throughput at the automatic machine’s maximum capacity is certainly a non-questionable approach to expand our understanding (Gill, Halweg-Edwards, Clauset, & Way, 2016) . Furthermore, computation power should be incorporated into the design process as early as possible. More than 30 computation tools are available for evaluating and guiding metabolic pathway design now. It is an effective complementation or correction to human intuition to predict, confirm and prioritize unrevealed problems and to avoid those problems (Medema, van Raaphorst, Takano, & Breitling, 2012). Metabolomics analysis should also be incorporated into the iterative design process widely. The feedback that the engineered cellular systems send may not present in the way that we could predict. Metabolomics data will provide the ultimate panorama of metabolic networks

(Ellis & Goodacre, 2012). How the metabolomics data would interact with the computation power coherently in the metabolic engineering and synthetic biology study would be the top challenge for metabolic pathway designers in future (Johnson, Ivanisevic, & Siuzdak, 2016).

1.2 Synthetic Biology for improving carbon intake efficiency

The discipline of synthetic biology was applied to photosynthetic organism to address the ever-lasting problem of low photosynthetic efficiency. How to reduce carbon and energy loss during the process of photosynthesis is one of the top challenges for crop improvement (Figure 1-1) (Borak, Ort, & Burbaum, 2013). Although transformation efficiency and gene silencing is still the barrier for large scale of plant engineering (A. Z. Nielsen et al., 2016), the toolkit have expanded during the last decades, for example, RNAi technology and sequence-specific nucleases (Baltes & Voytas, 2016). Several frontier attempts started to pave the way for future plant synthetic biology. The most common strategy in plant to increase the carbon yield including: "Learn from C4 plants (Schuler, Mantegazza, & Weber, 2016)", "Learn from cyanobacteria (Gonzalez-Esquer, Shubitowski, & Kerfeld, 2015) (Ducat & Silver, 2012)" as well as strategy to recycle photorespiration product(Kebeish et al., 2007) . While the urgency of plants with desired traits has been sensed, however, when come to *de novo* design of advanced metabolic pathways, plants may not be the ideal photosynthetic organisms to exercise with iterative design cycles by far. The long development cycle, the sensitivity to multiple environmental stimulations and the intrinsic complicity caused by multiple organs, layered signal transduction pathways of model plants limited its status in the field of synthetic biology so far (Cook, Martin, & Bastow, 2014).

1.3 Cyanobacteria as a host for novel metabolic pathway design

Cyanobacteria are considered as the ancestor of the common organelle in plant: Chloroplast (Reyes-Prieto, 2015). The unique evolution status makes it an ideal platform to test the compatibility between synthetic designs and native photosynthetic machinery. The facile toolkit to manipulate cyanobacteria supports large scale of engineering of pathways deviant from native metabolic reactions. For example, the behavior of cyanobacteria TCA cycle has been altered from a bifurcated cycle into a complete cyclic manner by the introduction of Ethylene production pathway which drived away the carbon flux from TCA cycle intermediate (Xiong et al., 2015). Recently, a synthetic phosphoketolase pathway was engineered in *Synechococcus elongatus PCC 7942*. Calvin cycle intermediate becomes directly accessible for heterologous chemical synthesis(Chwa, Kim, Sim, Um, & Woo, 2016) . In this research, we fully take advantage of the plasticity of cyanobacteria genome and explore the possibility of construction of an alternative carbon fixation/incorporation pathway in a photosynthetic organism.

.

1.4 Figures

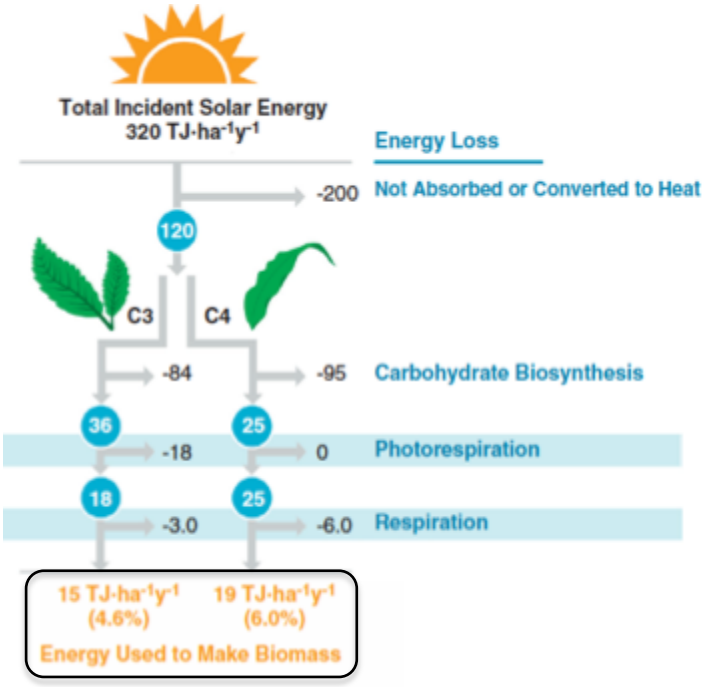

Figure 1- 1 Energy loss associated with biofuel production (Borak et al., 2013)**.**

1.5 Reference

Check Hayden E. Nature. 2015 Apr 9; 520(7546):141-2. doi: 10.1038/520141a

Baltes, N. J., & Voytas, D. F. (2016). Enabling plant synthetic biology through genome engineering. Trends in Biotechnology, 33(2), 120–131.

Borak, B., Ort, D. R., & Burbaum, J. J. (2013). Energy and carbon accounting to compare bioenergy crops. Current Opinion in Biotechnology, 24(3), 369–75.

Church, G. M., Elowitz, M. B., Smolke, C. D., Voigt, C. A., & Weiss, R. (2014). Realizing the potential of synthetic biology. Nat Rev Mol Cell Biol, 15(4), 289–294. Retrieved from

Chwa, J.-W., Kim, W. J., Sim, S. J., Um, Y., & Woo, H. M. (2016). Engineering of a modular and synthetic phosphoketolase pathway for photosynthetic production of acetone from CO2 in Synechococcus elongatus PCC 7942 under light and aerobic condition. Plant Biotechnology Journal.

Cook, C., Martin, L., & Bastow, R. (2014). Opportunities in plant synthetic biology. Journal of Experimental Botany .

Ducat, D. C., & Silver, P. A. (2012). Improving carbon fixation pathways. Current Opinion in Chemical Biology, 16(3-4), 337–44.

Ellis, D. I., & Goodacre, R. (2012). Metabolomics-assisted synthetic biology. Current Opinion in Biotechnology, 23(1), 22–8.

Gill, R. T., Halweg-Edwards, A. L., Clauset, A., & Way, S. F. (2016). Synthesis aided design: The biological design-build-test engineering paradigm? Biotechnology and Bioengineering, 113(1), 7–10.

Gonzalez-Esquer, C. R., Shubitowski, T. B., & Kerfeld, C. A. (2015). Streamlined Construction of the Cyanobacterial CO2-Fixing Organelle via Protein Domain Fusions for Use in Plant Synthetic Biology. The Plant Cell .

Hutchison, C. A., Chuang, R.-Y., Noskov, V. N., Assad-Garcia, N., Deerinck, T. J., Ellisman, M. H., … Venter, J. C. (2016). Design and synthesis of a minimal bacterial genome. Science, 351(6280).

Johnson, C. H., Ivanisevic, J., & Siuzdak, G. (2016). Metabolomics: beyond biomarkers and towards mechanisms. Nat Rev Mol Cell Biol, advance on.

Jullesson, D., David, F., Pfleger, B., & Nielsen, J. (2015). Impact of synthetic biology and metabolic engineering on industrial production of fine chemicals. Biotechnology Advances, 33(7), 1395–1402.

Kebeish, R., Niessen, M., Thiruveedhi, K., Bari, R., Hirsch, H.-J., Rosenkranz, R., … Peterhänsel, C. (2007). Chloroplastic photorespiratory bypass increases photosynthesis and biomass production in Arabidopsis thaliana. Nature Biotechnology, 25(5), 593–599.

Medema, M. H., van Raaphorst, R., Takano, E., & Breitling, R. (2012). Computational tools for the synthetic design of biochemical pathways. Nat Rev Micro, 10(3), 191–202.

Nielsen, A. Z., Mellor, S. B., Vavitsas, K., Wlodarczyk, A. J., Gnanasekaran, T., Perestrello Ramos H de Jesus, M., … Jensen, P. E. (2016). Extending the biosynthetic repertoires of cyanobacteria and chloroplasts. The Plant Journal : For Cell and Molecular Biology.

Nielsen, J., Fussenegger, M., Keasling, J., Lee, S. Y., Liao, J. C., Prather, K., & Palsson, B. (2014). Engineering synergy in biotechnology. Nat Chem Biol, 10(5), 319–322.

Reyes-Prieto, A. (2015). The Basic Genetic Toolkit to Move in with your Photosynthetic Partner . Frontiers in Ecology and Evolution .

Schuler, M. L., Mantegazza, O., & Weber, A. P. M. (2016). Engineering C4 photosynthesis into C3 chassis in the synthetic biology age. The Plant Journal : For Cell and Molecular Biology.

Smanski, M. J., Zhou, H., Claesen, J., Shen, B., Fischbach, M. A., & Voigt, C. A. (2016). Synthetic biology to access and expand nature's chemical diversity. Nat Rev Micro, 14(3), 135–149.

Way, J. C., Collins, J. J., Keasling, J. D., & Silver, P. A. (2016). Integrating Biological Redesign: Where Synthetic Biology Came From and Where It Needs to Go. Cell, 157(1), 151–161.

Xiong, W., Morgan, J. A., Ungerer, J., Wang, B., Maness, P.-C., & Yu, J. (2015). The plasticity of cyanobacterial metabolism supports direct CO_2 conversion to ethylene. Nature Plants, 1, 15053.

Chapter II Design and demonstration of reverse glyoxylate shunt pathway *in vitro* and in *E.coli*

2.1 Introduction

2.1.1 Problems of initial design of reverse glyoxylate shunt

Glyoxylate shunt exists in many bacteria and plants and it could convert two C2 units into one C4 unit for the purpose of energy generation and biosynthesis. The initial proof of concept of a reverse glyoxylate shunt was demonstrated in *E.coli* (Mainguet, Gronenberg, Wong, & Liao, 2013) (Figure 2-1). The reverse glyoxylate shunt pathway was constructed by malatethiokinase (MTK), malate-CoA lyase (MCL), isocitrate lyase (ICL), aconitase (ACN) and ATP-citrate lyase (ACL). The key enzyme for this pathway is MTK. The conversion from malate to glyoxylate and acetyl-CoA is thermodynamically unfavorable ($\Delta rG'^{\circ}$=44.4 kJ/mol). Instead, a MTK is able to couple the ATP hydrolysis to drive the reaction from malate to malyl-CoA that subsequently cleaved into glyoxylate and acetyl-CoA with thermodynamic favorability ($\Delta rG'^{\circ}$=-10.9 kJ/mol). The co-expression of the five enzymes and a malate transporter were able to rescue an oxaloacetate auxotroph mutant when malate and succinate were added into the medium. As the author predicted, if the reverse glyoxylate shunt pathway could be integrated with the *E.coli* central metabolism, particularly, the left branch of TCA cycle enzymes, Phosphoenolpyruvate carboxylase (PPC), Malate dehydrogenase (MDH) fumarase and fumarate reductase (FRD), a C3 metabolite could react with bicarbonate and become two acetyl-CoA molecules through this pathway. This pathway was denoted as “rGS-Citrate” pathway. It will significantly increase acetyl-CoA yield by 50% through glycolysis (Figure 2-2-A).

The efforts to re-route the central metabolism to suit the complete function of the rGS pathway from glucose will inevitably disturb the homeostasis of cellular metabolites. Most of the metabolic engineering works focus on achieving a steady state of intermediate metabolites. The non-native metabolic pathways didn't co-evolve with the rest of the metabolic networks. The expression level of pathway enzymes could be far beyond the optimal range. Therefore, the failure rate of the initial pathway design is really high. Intuitively, the branch point at malate of rGS-Citrate pathway could be problematic. The enzyme activity MDH, MTK and FUM need to be perfectly balanced in order to maintain the flux ratio between succinate and glyoxylate is 1 to 1. Otherwise, accumulation of succinate or glyoxylate would gradually drain out the pathway intermediate and lead to the crash of rGS cycle.

This concern was confirmed by simulation results. A new perspective to evaluate metabolic pathway design through stability was recently developed by *Lee, Y et al.* (Lee, Lafontaine Rivera, & Liao, 2014). They utilized Ensemble Modeling (Tan & Liao, 2012)for Robustness Analysis. In another word, they tested how the kinetic parameter of individual enzymes of a certain pathway change would affect the stability of whole pathway, for example, causing accumulation or depletion of metabolites. The investigated whether rGS pathway was robust enough to tolerate high level individual enzyme kinetic parameter drifting (Figure 2-2-B). They found out the fold changes of MTK even by two could cause very high chance of system failure. And a significant low MTK activity was also not within the desirable range.

2.1.2 Design of reverse glyoxylate shunt rGS-Glycerate pathway

An alternative design was required in order to overcome the limitation in term of metabolic pathway robustness. Glyoxylate need to be recycled as C3 metabolite in the rGS pathway. There

were three naturally existing pathways that could potentially assimilate glyoxylate and subsequently become the C3 metabolites that were compatible with initial rGS designs.

(1) Bacterial type glycerate pathway (Figure 2-3-A). With this pathway, two glyoxylate will be ligated as tartronic semialdehyde through glyoxylate carboligase (GCL). Then tartronic semialdehyde reductase (TSR) will reduce it into D-glycerate. D-glycerate will be further converted into 3-Phospho-glycerate through Glycerate Kinase (GK). 3-phospho-glycerate could be catalyzed into PEP through Enolase (ENO). This bacteria type glycerate pathway is part of glyoxylate and glycolate degradation pathway. Furthermore, Kebeish *et al* demonstrated its function as a bypass to efficiently channel photorespiration product into C3 compounds in Arabidopsis (Kebeish et al., 2007)..

(2) Glycine-serine cycle (Figure 2-3-B). This is the pathway that widely existed in many phototrophs (Kebeish et al., 2007) and methanotrophs (Schneider et al., 2012). Glyoxylate will receive the amino group from serine through transaminase. The resulting product glycine could further react with another C1 molecule to replenish serine molecules. The other transamination product, hydroxypyruvate, will be reduced into D-glycerate through hydroxypyruvate reductase (HPR). D-glycerate re-enter the rGS pathway through the same route as above.

(3) Propionyl-CoA: glyoxylate assimilation pathway (Figure 2-3-C). Glyoxylate is combined with propionyl-CoA to become β−methylmalyl-CoA through Methylmalyl-CoA Lyase. This product is dehydrated to mesaconyl-C1-CoA through Mesaconyl-CoA Hydratase. Intramolecular CoA transfer yields mesaconyl-C4-CoA and then it react with water to form (S)-Citramalyl-CoA. (S)-Citramalyl-CoA is cleaved into pyruvate and acetyl-CoA through Citramalyl–CoA Lyase (Fuchs & Berg, 2014). Pyruvate will be phosphorylated into PEP and

start another round of carbon fixation. The propionyl-CoA was originally synthesized from acetyl-CoA through the 3-Hydroxypropionate pathway (Saini, Kapoor, Kumar, Siddiqi, & Kumar, 2011).

If pathway (2), (3) could be successfully combined with the reverse glyoxylate shunt, it could a complete CO_2 fixation into acetyl-CoA cycle. Unlike the initial design of the rGS-Citrate pathway, no C3 metabolites would be required as the entry point of the cycle. However, due to the apparent technical feasibility, pathway (1) was selected to complete the recycling of the glyoxylate into the reverse glyoxylate shunt cycle. The new design was denoted as " rGS-Glycerate" cycle.

2.2 Materials and Methods

2.2.1 Protein expression and purification

Ppc, Eno and Mdh were purchased from Sigma. Mtk have two subunits A and B, each subunit was fused with His-tag at C-terminal and cloned within the same operon, while the remaining rGS genes including Pps, Mcl, Gcl, GlxR, Gark were fused with His tag at N-terminal. All His-tag rGS genes were cloned under T7 promoter and transformed into *E. coli* BL21 (DE3) cells for protein purification.

E. coli BL21 (DE3) cells were inoculated into LB medium with a 2/100 dilution of an overnight culture. Cells were grown at 37 degree with agitation rates of 250 rpm to mid-log phase and induced with 0.1mM IPTG. The culture was grown for an additional 6hr at 30 degree and cells were then harvested by centrifugation. Cell pellets were lysed and proteins were purified by His-Spin Protein Mini-prep columns (Zymo Research). Concentration of purified protein elute was determined using the BioRad Protein Assay kit, and protein purity was verified by standard SDS-PAGE with Coomassie staining methods. Purified protein was kept on ice and used the same day.

2.2.2 Pathway assay conditions and detection methods *in vitro*

The whole rGS in vitro assays were performed as following:

Pyruvate as initial substrate: The reactions were set up at 37 degree in a final volume of 400μL containing 50mMTris-Cl pH 7.5, 5mM $MgCl_2$, 0.5mM TPP, 2mM pyruvate, 5mM $NaHCO_3$, 8mM CoA, 10mM ATP, 10mM NADH with rGS enzymes including MtkAB, Mcl, Gcl, GlxR, GlxR, GarK, Ppc, Eno, Mdh and Pps(50units for each enzyme).

Glyoxylate as initial substrate: The reactions were set up at 37 degree in a final volume of 400μL containing 50mMTris-Cl pH 7.5, 5mM MgCl2, 0.5mM TPP, 2mM glyoxylate, 5mM NaHCO3,

4mM CoA, 6mM ATP, 6mM NADH with rGS enzymes including MtkAB, Mcl, Gcl, GlxR, GlxR, GarK, Ppc, Eno and Mdh(50 units for each enzyme). 50ul of the reaction was taken out at different time points and acetyl-CoA production was measured by HPLC. The detection methods was modified based on the protocol (Petrarulo et al., 1988).

2.2.3 *In vitro* enzyme assay condition

Measurement of rGS enzyme activities is performed as following:

Mtk-Mcl assay: MTK performs the ATP-dependent condensation of malate and CoA into malyl-CoA. MCL cleaves malyl-CoA into acetyl-CoA and glyoxylate, the latter reacting with phenylhydazine to form glyoxylate-phenylhydrazone which displays strong absorbance at 324 nm. Reactions were set up at 37 degree in a final volume of 200μL containing 50mMTris-Cl pH 7.5, 5mM $MgCl_2$, 2mM phenylhydrazine, 10mM malate, 2.5mM ATP, 2mM CoA, 15ug MtkAB and 5ug Mcl purified protein.

Gcl-GlxR assay: Gcl performs the reaction to condense two glyoxylate into one tartronic semialdehyde. GlxR converts tartronic semialdehyde to glycerate by NADH consumption which can be recorded at 340nM. Reactions were set up at 37 degree in a final volume of 200μL containing 50mMTris-Cl pH 7.5, 5mM $MgCl_2$, 0.5mM TPP, 5mM glyxoylate, 0.25mM NADH, 5ug Gcl and 5ug GlxR purified protein.

Mtk-Mcl-Gcl-GlxR assay: Gcl-GlxR proteins condense and reduce glyxoylate, produced by Mtk-Mcl from malate, to glycerate. NADH consumption can be used to record the reaction. Reactions were set up at 37 degree in a final volume of 200μL containing 50mMTris-Cl pH 7.5, 5mM $MgCl_2$, 0.5mM TPP, 2.5mM ATP, 2mM CoA, 0.25mM NADH, 10mM malate, 20ug MtkAB, 5ug Mcl, 10ug Gcl and 5ug GlxR.

GarK assay: Gark performs the ATP-dependent reaction to use glycerate as substrate to produce 2-phospho-glycerate and ADP. Pyk/Ldh enzyme mixture (purchased from Sigma) is used to measure ADP content in the reaction. Pyk uses ADP as a cofactor to convert PEP to pyruvate. Ldh enzyme reduces pyruvate to lactate by NADH consumption. NADH consumption can be recorded at 340nM. The whole reactions were set up at 37 degree in a final volume of 200μL containing 50mMTris-Cl pH 7.5, 5mM $MgCl_2$, 5mM glycerate, 2mM PEP, 2.5mM ATP, 0.25mM NADH, 10ug GarK purified protein and 1ul of Pyk/Ldh mixture.

GarK-Eno-Ppc-Mdh assay: Eno catalyzes the reaction of 2-phospho-glycerate, produced by GarK protein, to PEP. The latter reacts with bicarbonate to produce OAA by Ppc enzyme. Mdh performs the NADH-dependent reaction to reduce OAA to malate. The reactions were set up at 37 degree in a final volume of 200μL containing 50mMTris-Cl pH 7.5, 5mM $MgCl_2$, 2mM glycerate, 10mM $NaHCO_3$, 2.5mM ATP, 0.25mM NADH, 10ug Gark purified protein, 0.5ul of Ppc, 0.5ul of Eno and 0.5ul of Mdh. The reactions were measured by NADH consumption at 340nM.

Pps-Ppc-Mdh assay: Pps converts pyruvate to produce PEP. Ppc enzyme catalyzes CO2 fixation reaction to convert PEP (C3 carbon) to OAA(C4 carbon). The latter can be reduced to malate by Mdh enzyme. The reactions were set up at 37 degree in a final volume of 200μL containing 50mMTris-Cl pH 7.5, 5mM $MgCl_2$, 10mM pyruvate, 10mM $NaHCO_3$, 2.5mM ATP, 0.25mM NADH, 10ug Pps purified protein, 0.5ul of Ppc and 0.5ul of Mdh. The reactions were measured by NADH consumption at 340nM.

2.2.4 *E.coli* strain construction and test condition

(KmR: Kanamycin resistant; RBS: 5'-AGGAGCTATACC-3'; E.c: Escherischia Coli; M.c: Methylococcus capsulatus; R.s: Rhodobacter sphaeroides.)

△aceEF△poxB△pflB mutant strain was developed by Zelić et al.. The plasmids of pHY100 and pHY101 were transformed into △aceEF△poxB△pflB mutant *E.coli* cells were inoculated into fresh LB medium with a 2/100 dilution of an overnight culture. Cells were grown at 37 degree with agitation rates of 250 rpm to mid-log phase and induced with 0.1mM IPTG. The culture was grown for an additional 6 hrs at 30 degree and cells were then harvested by centrifugation. The cell pellet was washed by 1ml M9 1% Glucose twice and performed 2% inoculation into M9 liquid medium with 1% Glucose and 100uM IPTG addition. Cell density was measured at indicated time points. The same protocol was used in the growth rescue of the △maeAB△pck mutant.

2.3 Results and discussion

2.3.1 rGS-Glycerate cycle analysis by thermodynamics and EMRA

The rGS-Glycerate pathway was first analyzed and compared with rGS-Citrate cycle through thermodynamic calculation (Table 2-1). By comparison of the Gibbs energy of the two pathways, we could tell that rGS-Glycerate cycle was much more thermodynamically favorable. Since the rGS-Glycerate cycle consumed one more ATP than rGS-Citrate cycle, ATP hydrolysis could drive the pathway towards the direction of acetyl-CoA synthesis more efficiently.

The rGS-Glycerate pathway was further analyzed by the EMRA. The simulation results showed that the robustness of this design was greatly enhanced due to the bacterial glyoxylate assimilation pathway (Figure 2-4). The expression levels of the nine key steps enzymes were perturbed. No individual enzyme expression level change would greatly affect the stability of the full pathway.

2.3.2 reverse glyoxylate shunt pathway individual enzyme activity characterization

The activity of individual enzymes was first examined through *in vitro* assay (Figure 2-5) (Table 2-2). We still chose the MTK from *M. capsulatus* which has been shown as the most active enzyme to convert malate into Malyl-CoA (Mainguet et al., 2013). A more active Malyl-CoA lyase was found by bio-prospection. The specific activity of MCL from *M. extoquens* was shown to be 9 folds higher than the one from *R. sphaeroides.*

Four coupled assays were performed to ensure the function of a sub-pathway (Figure 2-6). The sub-pathways from Pyruvate to malate, from glyoxylate to glycerate and from glycerate to malate were verified through NADH consumption by the terminal enzyme of each sub-pathway.

The sub-pathway from malate to glyoxylate was verified through generation of the glyoxylate-phenylhydrazone derivatization product that has absorbance @324nm.

2.3.3 *In vitro* demonstration of reverse glyoxylate shunt pathway at theoretical yield

rGS-Glycerate cycle functions in a cyclic fashion, unlike a linear pathway, the starting metabolite for a cyclic pathway could be any intermediate metabolite. The starting metabolite will be catalyzed through the whole cycle enzymes sequentially and become acetyl-CoA eventually with cofactors as additional inputs. Therefore, all the C2, C3+C1 and C4 input could be metabolized into Acetyl-CoA at their Stoichiometric balance. We adopted two starting metabolites to initiate this cycle *in vitro:* Pyruvate and glyoxylate. Pyruvate is the most common precursor for Acetyl-CoA across many organisms, so that acetyl-CoA yield from pyruvate *in vitro* would be the essential parameter to evaluate the performance of full cycle. Based on our design, the efficiency of glyoxylate recycling into C3 determined the stability of the rGS-glyoxylate cycle. Therefore, the conversion ratio between glyoxylate and acetyl-CoA would be another key feature to investigate *in vitro*.

2mM pyruvate and 2mM glyoxylate were added to the assay mixture respectively. After 3 hours, all of the substrate pyruvate and glyoxylate were consumed (Data not shown). 3.88mM Acetyl-CoA was detected in the assay mixture with pyruvate while 1.2mM Acetyl-CoA was detected in the assay mixture without GCL (Figure 2-7). It was surprised to find out that the Pyruvate/Acetyl-CoA yield was almost reached its theoretical value while Pyruvate/Acetyl-CoA yield through the partial pathway was only 60% of its theoretical value (2mM). Even with much more enzymatic reactions, it seems that the thermodynamics was able to boost the total conversion rate. 1.73 mM Acetyl-CoA was also detected in the assay mixture with glyoxylate

while no Acetyl-CoA was found if GCL or MTK was missing. Up to 86% conversion rate from glyoxylate successfully demonstrated the function of recycling branch of the rGS-Glycerate cycle *in vitro.*

2.3.4 *In vivo* demonstration of reverse glyoxylate shunt-citrate pathway in *E.coli*

For the eight enzymes that were required for the rGS-citrate pathway, six of them are indigenous to *E.coli*. The only heterologous enzymes are malate-CoA thiokinase and Malyl-CoA lyase. The original work on reverse glyoxylate shunt in *E.coli* successfully demonstrated oxaloacetate production facilitated by malate-CoA thiokinase. However, there was no direct evidence that significant amount of Acetyl-CoA production could also be driven by this enzyme. An acetyl-CoA auxotroph strain (Δ***aceEF*** Δ***poxB*** Δ***pflB)*** (Zelić et al., 2003)was utilized as the platform to detect overexpression effect of MTK/MCL in *E.coli. Gcl* was knocked out to prevent glyoxylate decarboxylation in the auxotroph strain. (Figure 2-8-A) showed that the introduction of the MTK/MCL was able to rescue the acetyl-CoA auxotroph strain in the glucose minimal medium within 40 hrs. Overexpression of GCL could accelerate the rescue effect and enhanced growth rate appeared at 8 hours after induction. However, almost no effect was observed by additional overexpression of GlXR. Figure 2-8-B showed that no growth would be detected without the supplement of acetate.

Meanwhile, we utilized a pyruvate auxotroph strain to exanimate whether glyoxylate produced by MTK/MCL could be converted into the C3 metabolite. Pathways that could convert C4 TCA cycle intermediate into C3 were blocked in the pyruvate auxotroph strain (Δ*maeAB,* Δ*pck)*. Figure 2-8-C showed that MTK/MCL overexpression successfully rescue the pyruvate auxotroph

strain with Aspartate in the medium. As long as GCL was missing, no growth rescue effect was detected within 5 days. In conclusion, it confirmed the role of GCL in terms of recycling C2 into the C3 intermediate in the rGS-citrate cycle. Figure 2-8-D showed that no growth of pyruvate auxotroph strain would be detected without the supplement of C3.

2.4 Figures

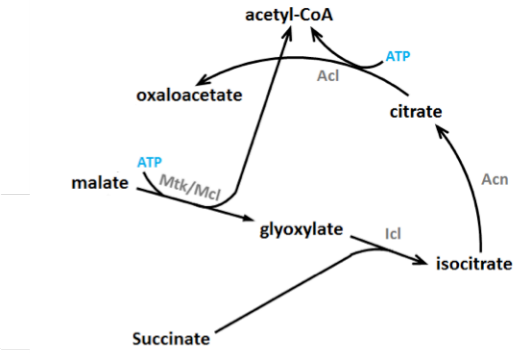

Figure 2- 1 Initial demonstration of reverse glyoxylate shunt pathway in E.coli

The initial design reverse glyoxylate shunt pathway include mtk/mcl, icl, acn and acl. It enables the conversion from malate into OAA and was demonstrated in *E.coli.* (Mainguet et al., 2013)

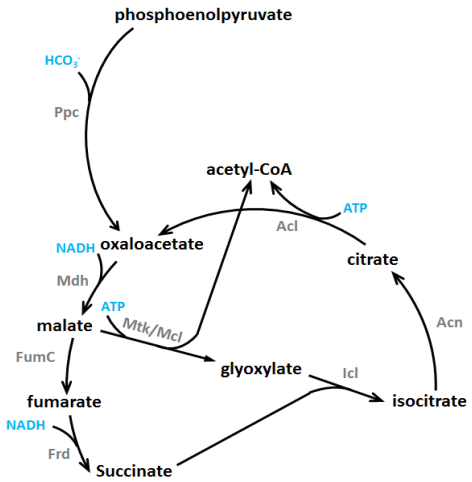

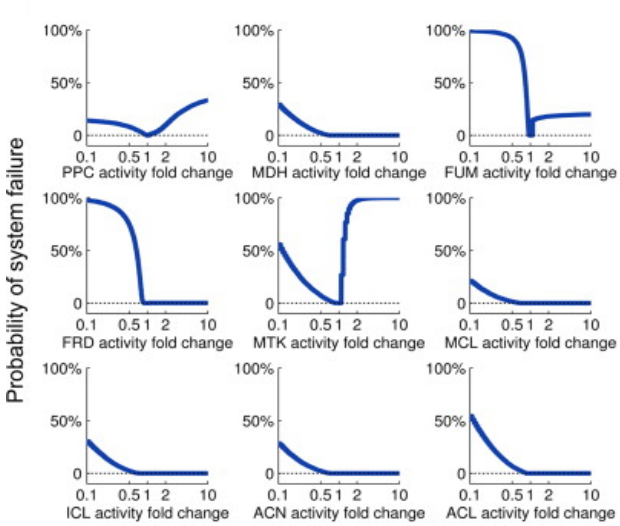

Figure 2-2-A

Figure 2-2-B

Figure 2- 2 reverse glyoxylate shunt-citrate design and EMRA simulation

Figure 2-2-A Design of rGS pathway to increase Acetyl-CoA yield from PEP

Figure 2-2-B Simulation through the EMRA showed that MTK activity changes could potentially cause the robustness issues of the initial design of rGS pathway. (Lee, Lafontaine Rivera, & Liao, 2014)

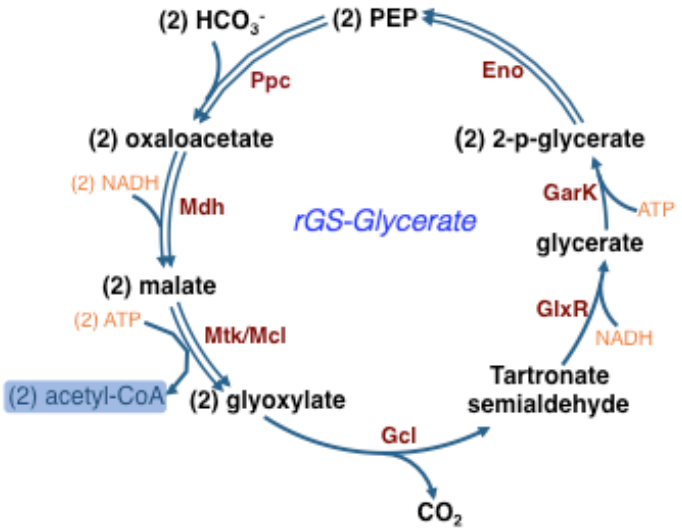

Figure 2-3-A rGS-Glycerate pathway with glyoxylate recycled through bacterial like pathway

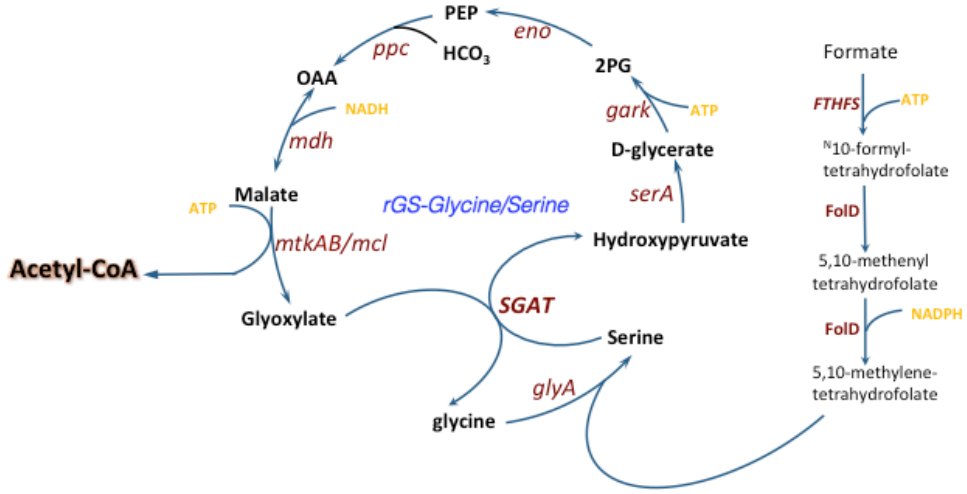

Figure 2-3-B rGS-Glycine/Serine pathway with glyoxylate recycled through SGAT

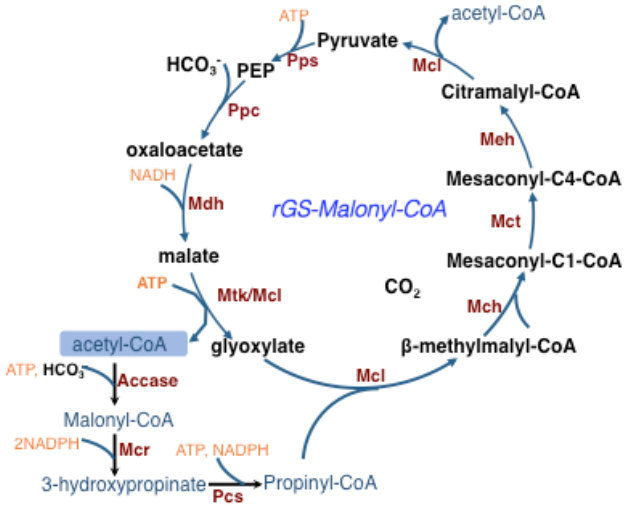

Figure 2-3-C rGS-Malonyl-CoA pathway with glyoxylate recycled through Propionyl-CoA: glyoxylate assimilation pathway

Figure 2- 3 Design of different pathways of recycling glyoxylate into reverse glyoxylate shunt pathway

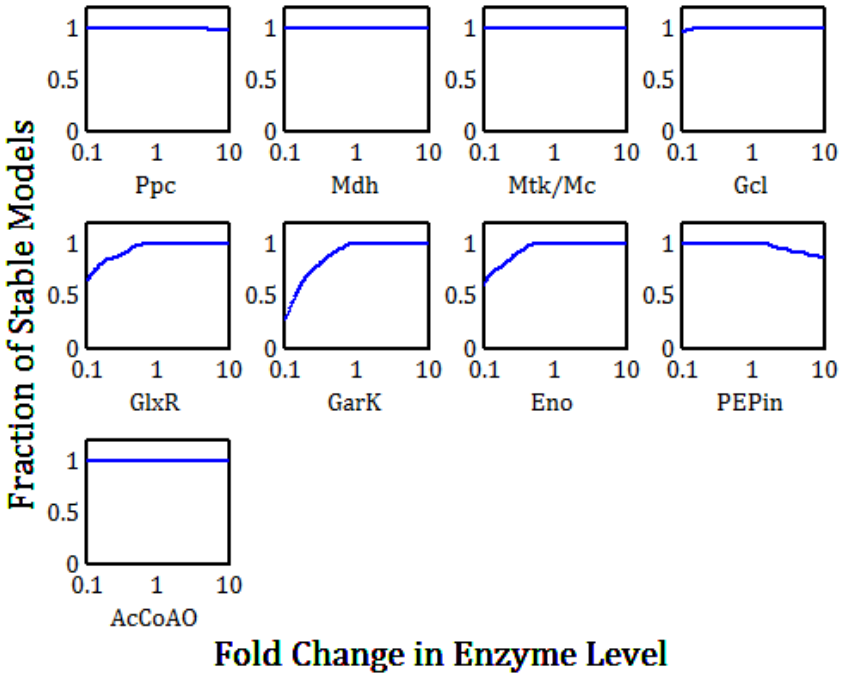

Figure 2- 4 Ensemble Modeling Robustness Analysis of rGS-glycerate pathway (By Matthew Theisen, unpublished work)

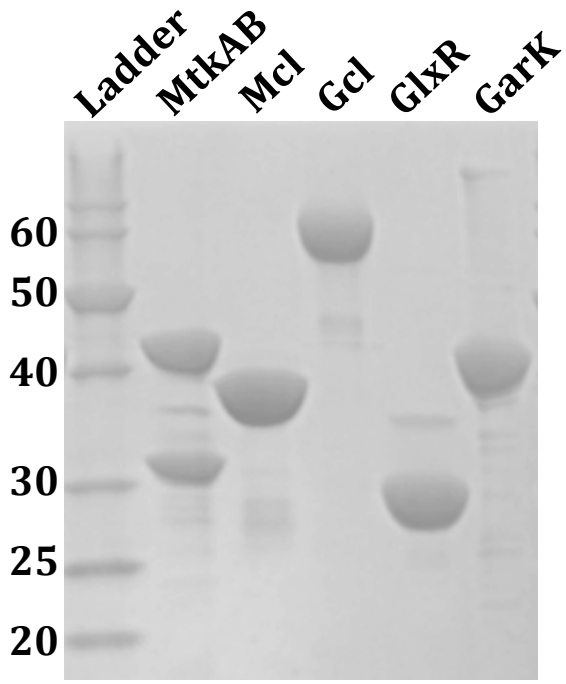

Protein	Organism	MW(kD)
MtkA	*M. capsulatus*	41.8
MtkB	*M. capsulatus*	31.3
Mcl	*M. extorquens*	35.5
Gcl	*E.coli*	64.7
GlxR	*E.coli*	30.8
GarK	*E.coli*	42.1

Figure 2- 5 His-tag purification of individual enzymes

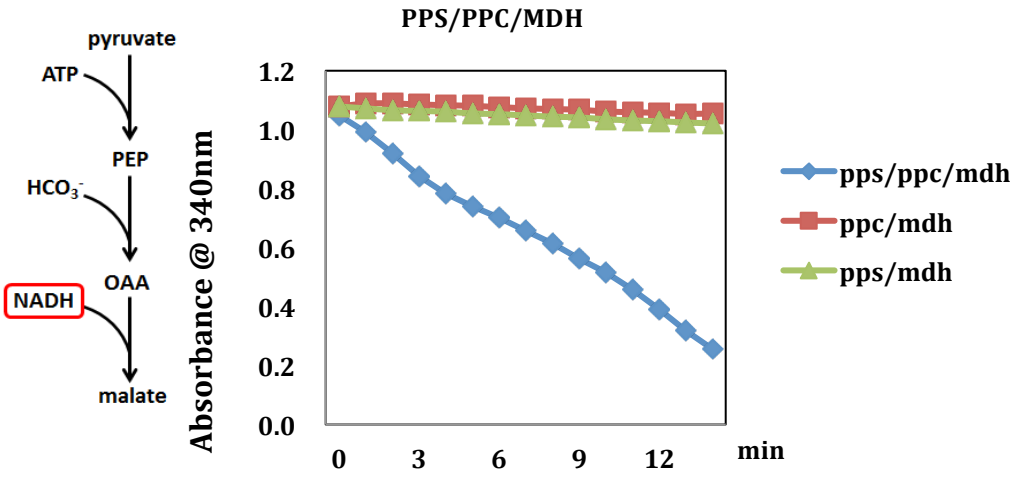

Figure 2-6-A Couple enzyme assay of PPS/PPC/MDH

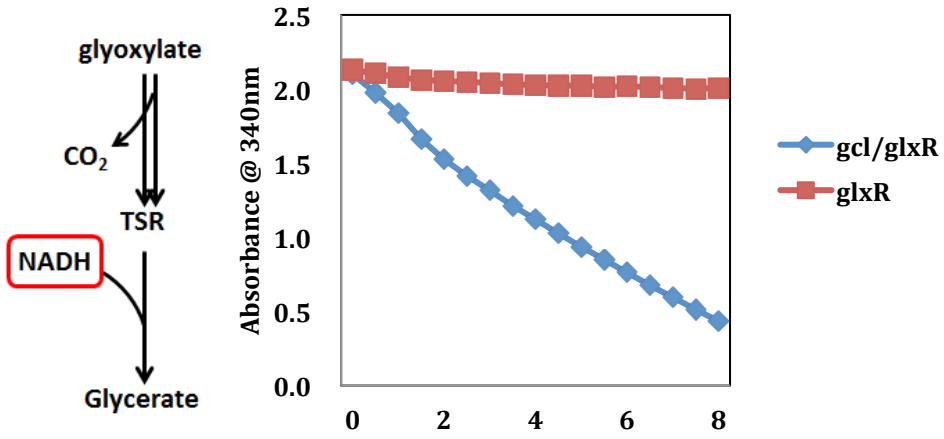

Figure 2-6-B Couple enzyme assay of GCL/GLXR

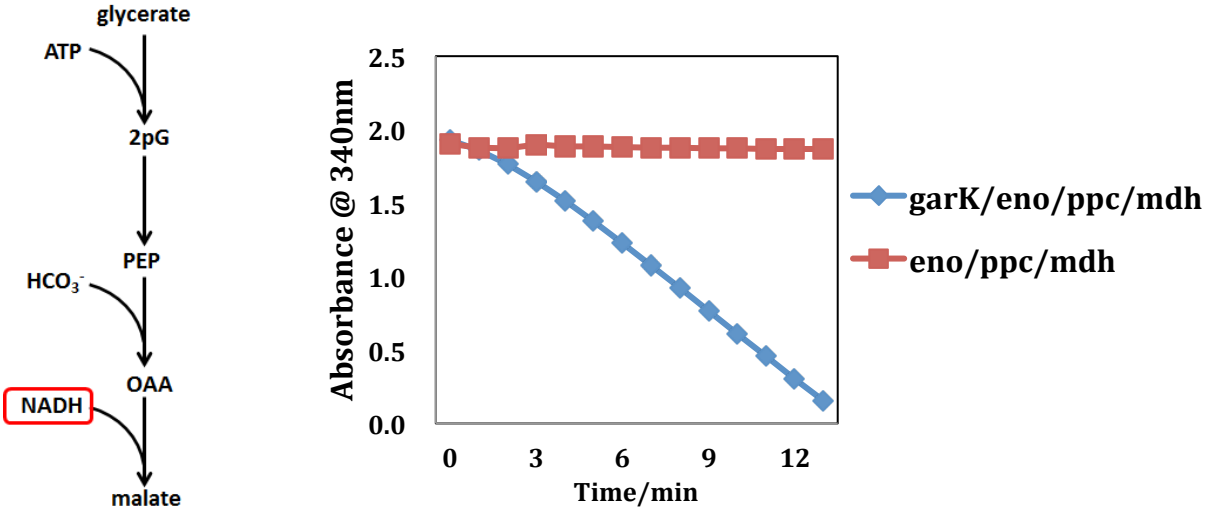

Figure 2-6-C Coupled enzyme assay of GarK/Eno/Ppc/Mdh

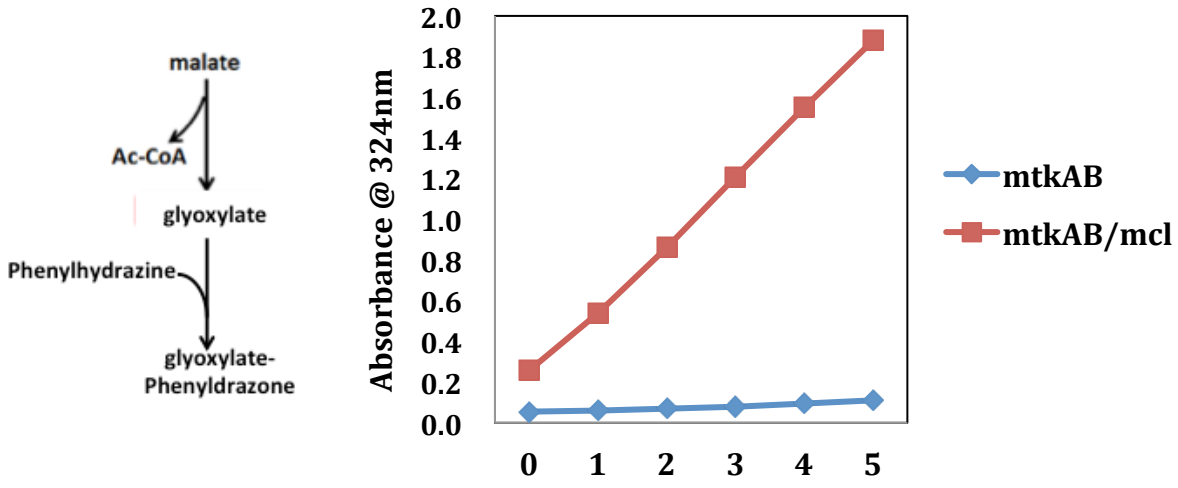

Figure 2-6-D Coupled enzyme assay of Mtk/Mcl

Figure 2- 6 Test of functions of sub-pathway of rGS-Glycerate cycle *in vitro*

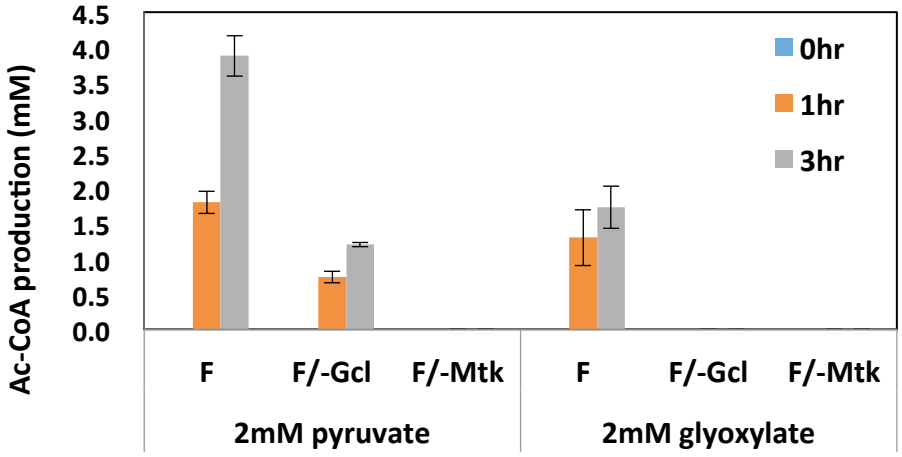

Figure 2-7-A Acetyl-CoA production

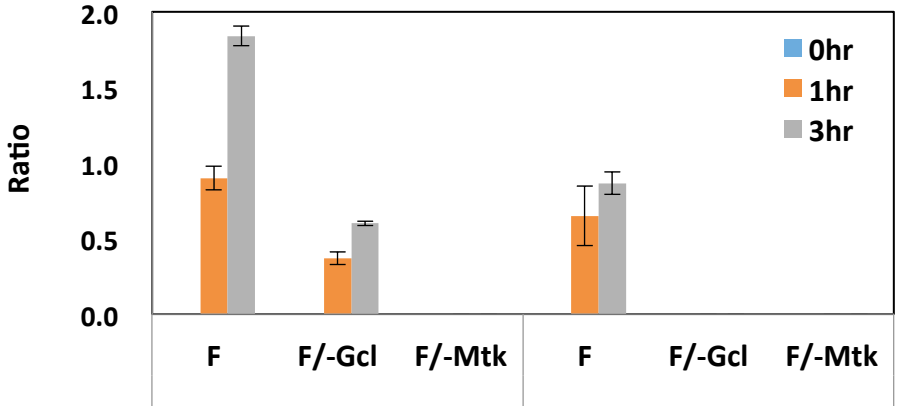

Figure 2-7-B PEP/Acetyl-CoA ratios

Figure 2- 7 *In vitro* demonstration of full rGS-citrate pathway

Figure 2-7-A: 2mM pyruvate and 2mM glyoxylate were added to the assay mixture respectively. After 3 hours, all of the substrate pyruvate and glyoxylate were consumed. 3.88mM Acetyl-CoA was detected in the assay mixture with pyruvate while 1.2mM Acetyl-CoA was detected in the assay mixture without GCL. 1.73 mM Acetyl-CoA was also detected in the assay mixture with glyoxylate while no Acetyl-CoA was found if GCL or MTK is missing.

Figure 2-7-B: PEP/Acetyl-CoA ratios *in vitro*. Pyruvate/Acetyl-CoA yield is almost reaches its theoretical value while Pyruvate/Acetyl-CoA yield through the partial pathway is only 60% of its theoretical value (2mM). Up to 86% conversion rate from glyoxylate successfully demonstrate the function of recycling branch of the rGS-citrate cycle *in vitro*.

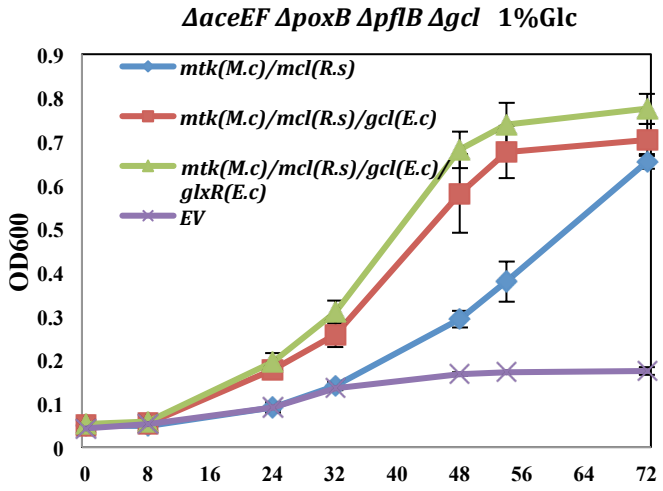

Figure 2-8-A Growth rescue with rGS-glycerate pathway gene for Acetyl-CoA production

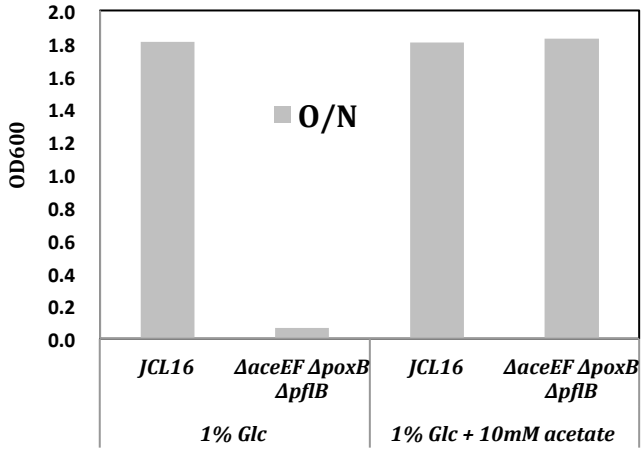

Figure 2-8-B Growth of acetyl-CoA auxotroph with acetate

Figure 2-8-A An acetyl-CoA auxotroph strain (Δ***aceEF*** Δ***poxB*** Δ***pflB)*** (was utilized as the platform to detect overexpression effect of MTK/MCL in *E.coli.* Gcl was also knocked out to prevent glyoxylate decarboxylation in the auxotroph strain showed that the introduction of the MTK/MCL was able to rescue the acetyl-CoA auxotroph strain in the glucose minimal medium within 40 hrs. Overexpression of GCL could accelerate the rescue effect and enhanced growth rate appeared at 8 hours after inoculation.

Figure 2-8-B confirmation of Acetyl-CoA auxotroph with addition of acetate.

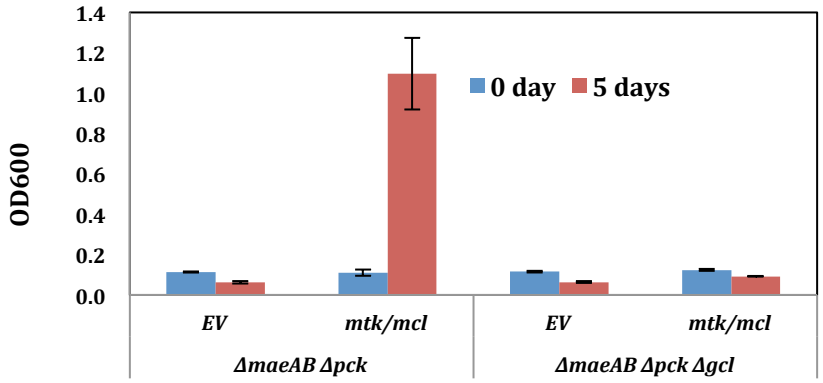

Figure 2-8-C Growth rescue with rGS-glycerate pathway gene for C3 production

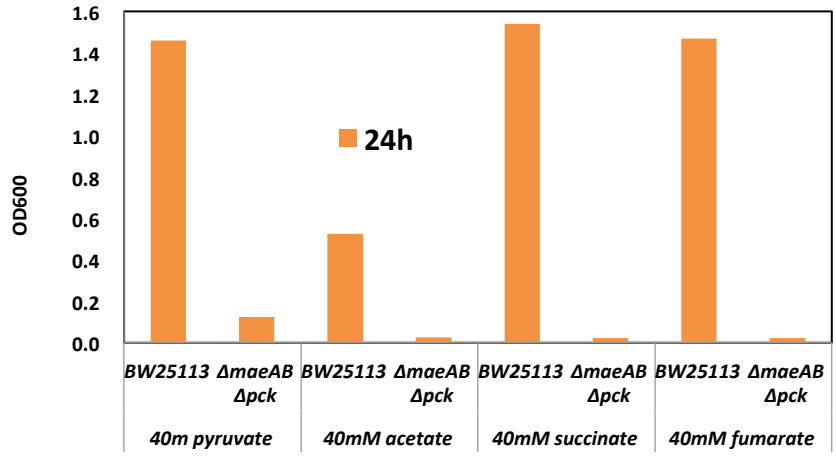

Figure 2-8-D Growth of pyruvate auxotroph with pyruvate

Figure 2-8-C :Pathways that could convert C4 TCA cycle intermediate into C3 were blocked in the pyruvate auxotroph strain (ΔmaeAB, Δpck). MTK/MCL overexpression successfully rescue the pyruvate auxotroph strain with Aspartate was added into the medium. As long as gcl is missing, no growth rescue effect was detected within 5 days.

Figure 2-8-D confirmation of pyruvate auxotroph with only addition of pyruvate.

Figure 2- 8 *in vivo* demonstration of rGS-citrate cycle in *E.coli*

2.5 Tables

	rGS-Citrate Reaction name	$\Delta_r G'^m$(KJ/mol)※	Number	Per Step ΔrG'm (KJ/mol)
1	Phosphoenolpyruvate(aq) + HCO3-(aq) ⇌ Oxaloacetate(aq) + Pi(aq)	-33.6	1	-31.9
2	NADH + Oxaloacetate = NAD+ + (S)-Malate	-30.3	2	-60.6
3	malate + coenzyme A + ATP -> malyl-CoA + ADP +phosphate	-6.7	1	-6.7
4	Malyl-CoA(aq) ⇌ Acetyl-CoA(aq) + Glyoxylate(aq)	-4.2	1	-4.2
5	Malate = Fumarate + H2O	3.50	1	3.5
6	fumarate +NADH -> Succinate +NAD	-63.20	1	-63.2
7	Succinate + glyoxylate ->isocitrate	-8.60	1	-8.6
8	Isocitrate = cis-Aconitate + H2O	0.70	1	0.7
9	cis-Aconitate + H2O = Citrate	-8.30	1	-8.3
10	Citrate + ATP + Coenzyme A = Oxaloacetate + Acetyl-CoA + ADP + Phosphate	8.20	1	8.2
Total	Phosphoenolpyruvate + 2HCO3- + 2 coenzyme A + 3 NADH + 3 ATP ⇌ 2 Acetyl-CoA + 3 NAD+ 3 ADP +4 Pi +H2O +CO2			-172

Table 2-1-A

	Reaction name	$\Delta_r G'^m$(KJ/mol)	Number	Per Step ΔrG'm(KJ/mol)
1	Phosphoenolpyruvate(aq) + HCO3-(aq) ⇌ Oxaloacetate(aq) + Pi(aq)	-33.6	2	-67.2
2	NADH + Oxaloacetate = NAD+ + (S)-Malate	-30.3	2	-60.6
3	malate + coenzyme A + ATP -> malyl-CoA + ADP +phosphate	**-6.7**	2	-13.4
4	Malyl-CoA(aq) ⇌ Acetyl-CoA(aq) + Glyoxylate(aq)	**-4.2**	2	-8.4
5	2glyoxylate -> Tartronate semialdehyde +CO2	**-19.6**	1	-19.6
6	Tartronate semialdehyde + NADH -> D-glycerate +NAD	**-33.3**	1	-33.3
7	d-glycerate +ATP -> ADP +2-Phospho-D-glycerate	**-6.7**	1	-11
8	2-Phospho-D-glycerate = Phosphoenolpyruvate + H2O	**-4.1**	1	-4.1
Total	Phosphoenolpyruvate + 2HCO3- + 2 coenzyme A + 3 NADH + 3 ATP ⇌ 2 Acetyl-CoA + 3 NAD+ 3 ADP +4 Pi +H2O +CO2			-217.6

Table 2-1-B

Table 2- 1 Thermodynamic calculation of reverse glyoxylate shunt Pathway Gibbs Energy

The reaction Gibbs energy was calculated through eQuilibrator software. $\Delta_r G'^m$(KJ/mol) is the free Gibbs energy when the reactant concentration was set to be 1mM, PH=7 and ionic strength is 0.1M.

Table 2-1-a showed the pathway Gibbs energy of rGS-citrate cycle in the defined condition.

Table 2-1-b showed the Gibbs energy of rGS-glycerate cycle in the defined condition

Enzyme	Organism	Other enzymes added	Substrate	Specific activity (µmol/mim/mg protein)
Pps	*E.coli*	Ppc, Mdh	5mM pyruvate	**5.6**
Ppc		Mdh	5mM PEP 5mM $NaHCO_3$	**1.15**
Mdh			8mM OAA	**3.1**
MtkAB	*M. capsulatus*	Mcl	10mM malate	**2.7**
Mcl	*R. sphaeroides*	MtkAB	10mM malate	**3.3**
Mcl	*M. extorquens*	MtkAB	10mM malate	**30.3**
Gcl	*E.coli*	GlxR	10mM glyoxylate	**2.8**
GlxR	*E.coli*	Gcl	10mM glyoxylate	**27.8**
GarK	*E.coli*	Eno, Ppc,Mdh	5mM glyceric acid 10mM $NaHCO_3$	**2.5**

Table 2- 2 Specific activity characterization of individual enzymes of reverse glyoxylate shunt–Glycerate cycle

Plasmid Name	Description
pHY100	*ColA-ori, KmR, LacI, PLlacO1:MtkA(M.c)-MtkB(M.c)-Mcl(R.s)*
pHY101	*ColA-ori, KmR, LacI, PLlacO1:MtkA(M.c)-MtkB(M.c)-Mcl(R.s)- PLlacO1:Gcl(E.c)*

Table 2- 3 plasmids used in E.coli growth rescue

2.6 Reference

Fuchs, Georg, and Ivan A Berg. 2014. "Unfamiliar Metabolic Links in the Central Carbon Metabolism." *Journal of Biotechnology* 192, Part : 314–22.

Kebeish, Rashad et al. 2007. "Chloroplastic Photorespiratory Bypass Increases Photosynthesis and Biomass Production in Arabidopsis Thaliana." *Nature biotechnology* 25(5): 593–99.

Lee, Yun, Jimmy G Lafontaine Rivera, and James C Liao. 2014. "Ensemble Modeling for Robustness Analysis in Engineering Non-Native Metabolic Pathways." *Metabolic engineering* 25: 63–71.

Mainguet, Samuel E, Luisa S Gronenberg, Sio Si Wong, and James C Liao. 2013. "A Reverse Glyoxylate Shunt to Build a Non-Native Route from C4 to C2 in Escherichia Coli." *Metabolic engineering* 19: 116–27.

Petrarulo, Michele et al. 1988. "High-Performance Liquid Chromatographic Determination of Glyoxylic Acid in Urine." *Journal of Chromatography B: Biomedical Sciences and Applications* 432: 37–46.

Saini, Rashmi et al. 2011. "CO2 Utilizing Microbes — A Comprehensive Review." *Biotechnology Advances* 29(6): 949–60.

Schneider, Kathrin et al. 2012. "The Ethylmalonyl-CoA Pathway Is Used in Place of the Glyoxylate Cycle by Methylobacterium Extorquens AM1 during Growth on Acetate." *Journal of Biological Chemistry* 287 (1): 757–66.

Tan, Yikun, and James C Liao. 2012. "Metabolic Ensemble Modeling for Strain Engineers." *Biotechnology Journal* 7(3): 343–53.

Zelić, B et al. 2003. "Fed-Batch Process for Pyruvate Production by Recombinant Escherichia Coli YYC202 Strain." *Engineering in Life Sciences* 3(7): 299–305.

Chapter III. Engineering a reverse glyoxylate shunt facilitated carbon fixation cycle in cyanobacteria for enhanced acetyl-CoA derived metabolites production

3.1 Introduction

3.1.1 Insufficient photosynthesis by RuBisCO and alternative carbon fixation/incorporation cycles evaluations

The highest solar conversion efficiency has been reported to be lower than 5% in C plants. One of the solution to close the gap between the actual and theoretical efficiency is to expand the photosynthetic capacity under light illumination (Zhu, Long, & Ort, 2008). Endless efforts have been devoted into reengineering the rate-limiting RubisCO and eliminating the regulations around RubisCO expression. Limited success has been achieved to improve the performance of the most abundant protein in plants (Parry et al., 2013) . Alternatively, a photorespiration bypass was incorporated into the chloroplast to reduce carbon loss and increase local concentration of RubisCO. However, the highest efficiency is predicted to be 5.2% (Kebeish et al.,d 2007) in the plant contained the bypass. Cyanobacteria are the best model organism to test the compatibility between photosynthetic machinery and innovative metabolic pathway designs. The gradually upgraded carbon concentration system in cyanobacteria could potentially bring about new perspective to plant metabolic engineering (Sun et al., 2016). A carbon sink, accumulation of 2, 3 butanediol pathway has been shown to increase the total carbon fixation productivity of cyanobacteria by 1.8 fold. However, further carbon partition towards the product damaged the cell growth as well as the total carbon fixation rate (Oliver & Atsumi, 2015). Likewise,

isobutanol pathway has been shown as a significant carbon sink to resuce *glgC* mutant. However, the additional carbon sink didn't increase the total carbon fixation capacity (Li, Shen and Liao, 2014)

The performance of RuBisCO imposed the upper limit of total carbon fixation capacity. Fortunately, nature prepared a lot of other types of carbon fixation pathways that could potentially be incorporated into the existing carbon fixation configuration of photosynthetic organism. For example: reductive TCA cycle, 3-hydroxypropionate bi-cycle, 3-hydroxypropionate/4-hydroxybutylrate cycle and Dicarboxylate-4-hydroxybutylrate cycle. Since none of those heterologous cycles or any derived synthetic cycles have been co-evolved with native Calvin cycle. The feasibility to implement those cycles needs to be throughout assessed.

3.1.2 Design of rGS core module

Among all the carboxylases discovered so far, PEP carboxylase seems to be a good candidate to be included for any synthetic carbon fixation pathway. Irreversible enzyme is an important pathway valve to drive the product synthesis. PEP carboxylase catalyzed the irreversible reactions under physiological conditions. Compared to other type of carboxylase (for example, Acetyl-CoA Carboxylase, Propionyl-CoA carboxylase, Pyruvate Carboxylase, Isocitrate Dehydrogenase and Crotonyl-CoA carboxylase/Reductase) it has the highest Gibbs free energy (Bar-Even, Noor, Lewis, & Milo, 2010). The substrate for PEP carboxylase is bicarbonate. Since bicarbonate becomes preferentially more soluble under alkaline conditions, it would be beneficial for organisms that grow in alkaline environments (cyanobacteria and eukaryotic algae)(Ducat & Silver, 2012). In addition, PEP carboxylase has very high affinity towards inorganic carbon. As a native enzyme in plants, PEP didn't encounter any oxygen sensitive

issues as the carboxylase exist in anaerobes. PEP would catalyze the conversion from C3 compounds into C4 compounds. Meanwhile, The pathway of converting malate (C4) into C2 metabolites, glyoxylate and acetyl-CoA, has been demonstrated (Mainguet et al., 2013). Combing the PEP carboxylase and the non-native route from C4 to C2, we have the original design of core module of reverse glyoxylate shunt (rGS) (Figure 3-1-A).

In order to complete the minimal carbon fixation cycle, at least one of the C2 metabolite need to react with one more C1 molecule and become C3 metabolite. The carbon fixation product could be Acetyl-CoA, glyoxylate or C3 metabolite (PEP or pyruvate). If there is a pathway or an enzyme that could fix one more carbon with Acetyl-CoA and become C3 metabolite, the carbon fixation product is glyoxylate (Figure 3-1-B). Likewise, if there is a pathway or an enzyme that could fix one more carbon with glyoxylate and become C3 metabolite, then the carbon fixation product is Acetyl-CoA (Figure 3-1-C). If there are one pathway or an enzyme that could fix two carbons with Acetyl-CoA and the other pathway that could recycle glyoxylate back into C3 metabolite, then C3 metabolite could be the output for this carbon fixation cycle (Figure 3-1-D). Likewise, if there are one pathway or an enzyme that could fix two carbons with glyoxylate and the other pathway that could recycle Acetyl-CoA back into C3 metabolite, then C3 metabolite could be the output for this carbon fixation cycle (Figure 3-1-E). Alternatively, if there are pathways that could fix one carbon with both of the Acetyl-CoA and glyoxylate simultaneously, then the carbon fixation product is C3 metabolite as well (Figure 3-1-F). (Bar-Even et al., 2010) showed that Acetyl-CoA carbon fixation cycle is thermodynamically advantageous to pyruvate, glyoxylate carbon fixation cycles under physiological conditions. However, appropriate amount of ATP hydrolysis still need to be compensated in order to drive those carbon fixation cycles *in vivo*.

3.1.3 Design of carbon fixation/incorporation into Acetyl-CoA pathway with rGS core module

The simplest step to complete the carbon fixation cycle would be using Pyruvate Ferredoxin oxidoreductase (PFOR). The enzyme could catalyze the reaction to convert Acetyl-CoA and CO_2 into pyruvate with the consumption of one reduced ferredoxin. However, most of the PFOR found in nature is oxygen sensitive and its mechanism of oxygen sensitivity is not clear (Ragsdale, 2003). PFOR would favor the function as a CoA dependent pyruvate decarboxylase (Furdui & Ragsdale, 2000) (Ma, Hutchins, Sung, & Adams, 1997) . The microorganisms with an functional PFOR and grow on rTCA cycles often were isolated from an extreme environment (High temperature, High salt condition, anaerobic condition) (Yamamoto, Ikeda, Arai, Ishii, & Igarashi, 2009) (Ikeda et al., 2010) (Tang & Blankenship, 2010). Attempts to overcome the oxygen sensitivity issue through mutagenesis approaches were not successful (Data not shown). Oxygen sensitivity seems to be one of major issues to limit the capacity of rGS modules in photosynthetic organisms.

Since metabolic pathways that resemble Figure 3-1-B, Figure 3-1-D, Figure 3-1-F require a functional pathway to convert Acetyl-CoA into pyruvate and no alternative oxygen tolerant pathways have been demonstrated by far, the focus of completing rGS module as a carbon fixation pathway has been shifted to designing metabolic routes to convert glyoxylate into C3 metabolite as in Figure 3-1-C. At first, we designed the pathway rGS-Malonyl-CoA pathway as a carbon fixation into Acetyl-CoA cycle (Figure 3-2-A). It is a combination of rGS core module and the right half of 3-Hydroxypropionate Pathway. 3-Hydroxypropionate bi-cycle is the only carbon fixation cycle that doesn't have the oxygen sensitive issues (Fuchs, 2011). However, when right half of 3-Hydroxypropionate Pathway enzymes (Mcl,Mch,Mct,Meh,Mcr,Pcs) were

overexpressed into cyanobacteria to improve the pyruvate production from glyoxylate, no clear phenotype was identified even with apparent enzyme activity. It was speculated that the thermophilic origin of those enzymes circumvents their performance in cyanobacteria. The effectiveness of Accase overexpression is also doubtful (Shih, Zarzycki, Niyogi, & Kerfeld, 2014). Subsequently, we designed the rGS-Serine pathway as carbon fixation into Acetyl-CoA cycle (Figure 3-2-B). It is the combination of rGS core module, formate assimilation pathway and glyoxylate to glycine conversion pathway. This is the pathway that doesn't have oxygen sensitivity issue. And since most of photosynthetic organisms are equipped with the glyoxylate to glycine conversion pathway, it could be easier for rGS-Serine pathway to be accommodated by native metabolic pathways.

Meanwhile, we found that even no additional carbon fixation step was added into the rGS core module, as long as glyoxylate could be converted into the rGS core module intermediate, the rGS core module contained pathway could function as a carbon incorporation pathway that would allow higher carbon intake by PEP carboxylase. Since the pathway from Malate to OAA has been demonstrated in *E.coli* (Mainguet et al., 2013), we first design rGS-citrate pathway(Figure 3-2-C). 2PG from Calvin cycle could enter the rGS-citrate cycle as the starting point. Two Acetyl-CoA could come out of the rGS-citrate cycle from one C3 starting metabolite. Instead of decarboxylation, rGS citrate pathway would fix one more carbon and double the Acetyl-CoA yield from C3. However, the rGS-citrate cycle was deemed unfavorable because of potential system instability issue caused by the branch point at the malate (Lee et al., 2014). In order to avoid the problematic branch point, we designed rGS-glycerate pathway (Figure 3-2-D). It is the combination of rGS core module and bacterial glyoxylate assimilation pathway. This pathway

could achieve similar biological function as rGS-citrate pathway in terms of doubling Acetyl-CoA yield.

In sum, the design of rGS-Glycerate pathway and rGS-Serine pathway were reduced to practice. The energy and reducing power usage were compared in (Table 3-1). Except for the rGS-Serine cycle, the NADPH usage for all the rest of synthetic carbon fixation was the same. All of the synthetic carbon fixation cycles were advantageous to Calvin cycle in term of energy consumption.

3.2 Materials and Methods

3.2.1 Strain culturing

For preculture, strains were grown in 20 mL of BG-11 (pH 7.5) with 50 mM $NaHCO_3$ and appropriate antibiotics at 30 °C with continuous shaking under 50 μmol/s/m^2 light condition until mid-log phase. The cultures were fed with 50 mM $NaHCO_3$ every day until OD_{730} reached 2 – 3.

For the main culture, the preculture was centrifuged at room temperature and the cells were resuspended in 5 mL of BG-11 (pH 7.5) medium with 50 mM $NaHCO_3$, appropriate antibiotics, 40 μM D-pantothenic acid (hemicalcium salt) and 0.2 mM Thiamine pyrophosphate at an OD_{730} equal to 0.5. The cultures were induced with 0.5 mM IPTG and grown with continuous shaking at 30 °C under 50 μE/(m^2.s) light intensity and low oxygen conditions. The cultures were fed everyday with BG-11 containing 500 mM bicarbonate, 40 μM D-pantothenic acid (hemicalcium salt), 0.2 mM Thiamine pyrophosphate and 0.5 mM IPTG. Samples for OD_{730} measurement and

supernatant analysis were taken every 2 days. Three different tubes were prepared for each strain as biological replicates.

3.2.2 Plasmids and strain construction

The strains used and constructed are listed in Table 3-3 based on homologous recombination using plasmids listed in Table 3-2. *S. elongatus PCC 7942* strains were transformed by incubating cells at mid-log phase (OD730 of 0.4 to 0.6) with 2 μg of plasmid DNA overnight in the dark. The culture was then spread on BG-11 plates supplemented with appropriate antibiotics for selection of successful recombination. For selection and culture maintenance, 20 μg/mL spectinomycin and/or10 μg/mL kanamycin and/or 10 μg/ml gentamicin were added into BG-11 agar plates and BG-11 medium where appropriate. Strain Segregation was confirmed by colony PCR. Cell growth was monitored by Beckman Coulter DU800 spectrophotometer at 730nm.

3.2.3 Enzyme assay measurement

Mtk-Mcl assay: MTK performs the ATP-dependent condensation of malate and CoA into malyl-CoA. MCL cleaves Malyl-CoA into Acetyl-CoA and glyoxylate, the latter reacting with phenylhydazine to form glyoxylate-phenylhydrazone that displays strong absorbance at 324 nm. Reactions were set up at 37 degree in a final volume of 200μL containing 50mMTris-Cl pH 7.5, 5mM $MgCl_2$, 2mM phenylhydrazine, 10mM malate, 2.5mM ATP, 2mM CoA, 15ug MtkAB and 5ug Mcl purified protein.

Gcl-GlxR assay: Gcl performs the reaction to condense two glyoxylate into one tartronic semialdehyde. GlxR converts tartronic semialdehyde to glycerate by NADH consumption which can be recorded at 340nM. Reactions were set up at 37 degree in a final volume of 200μL

containing 50mMTris-Cl pH 7.5, 5mM $MgCl_2$, 0.5mM TPP, 5mM glyxoylate, 0.25mM NADH, 5ug Gcl and 5ug GlxR purified protein.

GarK assay: Gark performs the ATP-dependent reaction to use glycerate as substrate to produce 2-phospho-glycerate and ADP. Pyk/Ldh enzyme mixture (purchased from Sigma) is used to measure ADP content in the reaction. Pyk uses ADP as a cofactor to convert PEP to pyruvate. Ldh enzyme reduces pyruvate to lactate by NADH consumption. NADH consumption can be recorded at 340nM. The whole reactions were set up at 37 degree in a final volume of 200μL containing 50mMTris-Cl pH 7.5, 5mM $MgCl_2$, 5mM glycerate, 2mM PEP, 2.5mM ATP, 0.25mM NADH, 10ug GarK purified protein and 1ul of Pyk/Ldh mixture.

GarK-Eno-Ppc-Mdh assay: Eno catalyzes the reaction of 2-phospho-glycerate, produced by GarK protein, to PEP. The latter reacts with bicarbonate to produce OAA by Ppc enzyme. Mdh performs the NADH-dependent reaction to reduce OAA to malate. The reactions were set up at 37 degree in a final volume of 200μL containing 50mMTris-Cl pH 7.5, 5mM $MgCl_2$, 2mM glycerate, 10mM $NaHCO_3$, 2.5mM ATP, 0.25mM NADH, 10ug Gark purified protein, 0.5ul of Ppc, 0.5ul of Eno and 0.5ul of Mdh. The reactions were measured by NADH consumption at 340nM.

3.2.4 Organic acids detection

Culture sample was centrifuged for 10min at 15,000 g. The supernatant was then directly analyzed by Agilent 1200 HPLC equipped with a BioRad HPX87 column. Ketoisocaproate concentration was monitored by photodiode array detector at 210 nm. The mobile phase used was 30mM H_2SO_4 at a constant flow rate of 0.6 mL/min. The column was maintained at 30 C.

3.2.5 GC/MS measurement methods

Place 50 μL of supernatant in a 2 mL microfuge tube. Add 1.8 mL of mixed solvent and mix. Incubate for 1 h at -30 C. Centrifuge. Transfer supernatant to a new tube (1 mL for LC and 300 μL for GC) For GC samples, add 150 μL of ultrapure H2O and mix. Centrifuge and transfer 300 μL to a new tube. Perform vacuum centrifugation. Perform freeze drying. Derivatization of GC samples: Add 50 μL of methoxyamine hydrochloride in pyridine (20 mg mL–1). Incubate at 30 °C, 1200 rpm for 90 min.Add 25 μL of N-methyl-N- (trimethylsilyl)trifluoroacetamide (MSTFA). Incubate at 37 °C, 1200 rpm for 30 min. Analyze within 24 h.

3.2.6 Metabolomics conditions

For sampling, culture broth equivalent to 5 mg dry cell weight was collected at day 0, day 4 and day 8 by fast filtration using a 0.2 μm Omnipore™ membrane filter (Millipore, MA, USA). The filter paper containing the cells was immediately immersed in liquid nitrogen for quenching and stored at -80°C until extraction.

For extraction, 3 mL of extraction solvent (Methanol/ Water/ Chloroform at 5:2:2 (v/v/v ratio) with 9 μg/L of (+)-10 camphorsulfonic acid as internal standard)) was added to the sample before mixing with a vortex and sonicator. The sample was then subjected to 3 cycles of freezing (-80°C for 1 h) and thawing (-30°C for 30 m). After mixing and centrifugation, 1 mL of the supernatant was collected to a new tube and added with 200 μL of ultrapure water. After mixing and centrifugation, 350 μL of the polar phase was filtered to a new tube using a 0.2 μm Millipore Millex-LG PTFE filter. Afterwards, centrifugal concentration (VC-36S, TAITEC, Japan) and lyophilization was performed. After dissolving in 50 μL of ultra-pure water, the sample was

centrifuged at 4°C, 16000 × g for 3 min and 40 µL of the supernatant was transferred to a LC glass vial for analysis.

Ion-pair LC/MS/MS analysis

A Nexera UHPLC system (Shimadzu, Kyoto, JAPAN) coupled with LCMS 8030 Plus (Shimadzu) was used for ion-pair LC/MS/MS analysis. The column used was a CERI (Chemicals Evaluation and Research Institute, Tokyo, JAPAN) L-column 2 ODS (150 mm × 2.1 mm, particle size 3 µm). The mobile phase A used was 10 mM tributylamine and 15 mM acetic acid in water, while mobile phase B was methanol. The flow rate was 0.2 mL/min and column oven temperature was 40°C. The concentration of mobile phase B was increased from 0% to 15%, 50%, and 100% from 1.0 to 1.5 min, 3.0 to 8.0 min, and 8.0 to 10.0 min, respectively, held until 11.5 min, decreased to 0% from 11.5 min, and held at 0% until 20 min. The analysis mode was negative ion mode. The injection volume was 3 µL, probe position was +1.5 mm, desolvation line temperature was 250°C, heat block temperature was 400°C, nebulizer gas flow was 2 L/min and drying gas flow was 15 L/min. The optimized multiple reaction monitoring (MRM) parameters for each metabolite are listed in Supplementary Table S1.

The acquired raw data was converted to an analysis base file format by using a freely available file format converter (Reifycs Inc., Tokyo, JAPAN). After file conversion, MRMPROBS (Tsugawa et al., 2013) was used for automatic peak picking and calculation of the peak area. The detected peaks were also confirmed manually.

Multivariate analysis

Principal component analysis (PCA) was performed using SIMCA-P+ version 13 (Umetrics, Umeå, Sweden). The metabolome data was normalized by an internal standard, mean centered and scaled to unit variance. A t-test was performed using MS Excel to determine statistically significant differences.

3.3 Results and discussion

3.3.1 Production of ketoisocaproate through rGS-Glycerate Pathway after iterative Engineering of *Synechococcus PCC 7942*

In order to build the rGS-citrate pathway in cyanobacteria, seven of the essential genes need to be introduced into the chromosomes. The complete incorporation rGS key genes would be able to double Acetyl-CoA yield while the partial rGS strain (*ppc,mdh,mtk.mcl*) would only be able to produce half of Acetyl-CoA amount in the full strain (Figure 3-3).

Since the enzyme activity of Malatethiokinase (MTK), Malyl-CoA lyase and glyoxylate carboligase are not native to cyanobacteria, we performed bioprospection to find a relative more active enzyme to ensure the function of those steps. MTK from *Methylococcus capsulatus* has been shown to be the most active enzyme from more than 20 candidates (Mainguet et al., 2013). We further found out that MCL from *Methylobacterium extorquens* could further increase the combinational activity of MTK/MCL for 3 folds (Figure 3-4-A). To screen a functional glyoxylate carboligase (GCL), we compared glyoxylate consumption rate in *E.coli* packed cell cultures with overexpression of GCL from different origins. Cell culture with initial OD=0.1 were induced with 0.5mM IPTG overnight. Then the cells were packed to OD=5 and were added with 10mM glyoxylate at the time 0. Glyoxylate carboligase from *Ralstonia* was found to

consume glyoxylate fastest (Figure 3-4-B). Based on their relative locations on the pathways, the seven genes were divided into two groups. *Ppc, mdh, mtk* and *mcl* were incorporated into Neutral Site I while *gcl, glxR,* and *glxK* were incorporated into Neutral Site II. We transformed those two set of genes separately at first and assayed the enzyme activity after transformation. Although Glycerate Kinase activity by *glxK* in *E.coli* has been shown to be essential enzyme for glyoxylate assimilation, we found that its activity in cyanobacteria was extremely low (Figure 3-4-C). We utilized *garK* from *E.coli* to replace *glxK* (Figure 3-4-D), which showed much higher activity. This results was consistent with the recent findings of physiological role of two Glycerate Kinases in *E.coli* (Zelcbuch et al., 2015). Finally, PPC *(E.coli),* MDH(*E.coli*), MTK(M.c) , Mcl(M.e) , Gcl(R.e), glxR(E.coli) and gark(*E.coli*) were overexpressed to construct the full strains.

Once the existence of all the genes were confirmed by colony PCR, we were looking for the potential phenotype that could be caused by enhanced intracellular acetyl-CoA synthesis. We hypothesized that excess Acetyl-CoA could be converted into Acetate through native Acetyl-CoA synthase. However, no acetate increase was detected in the rGS full strains as well as the control strains. Instead, we discovered two unknown peaks that came from the extracellular cell culture on HPLC with retention time at 17 mins and 20 mins respectively (Figure 3-5). The first unknown peak was relative unstable it showed up first and degraded quickly while the second peak accumulated by days. The retention time of those two peaks didn't match any of the rGS-Glycerate pathway intermediates as well as the any of TCA cycle intermediate. We checked the all the possible organic acids synthesis that Acetyl-CoA could possibly participate through online databases. We found out that Acetyl-CoA was also actively involved in the synthesis of ketoacids. Several ketoacids standards were tested on HPLC and we were surprised to find out

that retention time of the second unknown peak matched the retention time of ketoisocaproate (KIC). The existence of KIC was further confirmed by GC/MS (Figure 3-6). When the metabolic pathway for KIC synthesis was exanimated, we found that Acetyl-CoA was the precursor for KIC production. Meanwhile, another substrate, Ketoisovalerate (KIV) was also required for KIC synthesis. KIV is the precursor for isobutanol production in *Synechococcus elongatus PCC 7942*. It has been demonstrated that isobutanol production derived from KIV could achieve up to 450mg/L in cyanobacteria (Atsumi, Higashide, & Liao, 2009). It is an indication that the metabolite pool of KIV is relative abundant. Therefore, with higher supply of Acetyl-CoA, the carbon flux could be channeled into KIC (Figure 3-7).

Subsequently, the KIC productions from all strains were tested (Figure 3-8). Detectable amount of KIC was produced by both of the rGS-partial strains with *ppc,mdh,mtk/mcl* and rGS full strain after day 8. And it gradually accumulated to 0.06mM for the rGS-Full strain while rGS-partial strains with *ppc,mdh,mtk/mcl* could produce about 0.03mM KIC. This measured KIC production ratio between partial and full strains matched the theoretical ratio of acetyl-CoA yield between without and with glyoxylate recycling pathway. However, the introduction of the rGS-Glycerate pathway didn't bring any growth benefits to the strain. We hypothesized that TCA cycle of cyanobacteria would consume significant amount of newly synthesized acetyl-CoA. Then we created a relative low oxygen growth environment for cyanobacteria by flushing the headspace of cyanobacteria culture with non-oxygen gas (nitrogen, hydrogen, CO_2 mixture gas) daily. We found that cyanobacteria strains could maintain a relative high cell density under this condition and produced almost twice amount of the KIC that can be produced under the regular culture condition. The KIC production ratio between full strains and partial strain with *ppc,mdh,mtk/mcl* was still almost 2 to 1.

3.3.2 Inverse relationship between GCL activity and MTK/MCL activity as result of natural evolution to avoid intermediate toxicity

During the KIC production optimization, we found that there was significant discrepancy in KIC titer between different colonies as well as between different batches of the same colony (Figure 3-9-E). Enzyme assay of rGS-Glycerate pathway key enzymes, phosphoenolpyruvate carboxylase (PPC), malatethiokinase(MTK), malyl-CoA lyase(MCL), glyoxylate carboligase (GCL), 2-hydroxy-3-oxopropionate reductase(GLXR) and glycerate kinase(GLYCTK) were performed to check whether the instability of production was caused by the instability of enzyme activities. 13 colonies containing the full rGS-Glycerate pathway but were preserved in different ways were selected for the enzyme assay test. Figure 3-9-A showed that among the 13 colonies, the enzyme activity level of PPC, GLXR and GLYCTK were quite stable among colonies while there were significant fluctuations of MTK/MCL and GCL activities among different colonies. For example, the highest enzyme activity of MTK/MCL in plate-R6 is nearly 200 fold of that in plate-R7. At first we assumed that biosynthesis of glyoxylate could be source of toxicity. However, after analyzing MTKMCL activity in the partial strain that only contains *ppc,mdh,mtkmcl,* we found that the activity in up to 8 colonies were almost of the same level as the highest MTK/MCL activities measured in the rGS-Glycerate full strain (Figure 3-9-B) . In addition, we also found out that GCL activity in the partial strain with only *gcl,glxR,gark* overexpression was also quite stable and similar to the highest activity measured in the full stains (Figure 3-9-C). It seems that the enzyme activity fluctuations only existed in the full stain.

Since PPC and MTK/MCL were inserted in the neutral site I (NSI) and GCL, GLXR, GLYCTK were inserted into the neutral site II (NSII), to rule out the influence of recombination behaviors over enzymes activities among different individual colonie, MTK/MCL and GCL activity were

normalized by another enzyme activity of the same incorporation site within the same colony. (Figure 3-9-D) shows that cells tent to circumvent the cellular activity of either MTK/MCL or GCL.

Those evidences led to the hypothesis that that cyanobacteria cells tried to limit the biosynthesis of the rGS-Glycrate pathway intermediate, tartronic semialdehyde. Cells almost deactivated GCL in the colonies that had very high MTK/MCL activity. If MTK/MCL activity was very low, then GCL activity was not altered. The selective preservation of either MTK/MCL or GCL activity as result of the cyanobacteria cellular natural evolution could be the explanation of the instability of KIC production. A much more active GLXR or tartronic semialdehyde consumption pathway seems to be required in order to resolve the toxicity issue. The colonies with relative higher *gcl/gark* ratio tend to produce more than the ones with higher MTK/MCL activity. It indicated the importance of the glyoxyate recycling in term of improve Acetyl-CoA amount.

We also found out the Plate-restreaked R5 hosted relative balanced pathway enzyme activities. While the MTK/MCL reduced to 8% activity of the frozen stock, it still preserved nearly highest GCL activity. The one with the most balanced enzyme activity didn't seem to be the one that produced most KIC, however, its productivity was most stable (Figure 3-9-E). Plate-restreaked R5 was selected for further analysis and characterization for rGS-Glycerate full strain.

3.3.3 *LeuA* overexpression led to higher KIC production in cyanobacteria

2-isopropylmalate synthase (*LeuA*) is the enzyme to directly incorporate Acetyl-CoA for KIC synthesis (Figure 3-10-A). *LeuA* from *E.coli* was further overexpressed in the WT strain and Plate-restreaked R5 cyanobacteria colony that has balanced rGS-glycerate pathway enzyme activities. KIC production test (Figure 3-10-B) showed that the titer could reach as high as 3mM

after 8 days. With *LeuA* overexpression, KIC amount in the rGS-full strains was almost four fold of that in WT strains.

3.3.4 Metabolomics profile of rGS-glycerate pathways in *Synechococcus elongatus PCC7942*

(Metabolomics data were produced by Fukasaki Lab, Osaka University, Japan)

WT strain, Partial rGS (*ppc,mdh,mtkmcl*) and Full rGS strain (colony Plate-restreaked R5) were further characterized by metabolomics study. Cell cultures of three strains were sampled at day 0, day 4 and day 8. Their intracellular metabolites were extracted and analyzed through metabolomics equipment.

Figure 3-11-A showed that a transient Acetyl-CoA accumulation was found at Day 4 for the full strains. At the same time, the intracellular PEP amount drop significantly at Day 4 for both of the partial and full rGS strain and PEP amount was not able to resume to the WT level in the further measurement on Day 8. It indicated the function of PEP carboxylase in the rGS partial and full strains. Some of the TCA cycle intermediates were compared between those three strains (Figure 3-11-B). We found that there was a transient increase of isocitrate for both of the Partial rGS and Full rGS strain on Day 4. Potentially, the synthesized Acetyl-CoA and enhanced PEP carboxylase provide more substrate for citrate synthase, which led to the accumulation of isocitrate. However, 2-OG amount was not affected by the increase of isocitrate on Day 4. Figure3-11-C showed that most of the Calvin cycle intermediate remained unchanged except for SBP. SBP started to accumulate significantly ever since Day 4 in the rGS full strains. It indicated that the normal function of Calvin cycle was perturbed due to the introduction of a competing

pathway that draw away the Calvin cycle intermediate, 3PG. This could partially explain the growth retardation caused by the overexpression of the full rGS pathway genes (Figure 3-11-E). Fatty acids contents in all the strains were also analyzed. Figure 3-11-D showed that one of most abundant fatty acids (18:1) amount increased to 2.5 folds of WT FA (18:1) level on day 8. In addition, FA(18:2), FA(20:1), FA(20:2), FA (16:0) and FA(14:1) were all found increase to different levels in the rGS full strains.

3.3.5 Photosynthetic production of ketoisocaproic acid (KIC) in S*ynechococcus elongates PCC 7942* through rGS-Serine pathway

The carbon fixation into Acetyl-CoA cycle, rGS-Serine cycle was also constructed in *Synechococcus elongatus PCC7942* (Figure 3-12). Glyoxylate was converted into glycine through alanine-glyoxylate aminotransferase (AGXT). Glycine will react with 5,10-methylene-tetrahydrofolate that is original from formate to produce one Serine by Glycine hydroxymethyltransferase (SHMT). Serine then would be dehydrated to 2-aminoprop-2-enoate through L-serine dehydratase. 2-aminoprop-2-enoate spontaneously becomes pyruvate. Once pyruvate is re-introduced into the rGS cycle, it would be catalyzed into phosphoenolpyruvate(PEP) and initiate another round of carbon fixation.

Besides *ppc, mdh, mtk/mcl*, genes required to convert glyoxylate into pyruvate (*agx1, sda*), genes responsible for formate assimilation into 5,10-methylene-THF (*FolD,* FTHFS) and Formate dehydrogenase (*Fdh*) were also introduced in the cyanobacteria genomes. Glycine hydroxymethyltransferase (SHMT) was supplied by native *glyA* gene. All the strains were cultured under with and without formate addition conditions. Figure 3-13-A showed that the strains with "Glyoxylate-Glycine" conversion pathway and/or formate assimilation pathway

were sensitive to formate. While the addition of formate didn't cause any effect on control strains, it slowed down the growth of all the strains that contained formate consumption genes. From production profile (Figure 3-13-B), we were surprised to find out that KIC was also produced in all the rGS strain with the glyoxylate to glycine conversion pathway. However, the addition of formate didn't help to improve the KIC titer. In addition, the overexpression of formate assimilation system (*FolD,* FTHFS) in cyanobacteria didn't seem to help for KIC production as well. Furthermore, we found that KIC titer was also higher under the low oxygen condition (Figure 3-13-D). The strains with *agx1* and *sda* were able to produce up to 0.3 mM KIC. This titer was roughly of same level as the rGS-glycerate pathway.

Formate and formate assimilation were found not responsible for KIC production in the rGS-Serine full strain. One possible explanation is that the 5,10-methylene-THF is from the native glycine-cleavage system in cyanobacteria (Figure 3-14) other than formate. KIC production in rGS-Serine strains was a good indication that both of the C1 fixation steps (PEP carboxylase and SHMT) are working in cyanobacteria. However, if the 5,10-methylene-THF was generated from glycine cleavage system, then the general function of the rGS-Serine pathway would be same to rGS-glycerate pathway, which could only double the Acetyl-CoA yield. It partially explained why the highest titer of KIC by rGS-Serine strains was almost identical to rGS-glycerate strain.

For future research, in order to fully demonstrate the formate and bicarbonate fixation pathway through rGS-Serine pathway, it is necessary to knock out the native glycine cleavage system.

3.4 Figures

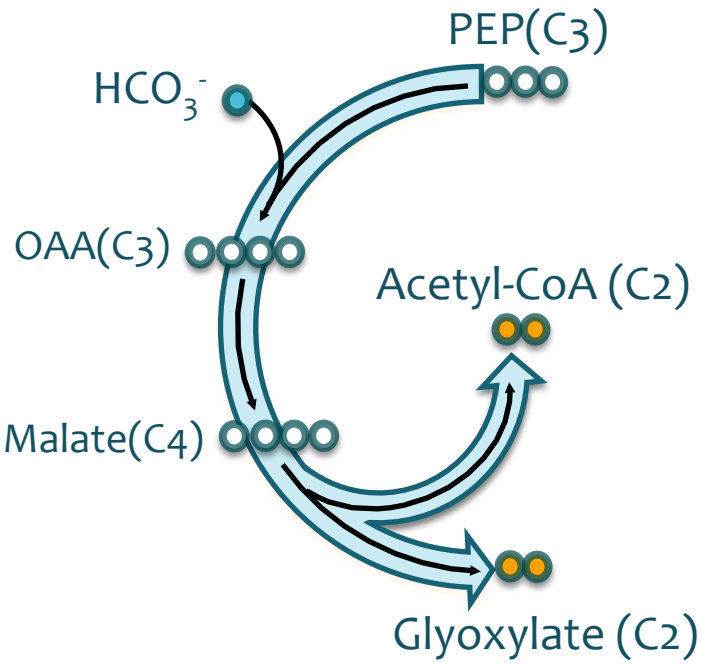

Figure 3- 1-A Core module of Reverse Glyoxylate Shunt(rGS)

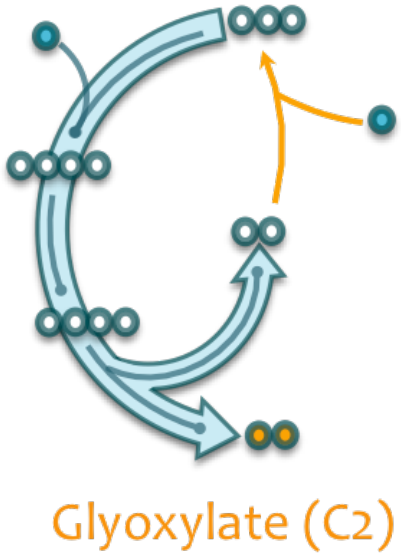

Figure 3- 1-B Glyoxylate as carbon fixation product of rGS module

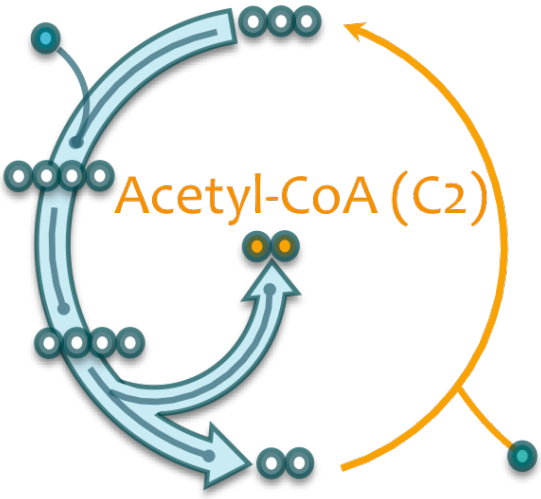

Figure 3- 1-C Acetyl-CoA as carbon fixation product of rGS module

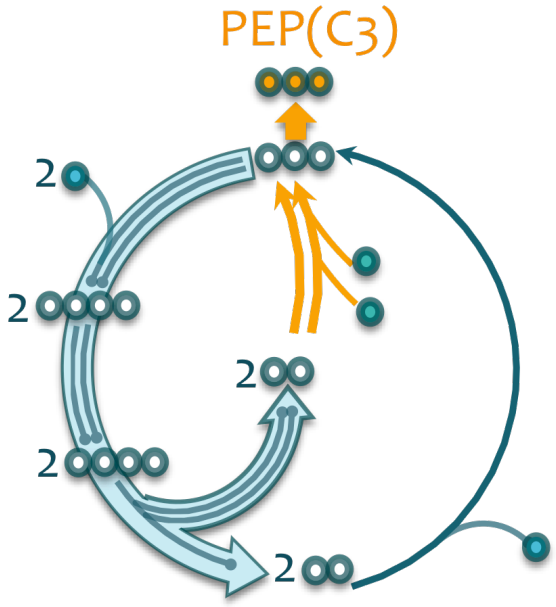

Figure 3- 1-D C3 metabolite as carbon fixation product of rGS module-I

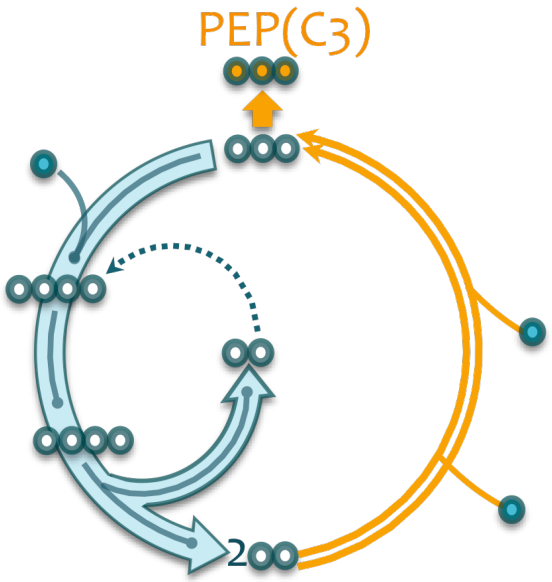

Figure 3- 1-E C3 metabolite as carbon fixation product of rGS module-II

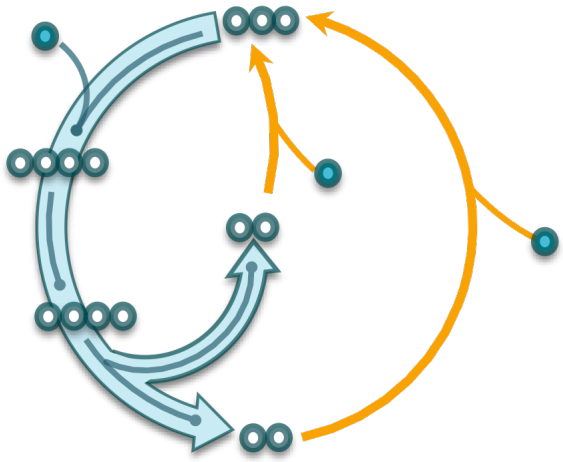

Figure 3- 1-F C3 metabolite as carbon fixation product of rGS module-III

Figure 3- 1 Schematic presentation of metabolic pathway design with rGS core module

Figure 3-1-A: The core module of a reverse glyoxylate shunt pathway contains PEP carboxylase, malate dehydrogenase, Malatethiokinase, Malyl-CoA lyase.

Figure 3-1-B: A pathway or an enzyme that could fix one more carbon with Acetyl-CoA and become C3 metabolite. The carbon fixation product is glyoxylate.

Figure 3-1-C: A pathway or an enzyme that could fix one more carbon with glyoxylate and become C3 metabolite, The carbon fixation product is Acetyl-CoA.

Figure 3-1-D: A pathway or an enzyme that could fix two more carbon with Acetyl-CoA. The other pathway could recycle glyoxylate back into C3 metabolite. C3 metabolite could be the output for this carbon fixation cycle

Figure 3-1-E: A pathway or an enzyme that could fix two more carbon with glyoxylate. The other pathway could recycle Acetyl-CoA back into C3 metabolite. C3 metabolite could be the output for this carbon fixation cycle

Figure 3-1-F: Both of the Acetyl-CoA and glyoxylate could fix one more carbon. The carbon fixation product is C3 metabolite.

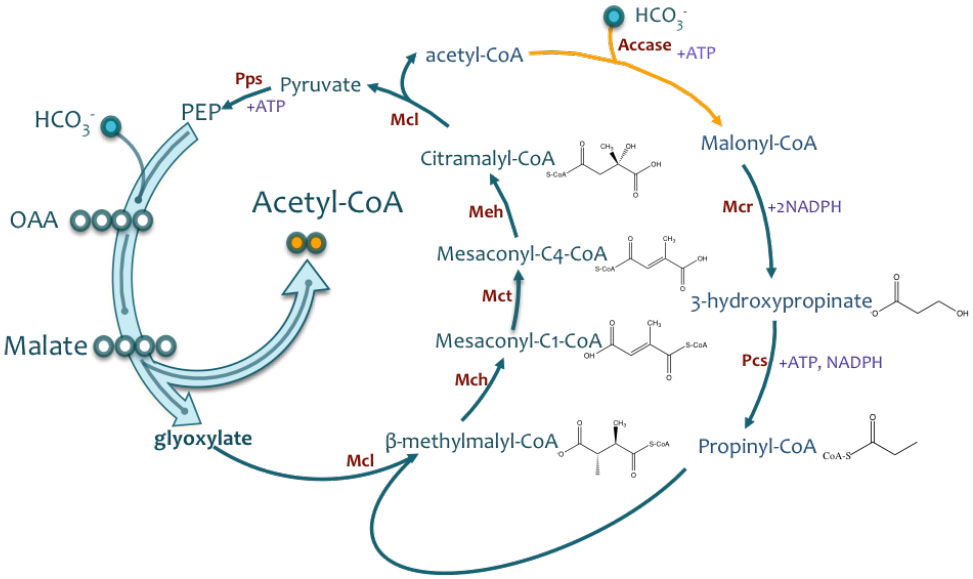

Figure 3-2-A Carbon fixation cycle rGS-Malonyl-CoA pathway

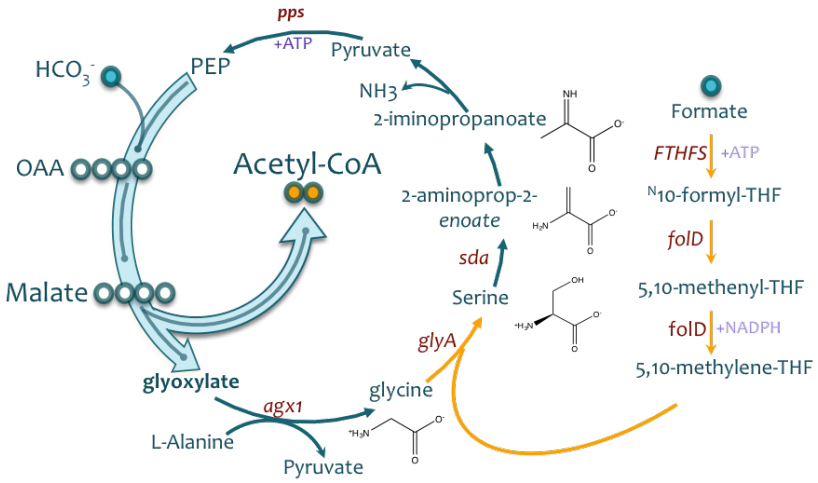

Figure 3-2-B Carbon fixation cycle rGS-Serine pathway

.

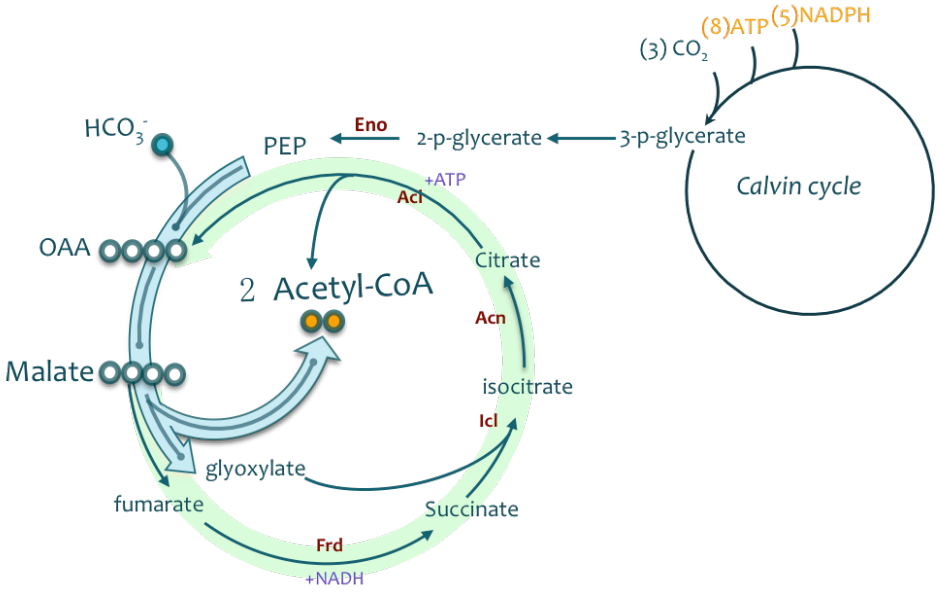

Figure 3-2-C Carbon incorporation cycle rGS-citrate pathway

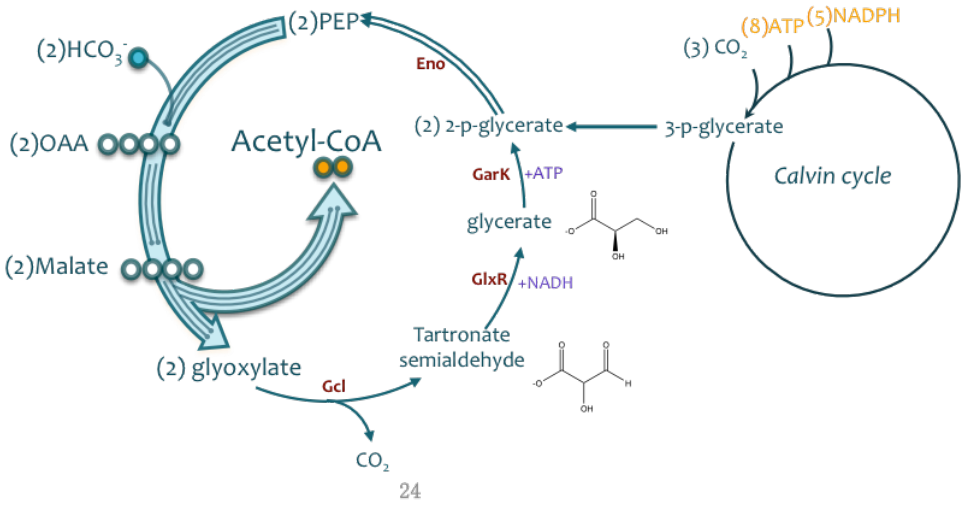

Figure 3-2-D Carbon incorporation cycle rGS-glycerate pathway

Figure 3- 2 Design of rGS core module contained Carbon fixation/incorporation pathway

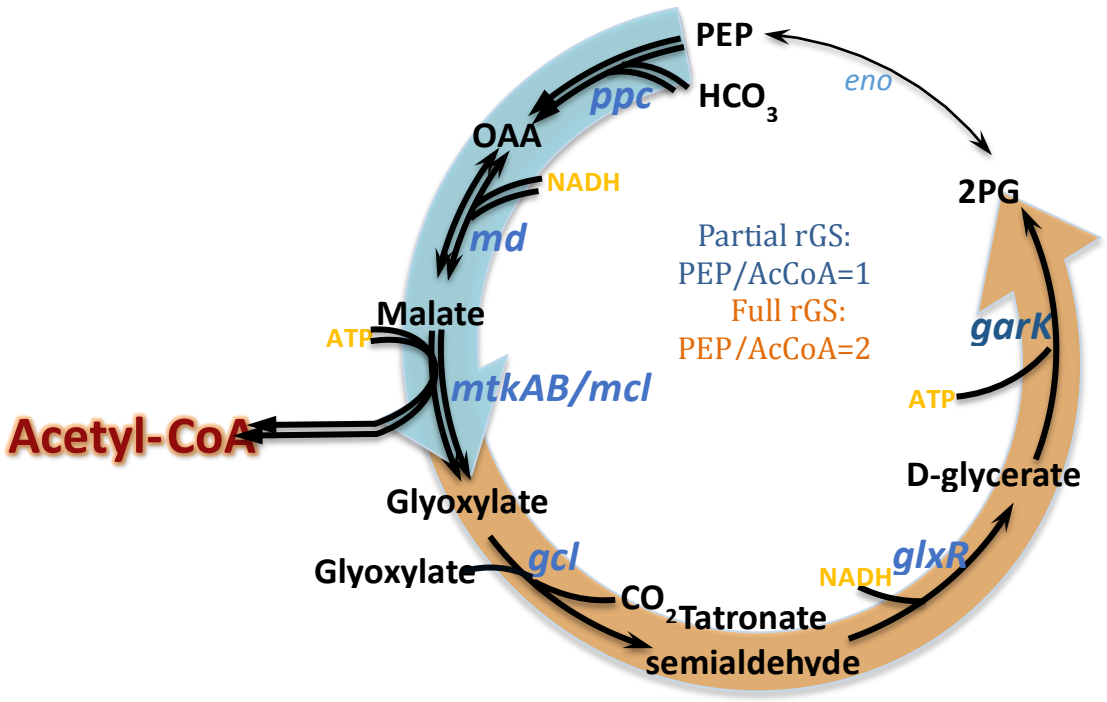

Figure 3- 3 Carbon fixation into acetyl-CoA cycle rGS-Glycerate

rGS-citrate is able to double the acetyl-CoA from PEP through glyoxylate recycling. Without Glyoxylate recycling, the PEP/AcCoA is 1 . With the full pathway, the PEP/AcCoA ratio reaches to 2.

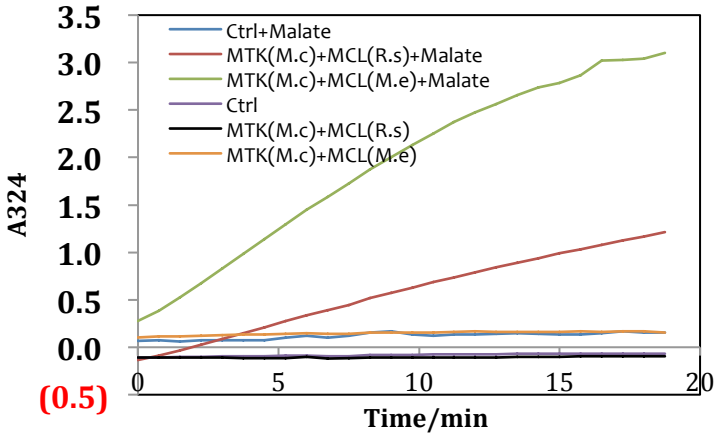

Figure 3-4-A Inceased MTK/MCL activity with MCL(M.e)

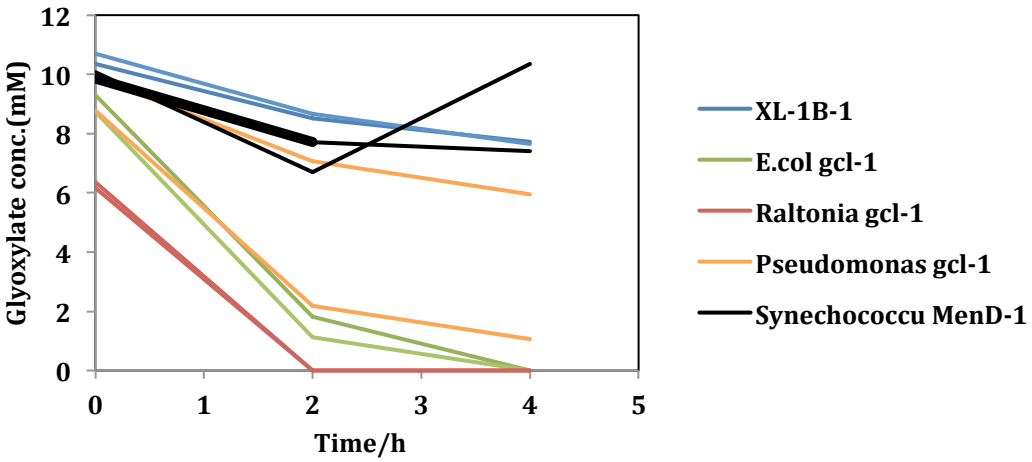

Figure 3-4-B Gcl bioprospection through glyoxylate consumption rate comparison

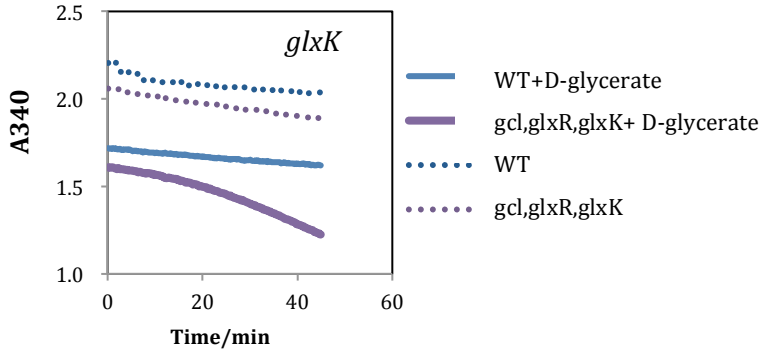

Figure 3-4-C Low Glycerate kinase activity by *glxK*

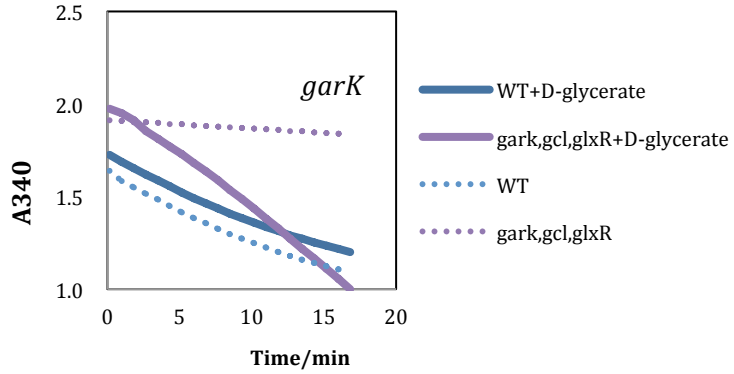

Figure 3-4-D Glycerate kinase activity by *garK*

Figure 3- 4 Enzyme Activity improvement for rGS-Glycerate Pathway

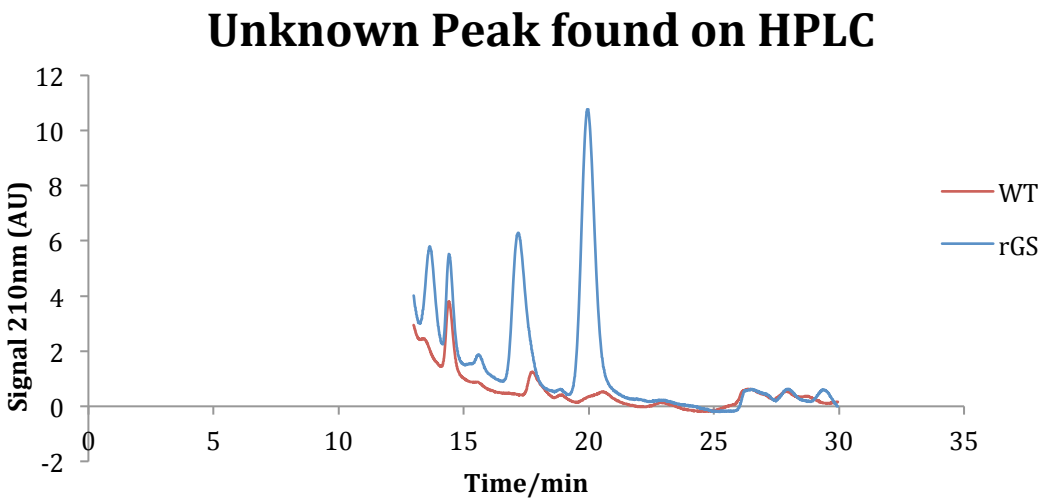

Figure 3- 5 Unknown peak from rGS-citrate full pathway strain

Two unknown peak with retention time at 17min and 19.8min were identified in the cyanobacteria culture with the full rGS-glycerate pathway on HPLC. The x-axis is the retention time; The Y-axis depicted the relative signal strength.

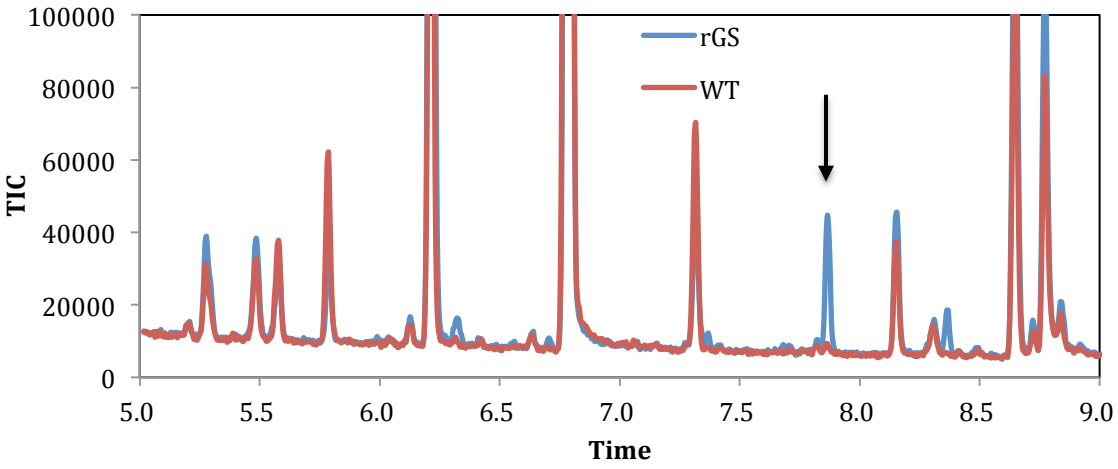

(A) GC chromatography comparison between rGS and WT strains

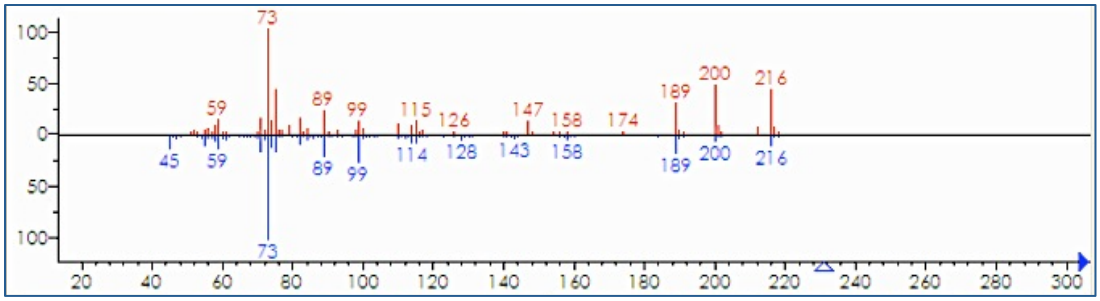

(B) MS Spectrum of the unknown peak from GC chromatography

Name: M000000_A132008-101-3_METB_0.00_FALSE_VAR5_ALK_Cap
Formula: $C_{10}H_{21}NO_3Si$
MW: 231 CAS#: N/A NIST#: N/A ID#: 1 DB: kic3
Other DBs: None
Comment: Boelling C., Liebig F., Erban A., Kopka J., Max Planck Institute
10 largest peaks:
73 999 | 99 254 | 89 187 | 189 159 | 75 155 |
71 152 | 59 128 | 45 118 | 74 110 | 216 86 |

(C) MS spectrum of ketoisocaproate

Figure 3- 6 GC-MS confirmation of ketoisocaproate

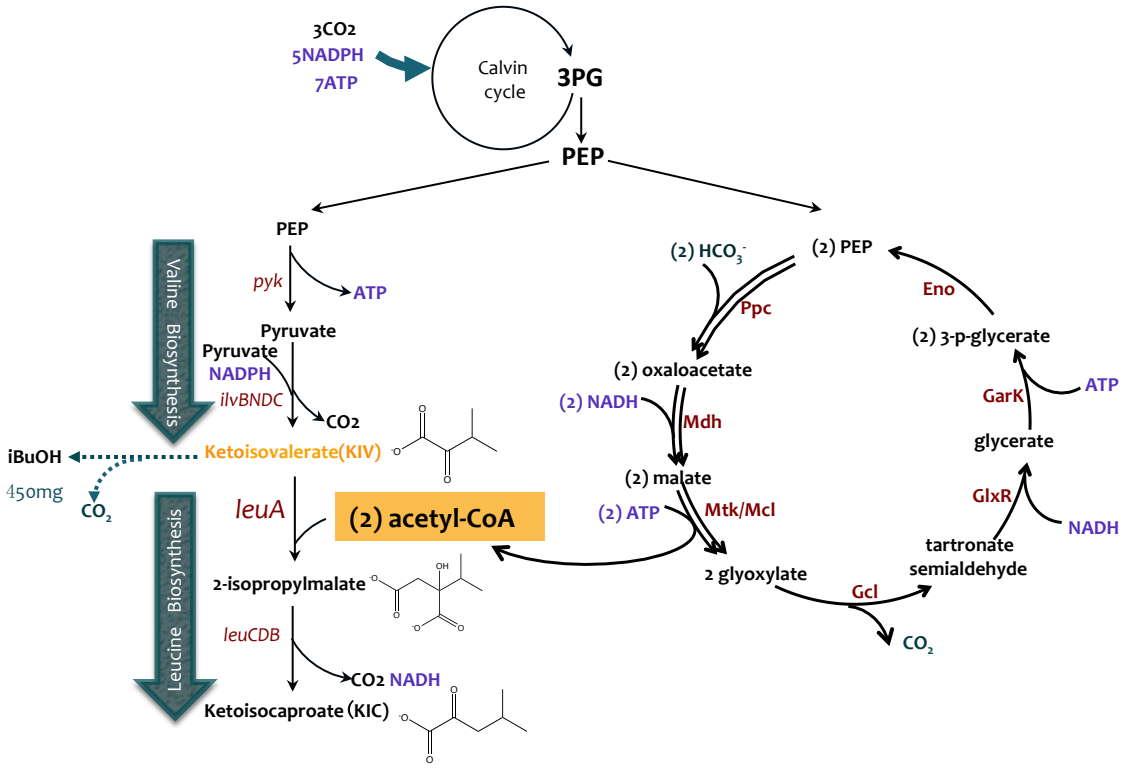

Figure 3- 7 Schematic presentation of KIC production from rGS-glycerate pathway

Acetyl-CoA was the precursor for KIC production. Ketoisovalerate (KIV) was also required for KIC synthesis. KIV is the precursor for isobutanol production in *Synechcoccus elongatus PCC 7942*. It has been demonstrated the isobutanol production derived from KIV could achieve up to 450mg/L in cyanobacteria (Atsumi et al., 2009). It is an indication that the metabolite pool of KIV is relative abundant. With higher supply of Acetyl-CoA, the carbon flux could be channeled into KIC.

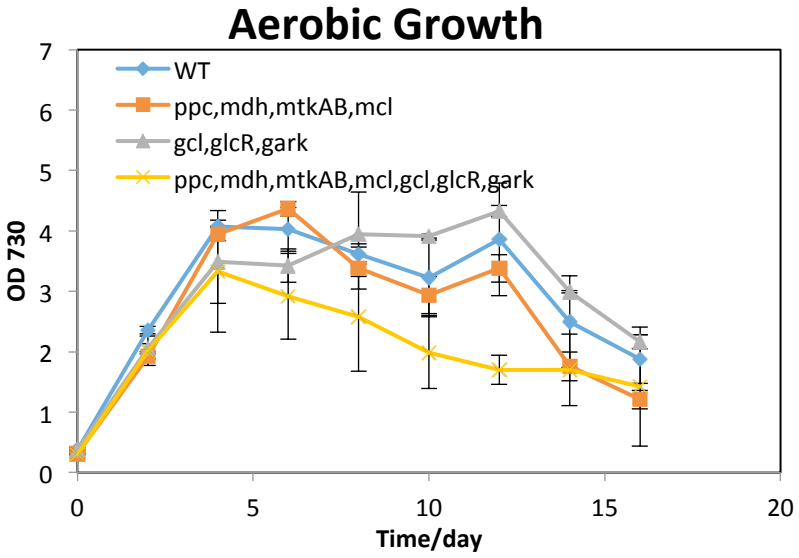

Figure 3-8-A Production of KIC under aerobic conditions

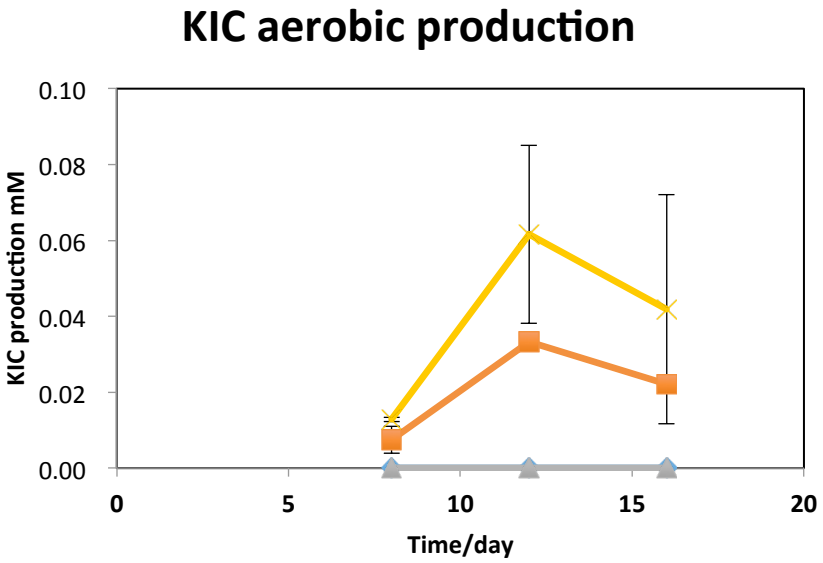

Figure 3-8-B Production of KIC under aerobic conditions.

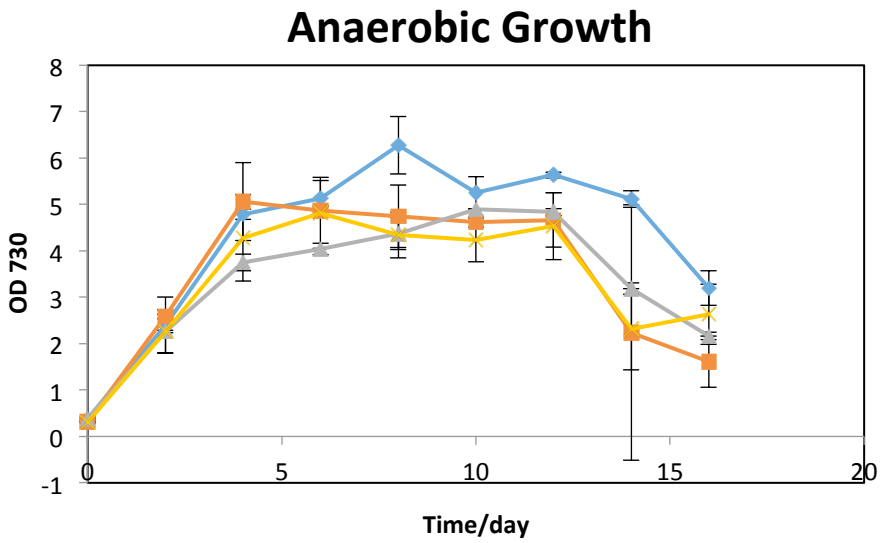

Figure 3-8-C Growth curve of rGS-glycerate strains under low oxygen condition

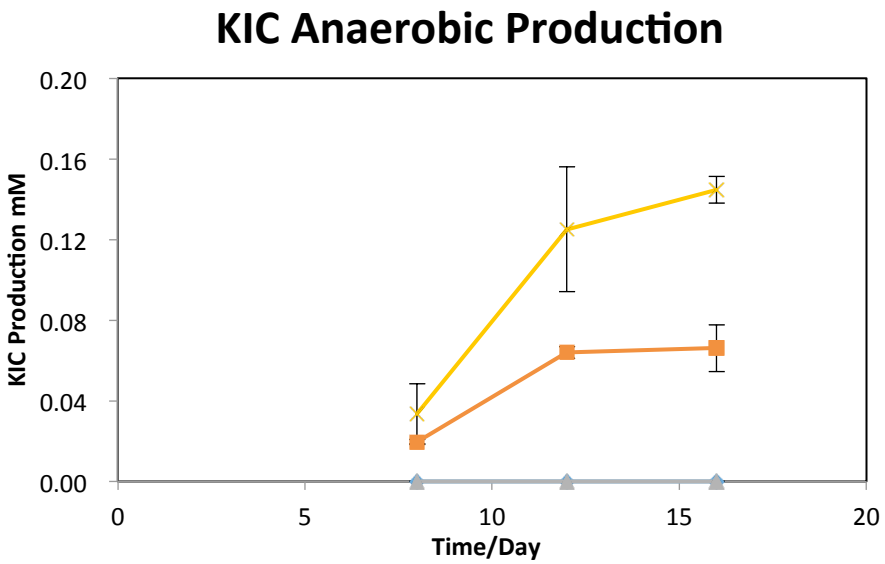

Figure 3-8-D Growth curve of rGS-glycerate strains under low oxygen conditions

Figure 3- 8 KIC production from rGS-glycerate pathway

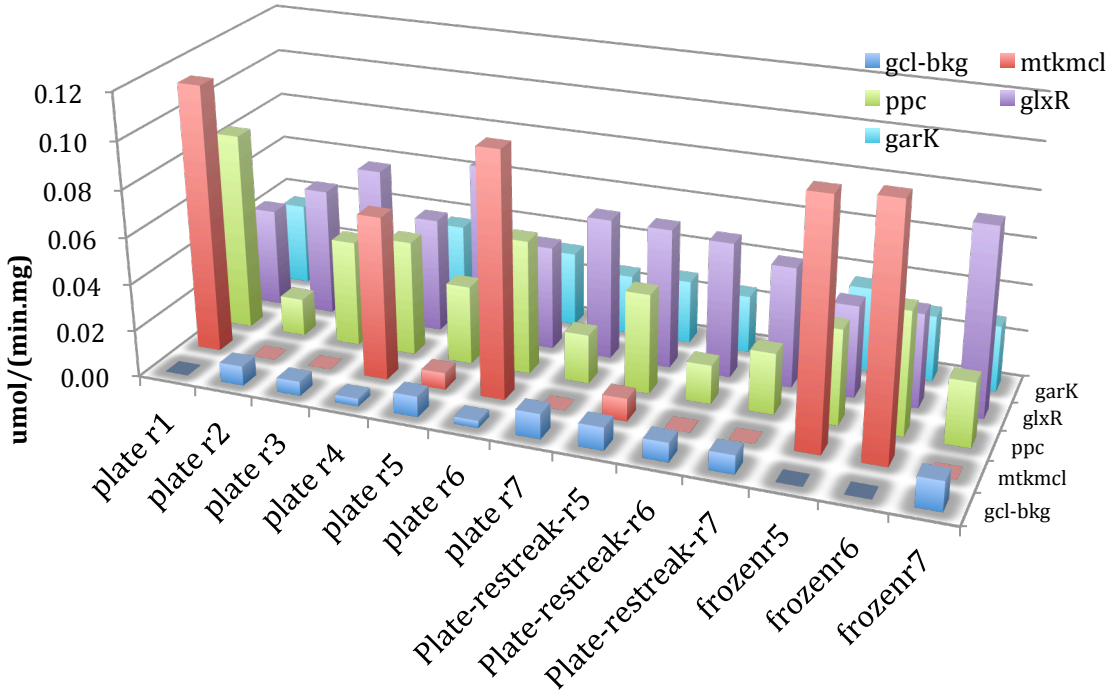

Figure 3-9-A Enzyme activities evolution of rGS- glycerate pathway

Seven colonies with the full pathway genes (R1 to R7) that were regularly maintained on the BG-11 plates were selected for the assay. 3 colonies (frozen5, frozen6, frozen7) revived from frozen stock as well as PR5, PR6,P R7 restreaked from a different parent single colony on the regularly maintained plated 3 generations ago were selected as the control group.

Figure 3-9-A showed that among the six colonies that were selected from the plates, the enzyme activity level of PPC and GLYCTK are quite even while there are a variety of distribution of MTK/MCL and GCL activities.

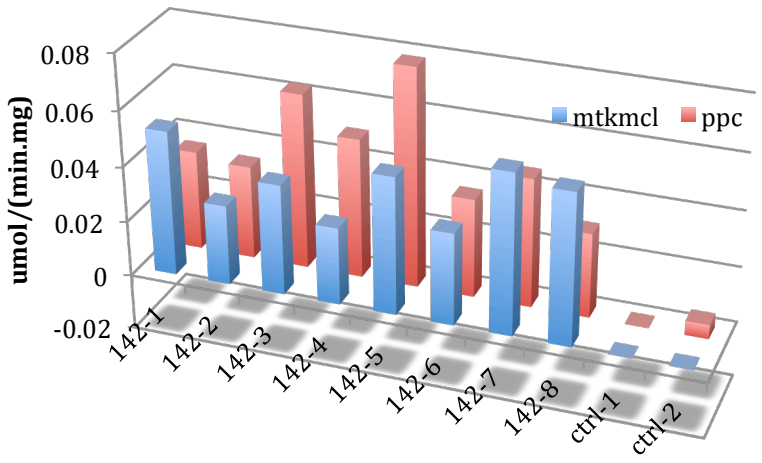

Figure 3-9-B MTKMCL activity in the partial rGS strains with *ppc,mdh,mtk/mcl*.

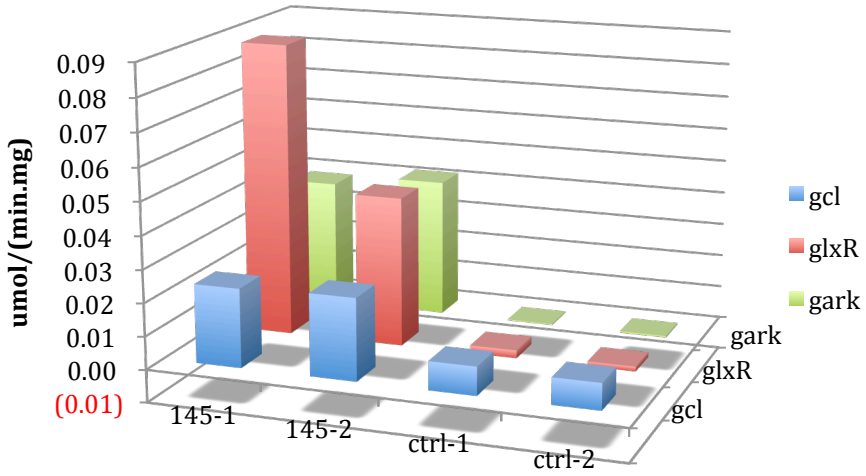

Figure 3-9-C GCL activity in the partial rGS strains with *gcl glxR,garK*.

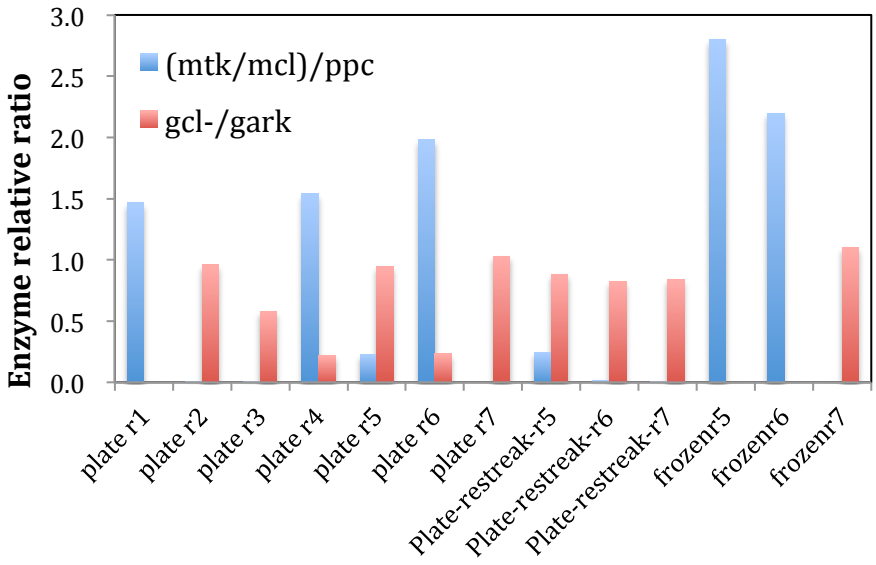

Figure 3-9-D *(mtk.mcl)/ppc* and *gcl/gark* ratio distribution in all rGS-full strain colonies

The activities of were first normalized by the average activity of the partial strain and then the activity ratio of (mtk.mcl)/ppc and gcl/gark were compared.

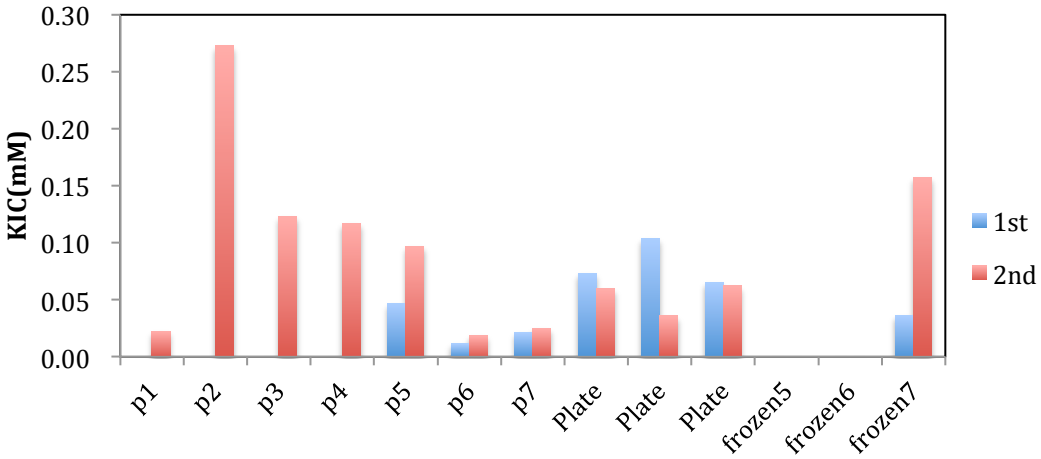

Figure 3-9-E Instability of KIC in the rGS full strains

Figure 3- 9 Enzyme activity evolution due to intermediate toxicity

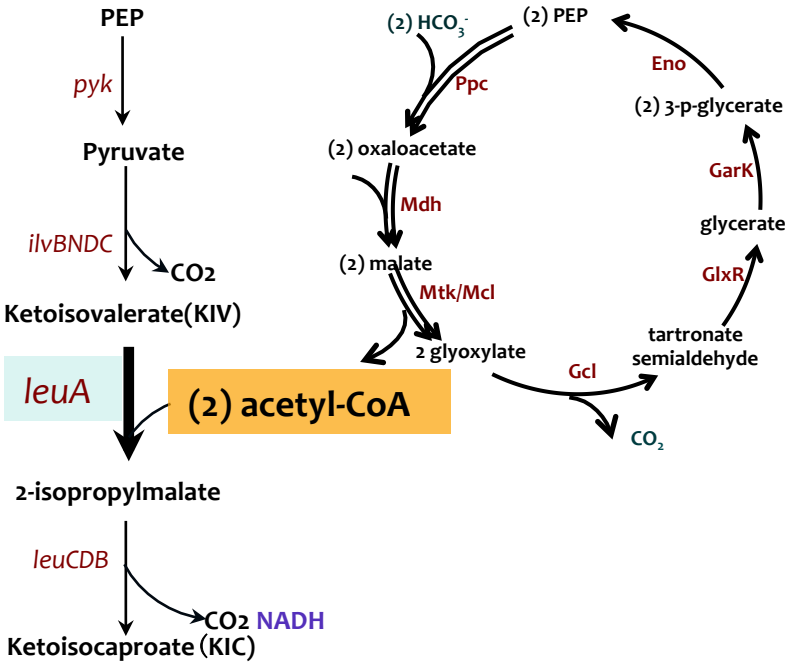

Figure 3-10-A Design of KIC optimization with *leuA* overexpression

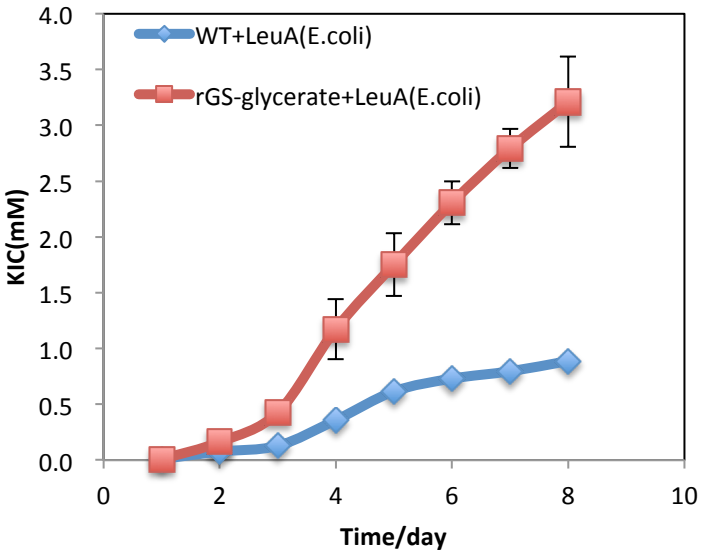

Figure 3-10-B KIC production optimization with *leuA* overexpression

Figure 3- 10 KIC production with *leuA* overexpression

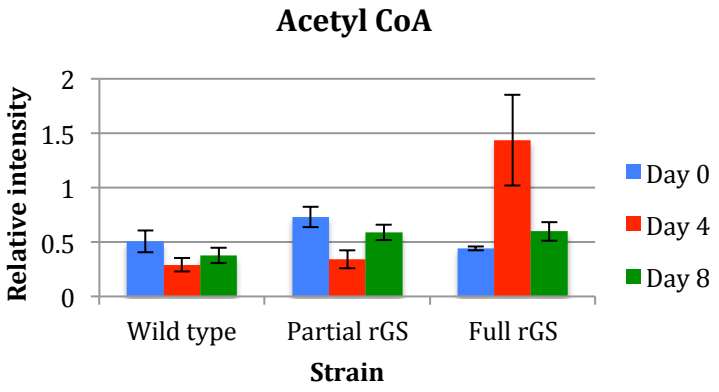

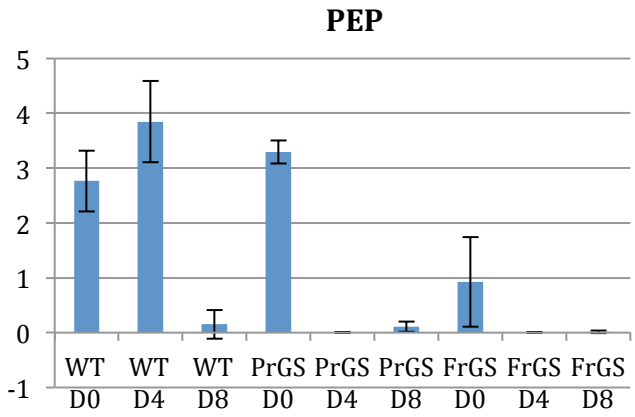

Figure 3-11-A Acetyl-CoA and PEP changes in the rGS-glycerate strains.

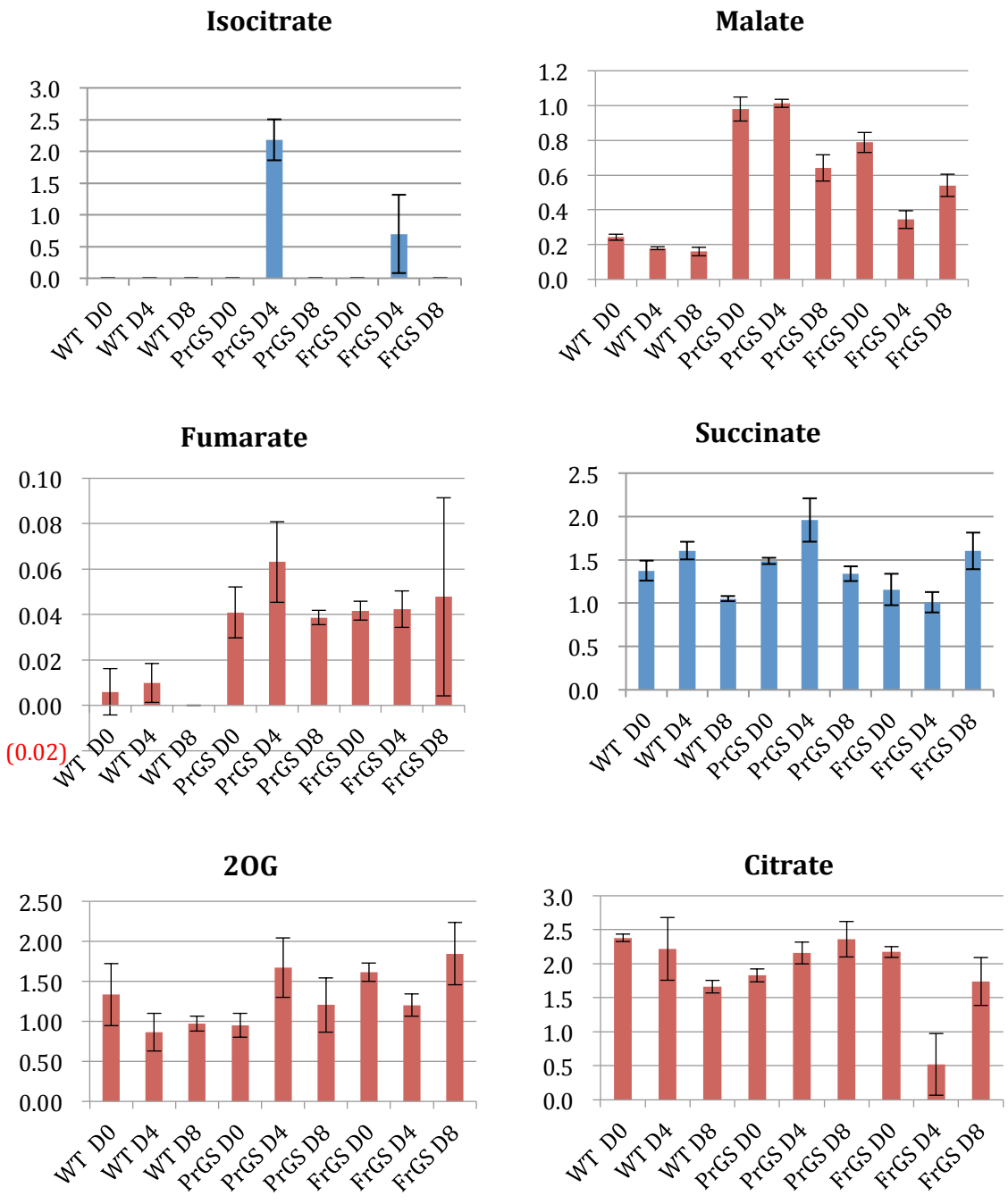

Figure 3-11-B TCA cycle intermediates changes in the rGS glycerate strains

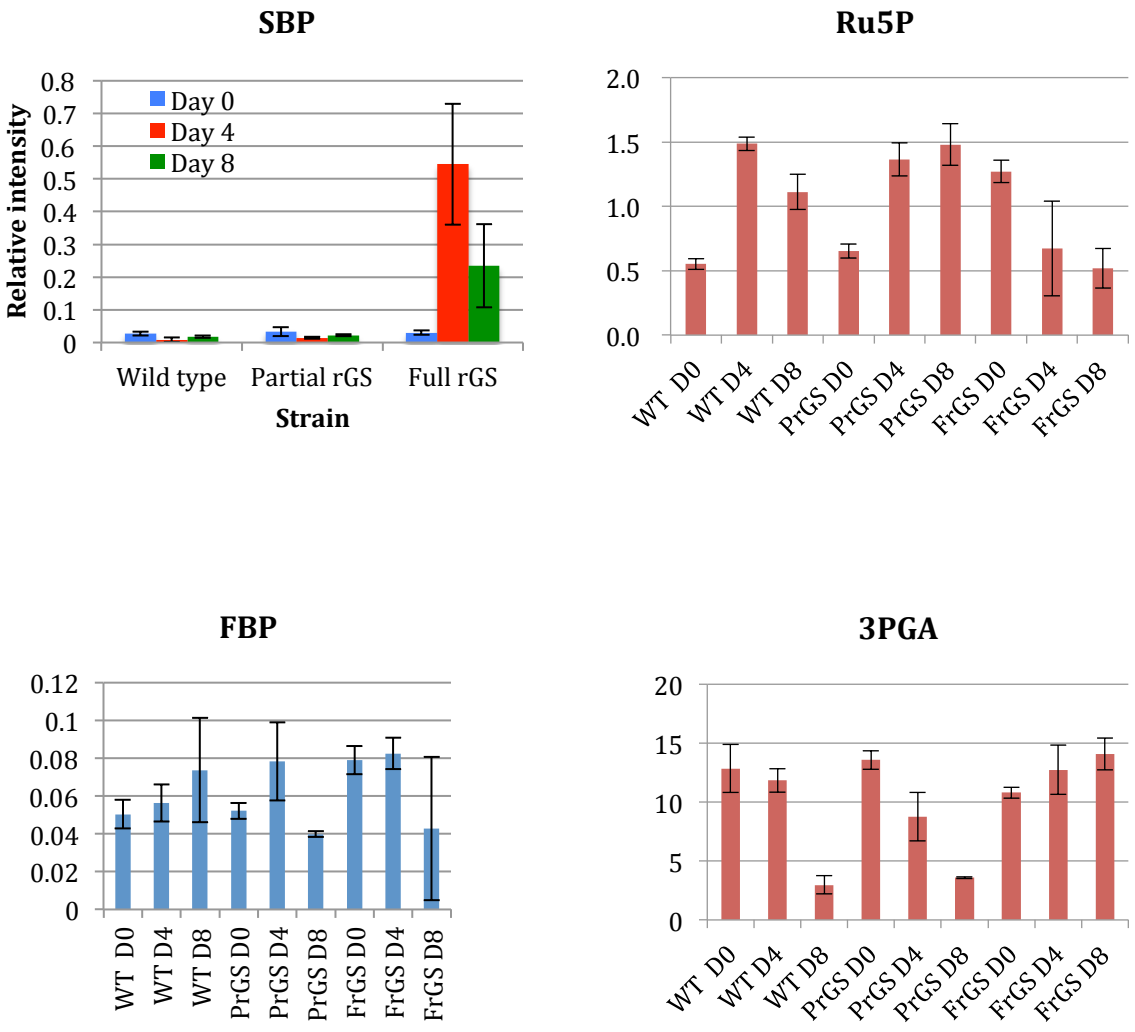

Figure 3-11-C Calvin cycle intermediates changes in the rGS glycerate strains

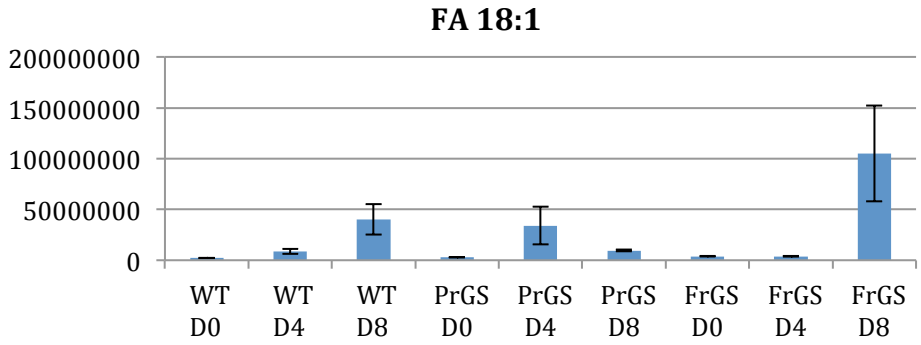
FA 18:1
200000000
150000000
100000000
50000000
0
WT D0
WT D4
WT D8
PrGS D0
PrGS D4
PrGS D8
FrGS D0
FrGS D4
FrGS D8

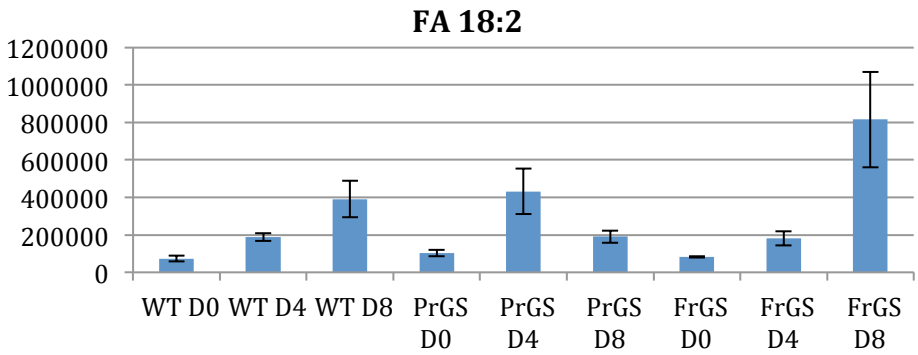
FA 18:2
1200000
1000000
800000
600000
400000
200000
0
WT D0
WT D4
WT D8
PrGS D0
PrGS D4
PrGS D8
FrGS D0
FrGS D4
FrGS D8

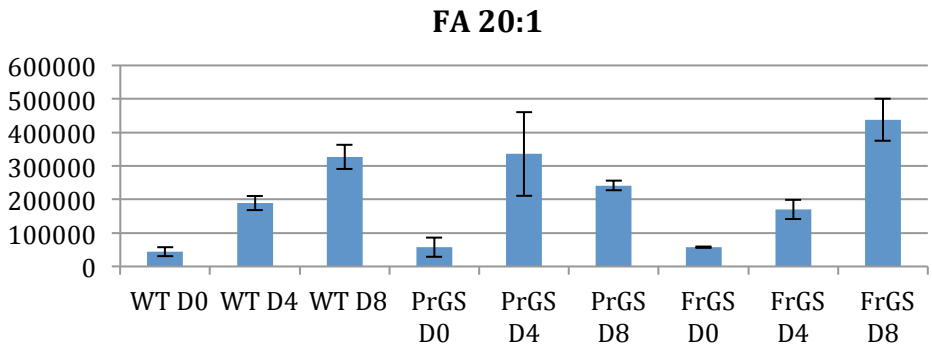
FA 20:1
600000
500000
400000
300000
200000
100000
0
WT D0
WT D4
WT D8
PrGS D0
PrGS D4
PrGS D8
FrGS D0
FrGS D4
FrGS D8

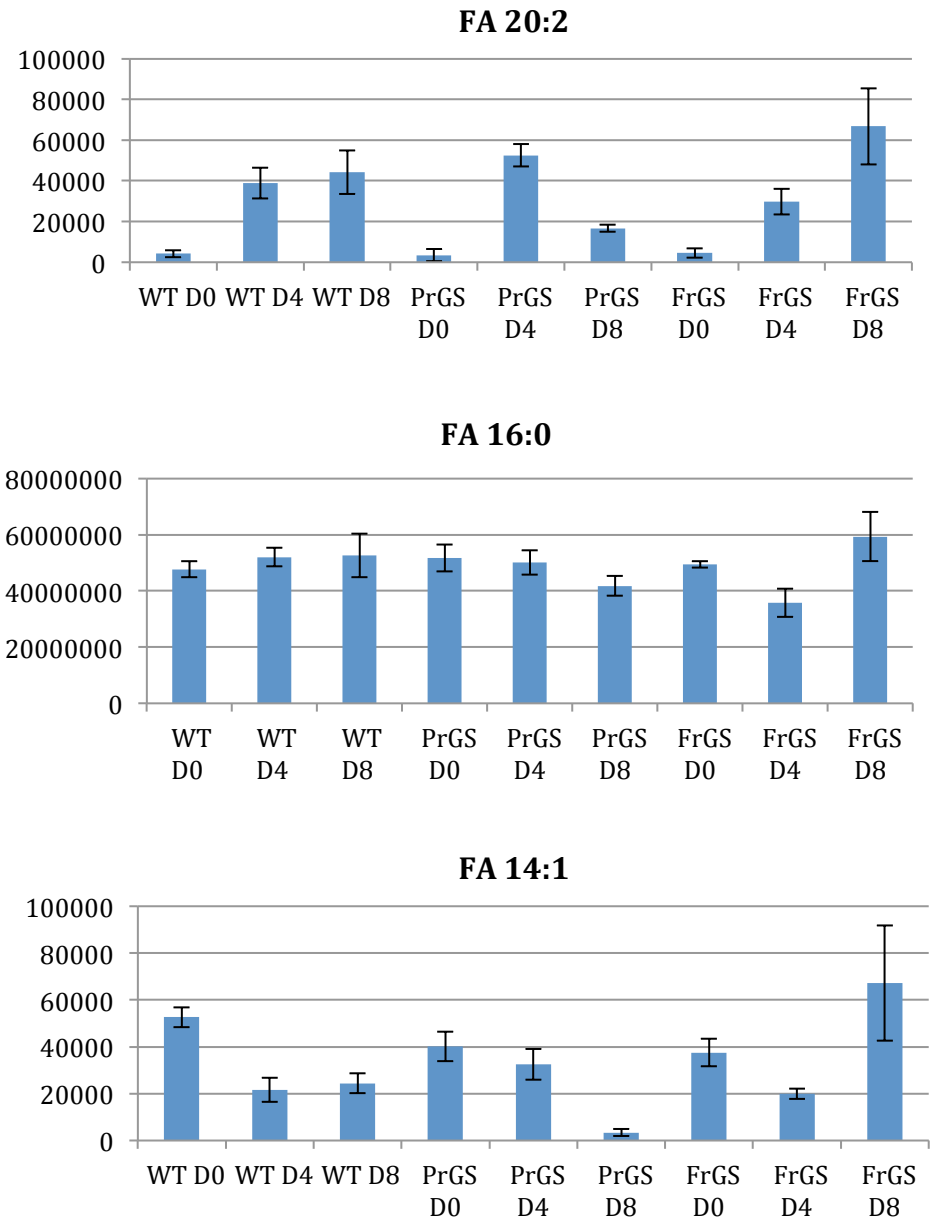

Figure 3-11-D key fatty acids accumulation changes in the rGS glycerate strains

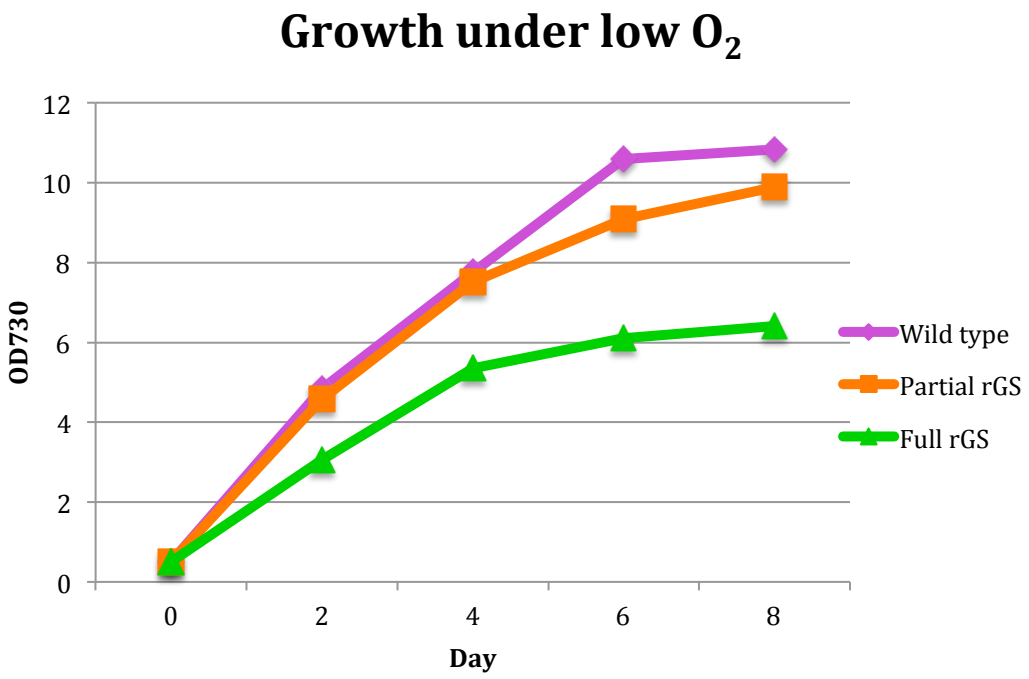

Figure 3-11-E Growth Curve of Strains Used in Metabolomics Study

Figure 3- 11 Metabolomics Study of rGS-glycerate pathway in cyanobacteria

WT strain, rGS partial strains (ppc,mdh,mtk/mcl) and rGS full strains (ppc,mdh,mtk/mcl,gcl,glxR,garK) intracellular metabolite were sampled and measured on Day 0, Day 4 and Day 8

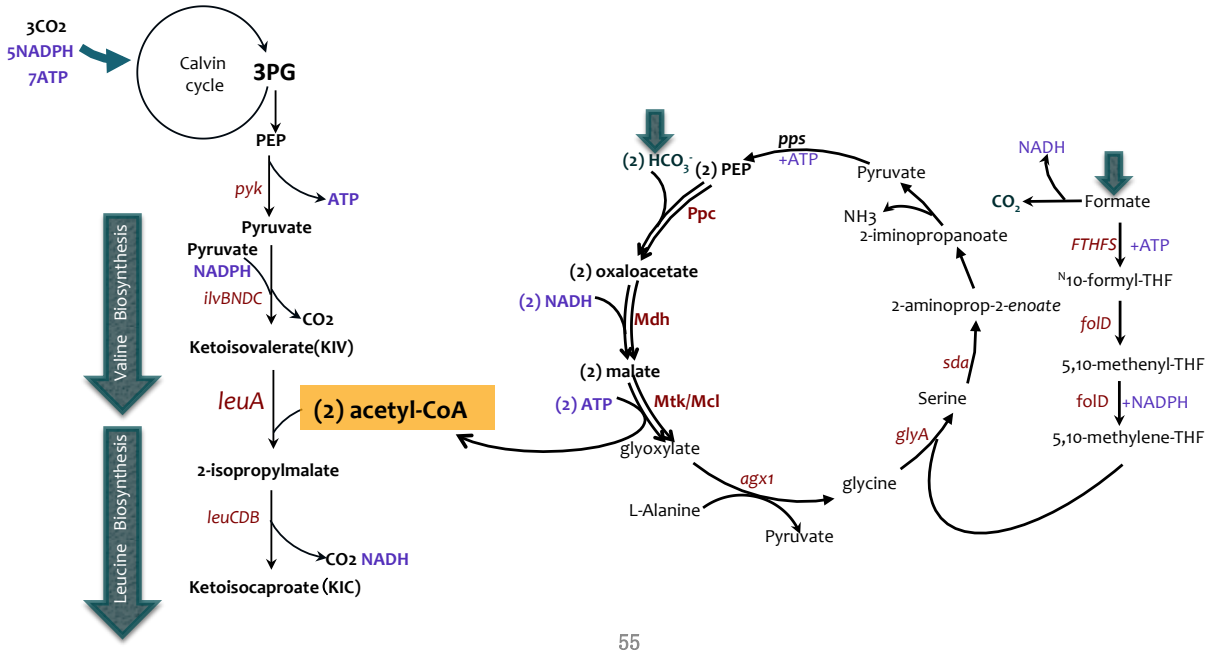

55

Figure 3- 12 Metabolic pathway design of KIC production with rGS-Serine pathway

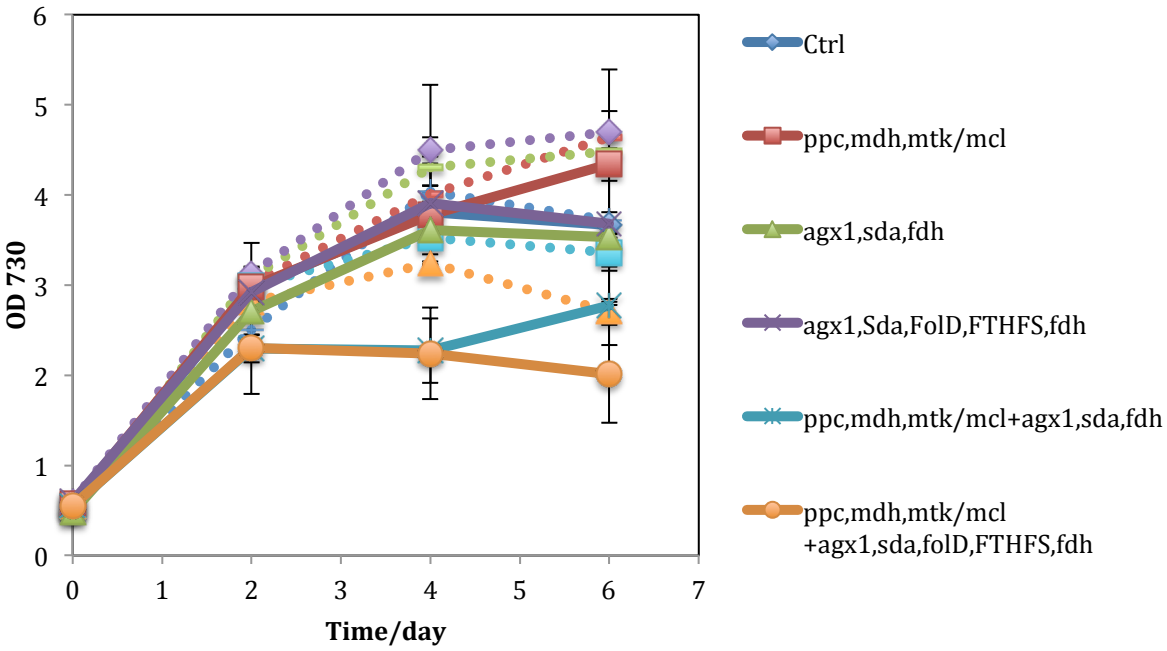

Figure 3-13-A Growth curves of rGS-Glycine/Serine pathway under aerobic condition

Solid lines indicate cultures with formate. Dotted lines indicate cultures without formate

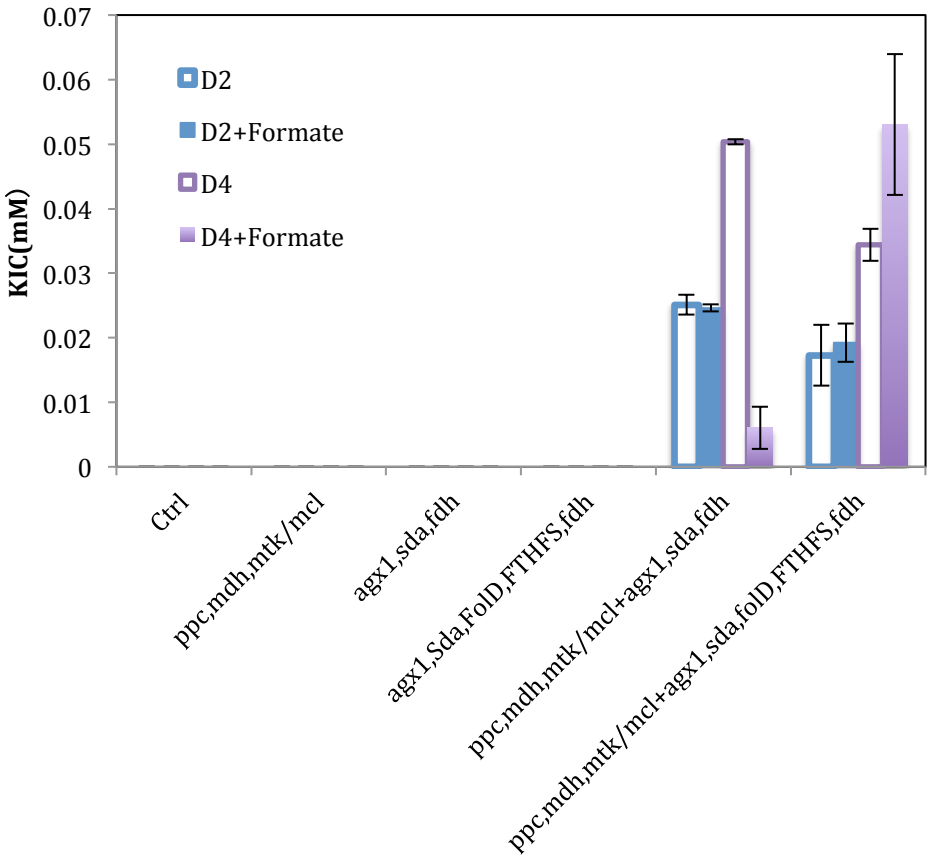

Figure 3-13-B KIC production of rGS-Serine pathway under aerobic condition

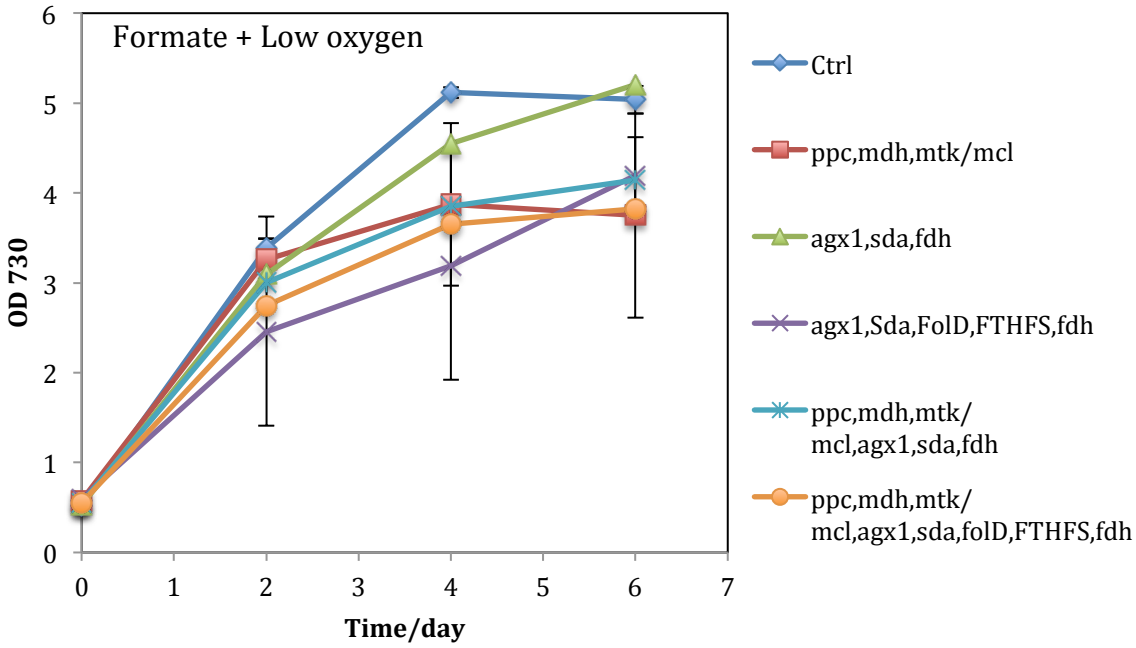

Figure 3-13-C Growth curves of rGS-Serine pathway under low oxygen condition

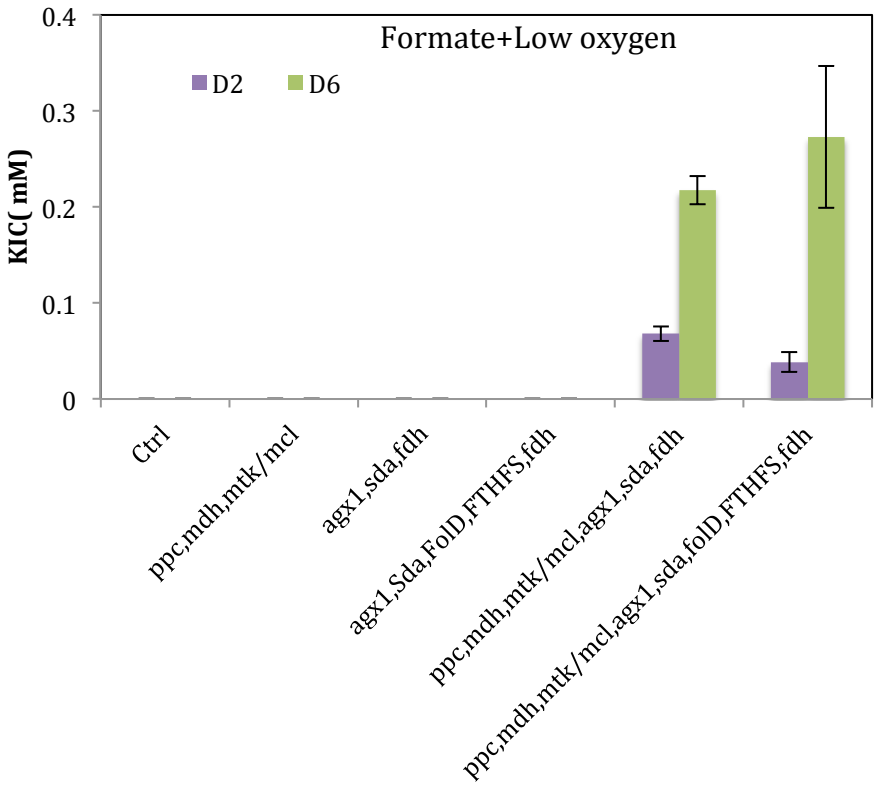

Figure 3-13-D KIC Production of rGS-Serine pathway under low oxygen condition

Figure 3- 13 Growth Curve and KIC production of rGS-Serine pathway

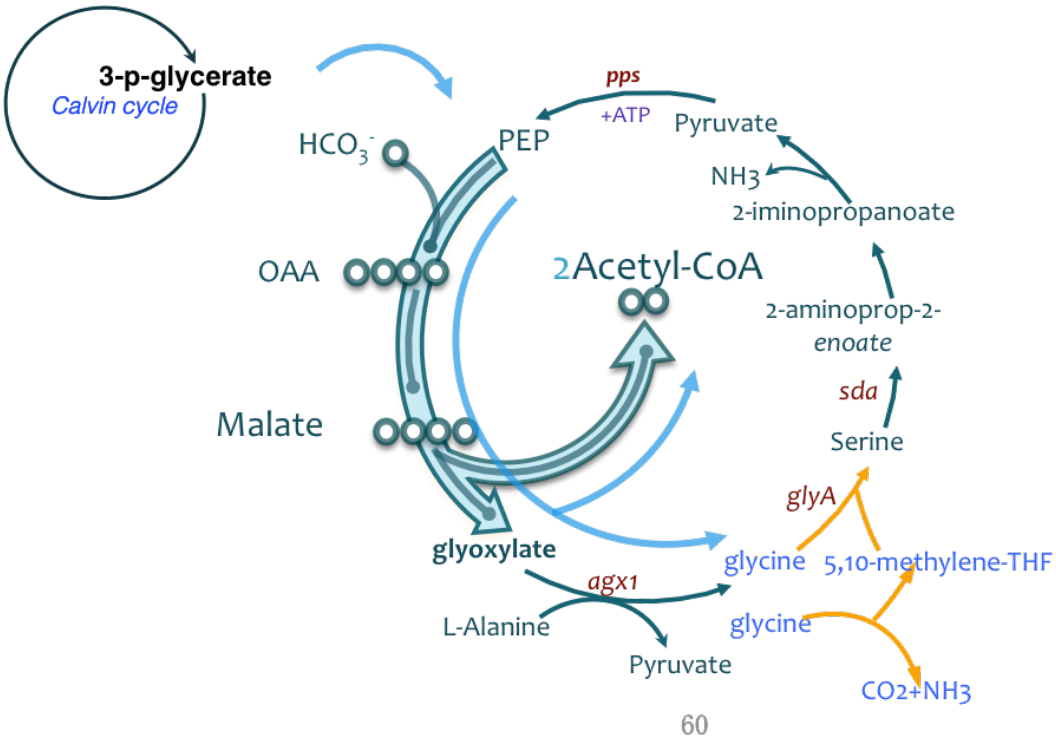

Figure 3- 14 rGS-Serine pathway with cyanobacteial Glycine Cleavage system

3.5 Tables

Per Acetyl-CoA Synthesis	ATP	NAD(P)H	CO_2	HCO_3-	Formate
Calvin cycle	7	4	2	0	0
Calvin cycle + rGS-glycerate	5.5	4	1	1	0
Calvin cycle + rGS-citrate	5	4	1	1	0
rGS - Malonyl-CoA	4	4	0	2	0
rGS - glycine/serine	3	2	0	1	1
rGS-glycine/serine (Glycine cleavage system)	5.5	4	1	1	0

Table 3- 1 Energy and reducing power consumption for Acetyl-CoA carbon fixation cycle

Integration site and plasmids	Gene	Origin
NSI site (Spec) pxl142	*ppc*	*E.coli*
	mdh	*E.coli*
	sucCD	*Methylococcus capsulatus*
	mcl	*Methylobacterium extorquens*
NSII site (Kan) pxl145	*gcl*	*Ralstonia eutropha*
	glxR	*E.coli*
	gark	*E.coli*
NSII site (Kan) pxl147	*Sda*	*Corynebacterium glutamicum*
	Agx1	*S. cerevisiae*
	fdh	*Candida Bodini*
NSII site (Kan) pxl147	*Sda*	*Corynebacterium glutamicum*
	Agx1	*S. cerevisiae*
	fdh	*Candida Bodini*
	FTHFS	*Moorella thermoacetica*
	folD	*Moorella thermoacetica*
NSIV (Gen)pxl154	*leuA*	*E.coli*

Table 3- 2 Plasmids used in this research

Engineered Strain name	*Plasmids*		
	NSI	*NSII*	*NSIV*
Ppc,mdh,mtkmcl	*Pxl142*		
Gcl,glxR,gark		*Pxl145*	
Ppc,mdh,mtkmcl, Gcl,glxR,gark	*Pxl142*	*Pxl145*	
Ppc,mdh,mtkmcl, Gcl,glxR,gark,leuA	*Pxl142*	*Pxl145*	*PXL154*
leuA			*PXL154*
sdaA,agx1,fdh		*Pxl147*	
sdaA,agx1,fdh, FTHFS,folD		*Pxl148*	
Ppc,mdh,mtkmcl sdaA,agx1,fdh	*Pxl142*	*Pxl147*	
Ppc,mdh,mtkmcl sdaA,agx1,fdh, FTHFS,folD	*Pxl142*	*Pxl148*	

Table 3- 3 Strains used in this research

3.6 Reference

Atsumi, Shota, Wendy Higashide, and James C Liao. 2009. “Direct Photosynthetic Recycling of Carbon Dioxide to Isobutyraldehyde.” *Nat Biotech* 27(12): 1177–80.

Bar-Even, Arren, Elad Noor, Nathan E Lewis, and Ron Milo. 2010. “Design and Analysis of Synthetic Carbon Fixation Pathways.” *Proceedings of the National Academy of Sciences*

Ducat, Daniel C, and Pamela A Silver. 2012. “Improving Carbon Fixation Pathways.” *Current opinion in chemical biology* 16(3-4): 337–44.

Fuchs, Georg. 2011. “Alternative Pathways of Carbon Dioxide Fixation: Insights into the Early Evolution of Life?” *Annual Review of Microbiology* 65(1): 631–58.

Furdui, Cristina, and Stephen W Ragsdale. 2000. “The Role of Pyruvate Ferredoxin Oxidoreductase in Pyruvate Synthesis during Autotrophic Growth by the Wood-Ljungdahl Pathway.” *Journal of Biological Chemistry* 275 (37): 28494–99.

Ikeda, Takeshi et al. 2010. “Enzymatic and Electron Paramagnetic Resonance Studies of Anabolic Pyruvate Synthesis by Pyruvate: Ferredoxin Oxidoreductase from Hydrogenobacter Thermophilus.” *The FEBS journal* 277(2): 501–10.

Kebeish, Rashad et al. 2007. “Chloroplastic Photorespiratory Bypass Increases Photosynthesis and Biomass Production in Arabidopsis Thaliana.” *Nature biotechnology* 25(5): 593–99.

Lee, Yun, Jimmy G Lafontaine Rivera, and James C Liao. 2014. “Ensemble Modeling for Robustness Analysis in Engineering Non-Native Metabolic Pathways.” *Metabolic engineering* 25: 63–71.

Li, Xiaoqian, Claire R Shen, and James C Liao. 2014. “Isobutanol Production as an Alternative Metabolic Sink to Rescue the Growth Deficiency of the Glycogen Mutant of Synechococcus Elongatus PCC 7942.” *Photosynthesis Research* 120(3): 301–10.

Ma, Kesen, Andrea Hutchins, Shi-Jean S Sung, and Michael W W Adams. 1997. “Pyruvate Ferredoxin Oxidoreductase from the Hyperthermophilic Archaeon, Pyrococcus Furiosus, Functions as a CoA-Dependent Pyruvate Decarboxylase.” *Proceedings of the National Academy of Sciences of the United States of America* 94(18): 9608–13.

Mainguet, Samuel E, Luisa S Gronenberg, Sio Si Wong, and James C Liao. 2013. “A Reverse Glyoxylate Shunt to Build a Non-Native Route from C4 to C2 in Escherichia Coli.” *Metabolic engineering* 19: 116–27.

Oliver, John W K, and Shota Atsumi. 2015. “A Carbon Sink Pathway Increases Carbon Productivity in Cyanobacteria.” *Metabolic engineering* 29: 106–12..

Parry, Martin A J et al. 2013. “Rubisco Activity and Regulation as Targets for Crop Improvement.” *Journal of Experimental Botany* 64 (3): 717–30.

Ragsdale, Stephen W. 2003. “Pyruvate Ferredoxin Oxidoreductase and Its Radical Intermediate.” *Chemical Reviews* 103(6): 2333–46. http://dx.doi.org/10.1021/cr020423e.

Shih, Patrick M, Jan Zarzycki, Krishna K Niyogi, and Cheryl A Kerfeld. 2014. “Introduction of a Synthetic CO2-Fixing Photorespiratory Bypass into a Cyanobacterium.” *Journal of Biological Chemistry* .

Sun, Yaqi et al. 2016. “Light Modulates the Biosynthesis and Organization of Cyanobacterial Carbon Fixation Machinery through Photosynthetic Electron Flow.” *Plant Physiology* .

Tang, Kuo-Hsiang, and Robert E Blankenship. 2010. “Both Forward and Reverse TCA Cycles Operate in Green Sulfur Bacteria.” *Journal of Biological Chemistry* 285 (46): 35848–54.

Tsugawa, Hiroshi et al. 2013. “MRMPROBS: A Data Assessment and Metabolite Identi Fi Cation Tool for Large-Scale Multiple Reaction Monitoring Based Widely Targeted Metabolomics.”

Yamamoto, Masahiro et al. 2009. “Carboxylation Reaction Catalyzed by 2-Oxoglutarate:ferredoxin Oxidoreductases from Hydrogenobacter Thermophilus .” *Extremophiles* 14(1): 79–85.

Zelcbuch, Lior et al. 2015. “An in Vivo Metabolic Approach for Deciphering the Product Specificity of Glycerate Kinase Proves That Both E. Coli’s Glycerate Kinases Generate 2-Phosphoglycerate.” *PloS one* 10(3): e0122957.

Zhu, Xin-Guang, Stephen P Long, and Donald R Ort. 2008. “What Is the Maximum Efficiency with Which Photosynthesis Can Convert Solar Energy into Biomass?” *Current Opinion in Biotechnology* 19(2): 153–59.

Chapter IV Isobutanol production as an alternative metabolic sink to rescue the growth deficiency of the glycogen mutant of Synechococcuselongatus PCC 7942

Disclaimer: This chapter was originally published with the same title in *Photosynthesis Researcch* **(2014) 120:301–310**

4.1 Abstract

Glycogen synthesis initiated by glucose-1-phosphate adenylyltransferase (glgC) represents a major carbon storage route in cyanobacteria which could divert a significant portion of assimilated carbon. Significant growth retardation in cyanobacteria with glgC knocked out (Δ glgC) has been reported in high light conditions. Here we knocked out the glgC gene and analysed its effects on carbon distribution in an isobutanol producing strain of Synechococcus elongatus PCC7942 and its parental wild-type strain. We showed that isobutanol production was able to partially rescue the growth of Δ glgC mutant where the growth rescue effect positively correlated with the rate of isobutanol production. Using NaH14CO3 incorporation analysis, we observed a 28% loss of total carbon fixation rate in the Δ glgC mutant compared to the wild-type. Upon expression of the isobutanol production pathway in Δ glgC mutant, the total carbon fixation rate was restored to the wild-type level. Furthermore, we showed that 52% of the total carbon fixed was redirected into isobutanol biosynthesis in the Δ glgC mutant expressing enzymes for isobutanol production, which is 2.5 times higher than that of the wild-type expressing the same enzymes. These results suggest that biosynthesis of non-native product such as isobutanol can serve as a metabolic sink for replacing glycogen to rescue growth and restore

carbon fixation rate. The rescue effect may further serve as a platform for cyanobacteria energy and carbon metabolism study.

4.2 Main text

4.2.1 Introduction

Cyanobacteria have become intriguing targets for metabolic engineering because of their ability to directly utilize of solar energy and CO2. Various efforts have focused on introducing non-native pathways and demonstrating feasibility in cyanobacteria for chemicals synthesis (Atsumi et al. 2009; Lan and Liao 2011, 2012; Shen and Liao 2012; Dexter and Fu 2009; Lindberg et al. 2010; Liu et al. 2011; Tan et al. 2011; Zhou et al. 2012; Oliver et al. 2013; Lan and Liao 2013; Ducat et al. 2011). The manipulation of non-native synthesis pathways provides a novel perspective on cyanobacterial energy and carbon metabolism. To efficiently channel harvested light energy into aimed product, it would be desirable to understand how heterogeneous pathways interact with cell physiology.

Since glycogen is the major carbohydrate storage metabolite, intuitively, removal of this cyanobacteria native carbon sink could redirect carbon to other biosynthetic processes which may favour increased growth. The synthesis of glycogen is catalyzed by glucose 1-phosphate adenylyltransferase (GlgC), glycogen synthase and 1, 4-alpha-glucan branching enzyme. GlgC catalyzes the first step of glycogen synthesis which converts glucose 1-phosphate into ADP-glucose. Several attempts have been made to break down glycogen synthesis in cyanobacteria. However, growth is not only unaffected under normal growth light conditions, ΔglgC was deleterious to cyanobacteria under high intensity light (Jacobsen et al. 2011; Miao et al. 2003a, b;

Suzuki et al. 2010). The photosynthetic activities of ΔglgC mutant are saturated at a lower light intensity with a relative lower oxygen evolution rate (Miao et al. 2003b; Suzuki et al. 2010; Gründel et al. 2012). On the basis of the high light sensitive phenotype, it is speculated that the deficiency in glycogen synthesis in the mutant prevents efficient electron transport in photosynthesis. Hence we hypothesized that a heterologous product formation pathway may serve as a non-native metabolic sink in the mutant lacking glycogen synthesis under excess light condition. With enhanced capacity to consume reducing equivalents and ATP in high radiance conditions, the mutant may overcome the growth limitation (Fig. 1). Biosynthesis of isobutanol initiates from pyruvate and utilizes NADPH as the reducing cofactor. Furthermore, isobutanol production has been demonstrated with high efficiency from cyanobacteria (Atsumi et al. 2009), thereby making it a suitable target as a metabolic sink. In this work, we knocked out the glgC gene in an isobutanol production strain of S. elongatus to explore the role of isobutanol pathway as an alternative carbon fixation driving force in the cell. In addition, we investigated the effects of glycogen deficiency on carbon flux distribution between cell mass and isobutanol synthesis.

4.2.2 Materials and methods

Culture medium and condition

All S. elongatus strains (Table 1) were grown on modified BG-11 (1.5 g/L NaNO3, 0.0272 g/L CaCl2•2H2O, 0.012 g/L ferric ammonium citrate, 0.001 g/L Na2EDTA, 0.040 g/L K2HPO4, 0.0361 g/L MgSO4•7H2O, 0.020 g/L Na2CO3, 1,000 × trace mineral (1.43 g/L H3BO3, 0.905 g/L MnCl2•4H2O, 0.111 g/L ZnSO4•7H2O, 0.195 g/L Na2MoO4•2H2O, 0.0395 g/L CuSO4•5H2O, 0.0245 g/L Co(NO3)2•6H2O), 0.00882 g/L sodium citrate dihydrate) agar (1.5% w ／ v)

plates. All S. elongatus strains were cultured in BG-11 medium containing 50 mM NaHCO3 in 100 mL flasks. Cultures were grown under 50μE s−1m−2 light, supplied by two Lumichrome F30W-1XX 6500K 98CRI light tubes on the top of the flasks at 30°C. Cell growth was monitored by measuring OD730 with Beckman Coulter DU800 spectrophotometer.

Mutant construction

Glucose-1-phosphate adenylyltransferase (glgC) of wild type (WT) and isobutanol strain (SA579) were knocked out by replacing native glgC with gentamicin cassette. Homologous flanking regions of 1,000 bp from each side were cloned from S. elongatus genomic DNA. The recombination vector pEL44 was constructed with glgC upstream flanking region, gentamicin cassette, downstream flanking region and replication origin ColE1. All primers for pEL44 were designed with 20 bp of overlapping sequence; those fragments were assembled through isothermal assembly methods(Gibson et al. 2009). The recombination vector was transformed into wild type S. elongatus and isobutanol strains SA579. Double crossover recombinants transformants XL18 and XL19 were selected on 2 ug/ml gentamicin plates. The insertion of gentamicin cassette at target position through double crossover was confirmed by colony PCR. XL27 was constructed by transforming XL18 with pSA150 which contained the kivd and yqhD. The transformants of XL27 were selected on 1 % agar plates of BG-11 medium containing 20 μg/ml spectinomycin and 2 μg/ml gentamicin. The insertions of kivd and yqhD were confirmed by colony PCR.

Culturing conditions for growth rescue test and alcohol production

Wild type S. elongatus and mutant strains were grown in 40 ml BG-11 medium with 50 mM NaHCO3 in 125 ml Pyrex shaker flasks. 10 mg/L thiamine was added to isobutanol producing cell culture ever day to provide the cofactors for pyruvate decarboxylase (Atsumi et al. 2009). Cells were grown at 30°C under fluorescent light (150 μE s−1m−2), which was provided by four fluorescent tubes placed on top of the cell culture. Cell growth was monitored by measuring OD730 of each culture. The culture was pre-cultured at 30 °C to OD730 of 0.4–0.6, at which point 1 mM IPTG was added. One tenth the total volume of cell culture was removed from the cell culture. Then the same volume of fresh medium containing 0.5 M NaHCO3 was added to cell culture every day. The pH of cell culture was adjusted to 7.5 with 10 N HCl once per day.

Quantification PCR of genomic DNA copy numbers

The genomic DNA was purified by Promega Wizard® Genomic DNA Purification Kit. The genomic DNA was diluted to 1 ng/ul for use. The primer was designed by NCBI/Primer-Blast tools. The primers used in the study were as follows: glgC-for (LX174): GCCGATGCGGTTCGCCAGTA, glgC-rev (LX175): GCTGAACTCGACCACCCGGC with product size 228bp; Gen-for (LX196): TCGCGGCTTACGTTCTGCCC, Gen-rev (LX197): CACTGCGGGATCGTCACCGT with product size 191bp; Icd-for (LX188): GGTGACGGCACTGGCGTTGA, Icd-rev (LX189): CACGCCGTACTCGCGGATCG with product size 192bp; RdoD-for (LX192): GCGCTCAAACCGGCGGAAAC, RdoD-rev (LX193): TGGCCGCCGCATCTTCATCC with product size 154bp;

The reagent for qPCR was BIORAD SsoFast™ EvaGreen® Supermix. The final PCR mixture contained forward and reverse primer at final concentration of 500nM in total volume of 10 l mixture cocktail. The Real-time PCR was performed by BIORAD CFX96 Real time system

C1000 Thermal cycler. The temperature cycling conditions was 3 min at 95 ℃, followed by 40 cycles of 10 s at 95° C and 30s at 60° C. The melting curve was from 65° C to 95° C at the increase of 0.5° C. Cycle threshold (Ct) values were obtained and analyzed by CFX Manage system Real-time System software threshold analysis.

The standard curve was generated through a dilution series of the genomic DNA (0.1 ng/µl, 0.02 ng/µl, 0.004 ng/µl and 0.0008 ng/µl). Standards were measured in triplicates for each concentration. Primer efficiency was calculated by CFX Manage 2.0 software. The Ct value threshold was set at 10000 RFU (Relative Fluorescence Units) for all samples. The primer sets used in this research all reached 100 % efficiency, which means both reference gene primer efficiency (Eref) and target gene primer efficiency (Etarget) equal to 1 (Fig.S1). The genomic DNA concentration in all samples was 0.1ng/µl. All samples were tested in triplicates (Fig.S2 a-d). The threshold values for reference gene (Ct ref) and target gene (Ct target) were all analyzed by CFX Manage 2.0 software (Table S1). The relative genomic DNA copy numbers of the samples were calculated with the average Ct value through absolute quantification according to the following formula below (Lee et al. 2006)

$$\textbf{Relative ratio} = \frac{(1+E_{Ref})^{Ct_{ref}}}{(1+E_{target})^{Ct_{target}}} \qquad (1)$$

The products were further loaded on the gel to verify specific the amplification of target genes (Fig.S2 e).

Glucose-1-phosphate adenylyltransferase Enzyme Assay

AGPase activity was measured based on previous protocol (Suzuki et al. 2010).The reaction mixture consisted of 50 mM HEPES-NaOH (pH 7.5), 2 M ADP-glucose, 2.4 mM Na

pyrophosphate, 1 mM 3-phosphoglycerate, 5 mM $MgCl_2$, 4 mM dithiothreitol (DTT), and enzyme crude extract in a total volume of 400 ul . The reaction was initiated by the addition of the crude cell extract and was carried out at 30 °C for 20 min. Finally, the reaction was terminated by heating at 100 °C in a water bath for 2 min. After centrifugation, 300µl of the supernatant was removed and mixed with an equal volume of 0.33 mM NADP+. Absorbance changes at 340nm were measured after the addition of 0.2 unit of phosphoglucomutase (Sigma-Aldrich) and 1unit of glucose 6-phosphate dehydrogenase (Sigma-Aldrich). Enzyme activities were normalized by total protein content (mg) in cell lysate .

Quantification of glycogen

Glycogen content was measured by the Biovision Glycogen Assay kit. Exponential phase cells were resuspended into distilled water with final OD equal to 1. The cell suspension was homogenized by beads beater for three times and the homogenates was boiled for 5 min to inactive the enzymes. The boiled samples were centrifuged at 13000rpm for 5 min to remove the insoluble materials. The supernatant of boiled sample were used for glycogen quantification based on protocols provided by Biovision Assay Kit.

Quantification of alcohols

Culture samples (1mL) were centrifuged for 5 min at 15,000 rpm and the supernatant was retrieved. The alcohol compounds in the supernatant were quantified by an Agilent model 6850 gas chromatograph (GC) system equipped with a flame ionization detector (FID), and an automatic injector, sampler and controller. The separation of alcohol compounds was carried through a DB-FFAP capillary column (30 m×320 µm.i.d×0.25 mm film thickness).The GC

oven temperature was initially held at 85 ℃ for 3 min and then raised to 235 ℃ with a temperature ramp of 45 ℃ min-1. The GC oven was then maintained at 235 ℃ for 1 min before completion of analysis. The column flow rate was 1.7 mL min-1. Helium gas was used as the carrier gas with an inlet pressure of 9.52 psi. The injector and detector temperatures were maintained at 225 ℃. The injection volume was 1mL. The supernatant of the culture broth was injected with a 1: 25 split ratio with1-pentanol as the internal standard

Calculation of cellular productivity

Daily isobutanol productivity was calculated through dividing the daily isobutanol concentration increment by the average of cell density during that day.

Quantification of Chlorophyll a content

S. elongatus cells were resuspended into BG-11 medium. 10ul suspension was put into 1ml 100% methanol and mix thoroughly. The cells were then centrifuged for 5 min at 12,000 rpm. The supernatant was taken for chlorophyll a measurement at the absorbance of 663 nm. The extinction coefficient for chlorophyll a is 82 ml•mg-1

Quantification of 14C labeled carbon flux

S. elongatus cells were harvested by centrifugation at 12,000 rpm for 5 min at room temperature. The supernatant was discarded and the cell pellet was washed twice with fresh BG-11 (pH 7.0). The cells were then resuspended at final OD equal to 1 with fresh BG-11 medium. 10 mg/L thiamine was added for induced isobutanol producing cells. 3 ml aliquots were

transferred into a sealed glass tube and pre-incubated for 1 hour under 80 μE/m2/s light conditions. The test was started by adding bicarbonate solution with 20% NaH14CO3 into the sealed glass tubes. The final concentration of total bicarbonate was 2 mM and final radio activity concentration was 10 μCi/ml. At 0 min, 30 min, 60 min, 0.3 ml of each cell culture were taken for analysis. Samples were measured in triplicates

(a) Cell mass NaH14CO3 incorporation analysis.

The cell pellet and aqueous phase were separated through silicone layer filtration. The method for cell mass separation was modified based on previous protocol (Ohnishi et al. 2010). A density gradient was formed with silicone oil AR20 and AR200 at the volume ratio 4:3.5. In a 1.5 ml Eppendoff tube, 100 μl silicone layers (AR20 and AR200) were first built on 20 μl termination buffer at the bottom. The termination buffer containing 25 mM CAPS and 0.75% SDS. Then, 100 μl cell culture was applied on the top of the silicone layers. After centrifugation at 12,000 rpm for 5 min, the silicone oil and the termination buffer with the supernatant of cell culture were aspired. The cell pellet was then resuspended in 100 μl 0.1 M NaOH solution for cell lysis. 50 ul cell lysate was used for scintillation counting to determine the whole carbon fixation amount.

(b) Isobutanol and 3-Methyl-1-butanol NaH14CO3 incorporation analysis.

Before we analyzed NaH14CO3 incorporation in extracellular alcohols, we first determined the extraction efficiency for both NaH14CO3 and alcohols by oleyl alcohol (Sigma-Aldrich) in our test. BG-11 medium containing NaH14CO3 were mixed with oleyl alcohol at various volume ratios and less than 0.25% scintillation reading was found in the extractant when extractant and medium mixing ratio was above 2:1. This result showed that the non-incorporated

NaH14CO3 could hardly be absorbed by oleyl alcohol (Table S2). Here we used volume ratios VOleyl alcohol:V medium = 2:1 to test the extraction efficiency for isobutanol and 3-Methyl-1-butanol (3MB). The extraction efficiency of isobutanol and 3MB was 30 % on average among all concentrations of isobutanol and 3MB that we have tested (Table S3). Therefore, the isobutanol and 3MB amount that were able to be quantified in oleyl alcohol would be approximately 30% of actual extracellular isobutanol and 3MB amount.

As for sample treatment, the cell pellet and supernatant were separated by centrifugation at 12,000 rpm for 5 min. 0.2 ml of the supernatant was added into 0.4 ml oleyl alcohol to extract isobutanol and 3MB. 20 μl of 5 M NaOH was added into the mixture to stabilize the non-incorporated bicarbonate. After mixing, 0.1 ml of the upper oily phase was transferred into a scintillation vial containing 3 ml scintillation cocktail. The 14C counting was performed by the Beckman LS6500 scintillation counter.

Calculations of NaH14CO3 incorporated rate

The relation between C14 scintillation reading and net carbon amount (mM) was characterized through a standard curve (Fig S3). To measure bicarbonate incorporation rate into cell mass and alcohols, scintillation reading at time 0, 30min and 60min for cell mass and alcohols for per unit cell culture were converted into equivalent bicarbonate incorporation amounts (mM). We then plot the net carbon incorporation amount at those three time points. The slope of the linear line (mM/h) that fits the plot represented the NaH14CO3 incorporated rate for per unit cell culture.

4.2.3 Results

Knocking out Glucose-1-phosphate adenylyltransferase (glgC) in the wild-type and isobutanol strains of S. elongatus

We first knocked out the glgC gene in the wild type (WT) strain, denoted as XL18, and isobutanol producing strain SA579, denoted as XL19, by replacing the coding region with a gentamicin cassette. Strain SA579 refers to the engineered S. elongatus strain which has the isobutanol biosynthesis genes alsS, ilvC, ilvD, kivd, and yqhD integrated into its chromosomes (Atsumi et al. 2009). Since multiple copies of chromosomes exist in S. elongatus, several approaches were employed to confirm the full segregation in the mutant strains. First we measured the relative gene copy number of glgC in strains XL19 and XL18 by quantitative PCR. Here we chose isocitrate dehydrogenase (Icd) and RNA polymerase sigma factor (RpoD) as two reference genes. As shown in Fig. 2a, the relative copy numbers of glgC were reduced to zero in strain XL18 and XL19 while the relative gene copy numbers of glgC in WT and SA579 were still around 1.0. The copy numbers of gentamicin cassette in XL18 and XL19 were almost identical to those of the reference genes. Those results confirmed the complete replacements of glgC by gentamicin cassette in all copies of chromosome of these two strains.

Subsequently, we examined the enzyme activities of glucose-1-phosphate adenylytransferase in the crude extract of XL18 and XL19. Compared with WT and SA579, the enzyme activities in XL18 and XL19 were not detected (Fig. 2b). Interestingly, the enzyme activity of glucose 1-phosphate adenylyltransferase in SA579 was almost triple of that in wild-type. This enzyme has been known to be conserved in higher plants, green algae and cyanobacteria, and is allosterically activated by 3P-glycerate (3PGA) and inhibited by inorganic phosphate (Gómez Casati et al.

1999). Since the total amount of glycogen in SA579 was less than that in WT, the precursor of glycogen synthesis, ADP-α-D-glucose, could be produced at lower level. As a result, less pyrophosphate could be generated and further hydrolyzed into inorganic phosphate. The high activity in SA579 could be ascribed to lower intracellular concentration of inorganic phosphate which allosterically inhibits the activity of glucose 1-phosphate adenylyltransferase.

Glycogen contents were also quantified in the cell lysate of glgC mutants. More than 40 ug/OD glycogen were stored in the glgC+ cells while almost no glycogen was detected in strain XL18 and XL19 (Fig. 2c). Taken together, these results confirmed the complete knock outs of glgC in both the isobutanol production strain and WT strain.

Alcohol production led to growth rescue of glycogen mutant

Various reports have stressed the growth inhibition in the glgC mutant strains due to the incapability of glycogen synthesis under high light conditions (Jacobsen et al. 2011; Miao et al. 2003a, b; Suzuki et al. 2010). Our observation is in accordance with previous reports. Interestingly though, the induction of the isobutanol pathway partially rescued the glgC mutant from growth retardation. In order to further characterize how isobutanol pathway genes could impact the growth of glgC mutants, we constructed strain XL27, which was XL18 (ΔglgC) with only two of the isobutanol pathway genes (kivd and yqhD) overexpressed. This partial overexpressed pathway was shown to produce isobutanol at a lower rate (Atsumi et al. 2009) .

We first confirmed that the introduction of the isobutanol pathway genes had no effect on the phenotype of glgC mutants, when those genes were uninduced. Fig. 3a indeed shows that all of the glgC null strains exhibited impaired growth compared to their glgC+ controls, with or

without the uninduced isobutanol synthesis genes. Next, we investigated the effect of isobutanol pathway activity on the phenotype of glgC null strains. Fig.3b shows that induction of the isobutanol pathway genes led to partial growth rescue in XL19. The induced culture of XL19 reached a final cell density that was about twice as high as that of the uninduced culture. In addition, the induced culture stayed green throughout culturing, whereas the uninduced culture turned yellow. The chlorophyll a content in the induced XL19 and XL27 cultures were also 50 % and 33 % higher than the uninduced cells respectively, which is consistent with the difference in cell density (Fig S3). The XL27 strain with partial isobutanol pathway genes showed slight rescuing effect. The growth recue effect was correlated with isobutanol productivity (Fig.3c), suggesting that the flux to isobutanol was responsible for such a phenotype reversal. These observations suggest that isobutanol synthesis could prolong the cell growth of glycogen mutants under light stress conditions.

Effects of defective glycogen synthesis on alcohols production

To investigate whether deletion of the glycogen synthesis pathway could enhance biofuel production, we quantified isobutanol and 3-Methyl-1-butanol (3MB) accumulations in the cell cultures under constant light conditions. 3MB is the side product of isobutanol pathway genes in cyanobacteria (Fig.1). In order to achieve the maximum productivity of alcohol productions in cyanobacteria, isobutanol strains SA579 and XL19 were tested in a high radiant environment (150 μE s−1m−2), which was consistent with previous isobutanol production conditions (Atsumi et al. 2009).

Under constant light conditions, the cell density of XL19 (ΔglgC) with the isobutanol pathway induced was almost half of the isobutanol strain SA579 (glgC+) during log phase and

stationary phase (Fig.4a). However, XL19 productivity of isobutanol and 3MB were slightly higher than SA579. Therefore, if we normalized the cell productivity by cell mass, we found that isobutanol productivity per cell was improved due to absence of glycogen synthesis. Per cell productivity (mg/L/OD/day) comparison (Table 2) showed that the maximum isobutanol cellular productivity (day 2) was improved up to 82 % under constant light conditions. It implies that S. elongatus starts to store glycogen during log-phase and glycogen synthesis is one major competing pathway for isobutanol synthesis. Nevertheless, the final titer of fuel production was hardly affected by the deletion of glycogen synthesis pathway (Fig.4b-4c). Cell cultures of XL19 and SA579 both accumulated about 550 mg/L of isobutanol and 70 mg/L 3MB after 8 days. It is possible that the final titer was limited by the toxicity of isobutanol pathway, either from isobutanol itself or a toxic intermediate.

Alcohols function as the alternative metabolic sink to change carbon flux distribution

Since isobutanol pathway prolong cell growth of glycogen mutant, we investigated the carbon flux distributions between cell mass and alcohols in these strains in order to clarify the role of isobutanol in cell rescue. To quantify the carbon flux into cell mass and extracellular products, a 14C labeled sodium bicarbonate incorporation assay was developed. Because isobutanol and 3MB were able to diffuse freely out of the cell membrane, the extracellular isobutanol and 3MB could be separated from the cell mass. Thus, the incorporated 14C bicarbonate was divided into two portions: cell mass (including glycogen) and products. Isobutanol-14C and 3MB-14C in the culture were extracted by oleyl alcohol (See methods). The extractant and cell pellet were then prepared for the scintillation counting respectively.

WT, SA579, XL18 and XL19 cells during the mid-log phase were analyzed for the 14C bicarbonate incorporation (Fig.5). For WT strain, about 1.1 mM bicarbonate was incorporated per hour per OD cells. Removal of glycogen synthesis in strain XL18 resulted in 28 % less cell mass incorporation compared to WT. For strain XL19 without induction, the cell mass incorporation was 26 % less than that of the isobutanol production strain SA579 under no induction conditions, which was consistent with the percentage difference between WT and XL18. Thus, glycogen synthesis typically accounted for 26-28% of carbon incorporated (Table.S4).

Comparing SA579 and WT, production of isobutanol and 3MB did not change the total amount of carbon fixation flux, but diverted 22% of total fixed carbon to alcohol synthesis. Comparing the total carbon fixation between the induced SA579 and XL19, we found that deletion of glgC increased the carbon flux towards isobutanol production, reaching 52% of total fixed carbon which is a 2.5 fold increase when comparing with and without ΔglgC (Table.S4). This result could potentially account for the increase in isobutanol productivity on per cell basis.

Due to a lack of glycogen as a metabolic sink, cyanobacteria lost a major route for spending its fixed carbon and reducing powers. As a result, carbon fixation rate is lowered while still receiving excess energy from light, which could cause the imbalance of cofactors. The total carbon fixation in induced XL19 cells was 38% higher than the uninduced cells (Table.S4), which indicated that isobutanol pathway restores carbon fixation rate of the glgC mutant back to the wild-type level. As mentioned above, the induced XL19 was able to divert 52% of the fixed carbon to alcohol biosynthesis (Fig. 5). This fraction was higher than the fraction normally

diverted towards glycogen biosynthesis (26-28%). Isobutanol production is therefore a highly efficient metabolic process to utilize fixed carbon and reducing power. As a result, isobutanol production can efficiently recycling cofactors and utilize the carbon fixing capacity that glycogen synthesis mutant cannot.

4.2.4 Discussion

This work describes the impacts of isobutanol pathway on glgC mutants growth phenotype as well as glycogen deficiency on isobutanol production in S.elongatus. Glycogen is generally accumulated when excess carbon is available and consumed under stress conditions in bacteria, however, unlike cyanobacteria, glycogen is not required for growth in heterotrophic bacteria such as E.coli, Clostridium pasteurianum since the glycogen deficiency mutant grow as well as their parental strain (Preiss and Romeo 1989). Glycogen synthesis was mainly associated with sporulation and differentiation in Bacillus subtilis and Streptomyces coelicolor (Ballicora et al. 2003). In such heterotrophic organisms such as E. coli, respiration and mixed acid fermentation products rather than glycogen served as metabolic sinks for recycling electron mediating cofactor NADH. Cyanobacteria, which is photoautotrophic and oxygenic, doesn't employ the fermentative pathway under light conditions naturally (Stal and Moezelaar 1997). Because of the high percentage of carbon flux directed into glycogen synthesis in cyanobacteria during growth phase, glycogen is a natural metabolic sink and plays an essentially physiological role in protecting the cells from light stress. The growth retardation effect of glgC deletion has been reported mainly under high light conditions (> 80 μE s−1m−2), whereas the mutant cell could grow normally in low light condition. In glgC mutants, the oxygen evolution rate reached saturation at a light intensity below one half of that observed in WT (Jacobsen et al. 2011; Miao

et al. 2003a, b; Suzuki et al. 2010). These observations implicate the occurrence of photoinhibition (Vonshak et al. 1996). Here we reported that the synthesis of non-native products could serve as an alternative metabolite sink to dissipate photosynthetic energy and maintain biosynthesis process. The cell growth of glgC mutants was spurred by a continuous carbon outlet that consumes NADPH and ATP, which facilitate the process of cofactor recycling. In plants, similar sink/source regulation strategy has been adopted for metabolite balance. The carbohydrate synthesis in the sink organs is responsible to release the inhibition of photosynthesis on the leaf (Arp 1991; Krapp et al. 1993). In S. elongatus, it has also been reported that expansion of sucrose synthesis could enhance the total carbon fixation rate (Ducat et al. 2012). However, a non native metabolite sink has never been demonstrated to improve cell growth rate in photosynthetic microbes.

Isobutanol production was not able to rescue the glgC phenotype completely. Although isobutanol could diffuse out of the cell membrane, which facilitates a continuous energy and carbon utilization, the rescue effect is still limited by the isobutanol pathway itself. This could be explained by several factors. First, when isobutanol concentration in the media reached the toxicity level, cell growth slowed down and the rescue effect compromised. Second, isobutanol production requires less ATP than glycogen formation. As a result, it is possible that using isobutanol as a metabolic sink still results in elevated intracellular ATP concentration as compared to using glycogen as a sink. Elevated ATP concentration may also have regulatory implications on cellular growth. Third, glycogen biosynthesis is known to play a role in response to osmotic stress.

As competing process for isobutanol and 3MB synthesis, glycogen stored nearly one third of fixed carbon in the WT strain. Thus, disruption of glycogen synthesis was able to boost cellular productivity on a per OD basis. Organic acid and sucrose production have been reported to benefit from incapability of glycogen synthesis in cyanobacteria as well (Carrieri et al. 2012; Ducat et al. 2012; Gründel et al. 2012) .Nevertheless, effect of product formation on rescuing the glgC growth retardation has never been reported. Because of the potential of growth rescue by non-native carbon sink, glgC mutants with diverse synthetic pathways could be utilized as a novel model for energy and carbon balance study for photosynthetic organism.

Acknowledgements

The authors would like to thank Ethan I. Lan for the plasmids and valuable discussions. This work is supported by PETRO program of the Advanced Research Projects Agency–Energy (ARPA-E) of DOE (Award number DE-AR0000201)

4.3 Figures

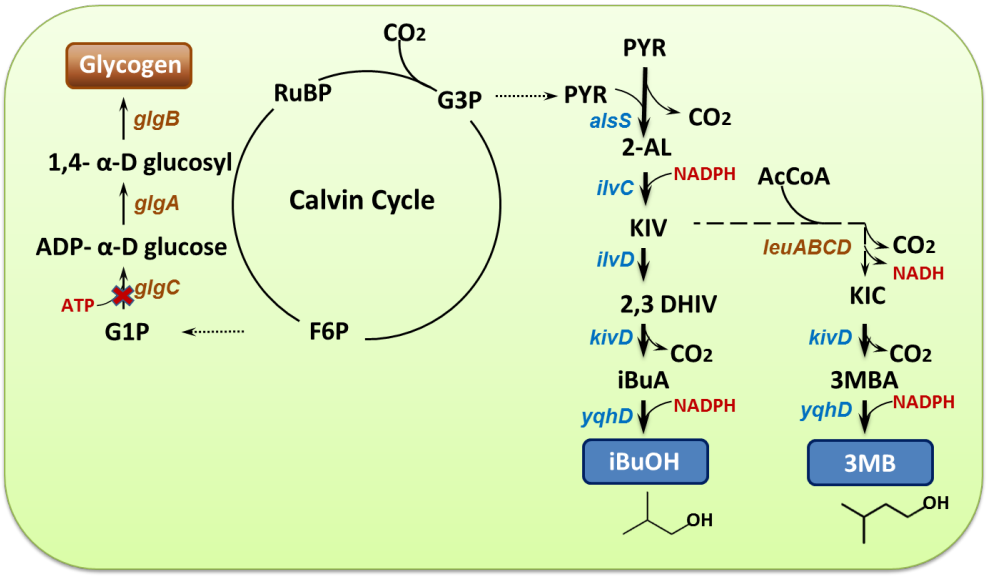

Figure 4-1 Competing carbon sinks between glycogen and isobutanol in cyanobacteria.

Bold arrows indicate the overexpressed isobutanol pathway constructed with *alsS, ilvCD, kivD and yqhD*. The thin arrows indicate the *S. elongatus* PCC 7942 *native* pathway. Dashed line indicates multiple steps in native pathways. Foreign genes introduced are in blue fonts while the native genes are in brown fonts. The essential cofactors are in red fonts.. **RuBP,** rubilose biphosphate; **G3P**, glyceraldehyde-3-phosphate; **PYR,** pyruvate; **2-AL**,2-acetolactate; **KIV**, ketoisovalerate; **2,3 DHIV**,2,3 dihydroxyisovalerate; **iBuA**, isobutyraldehyde; **iBuOH**, isobutanol; **AcCoA,** acetyl-CoA; **KIC**, ketoisocaproate; **3MBA,** 3Methyl butyraldehyde; **3MB**, 3-Methyl-1- butanol;

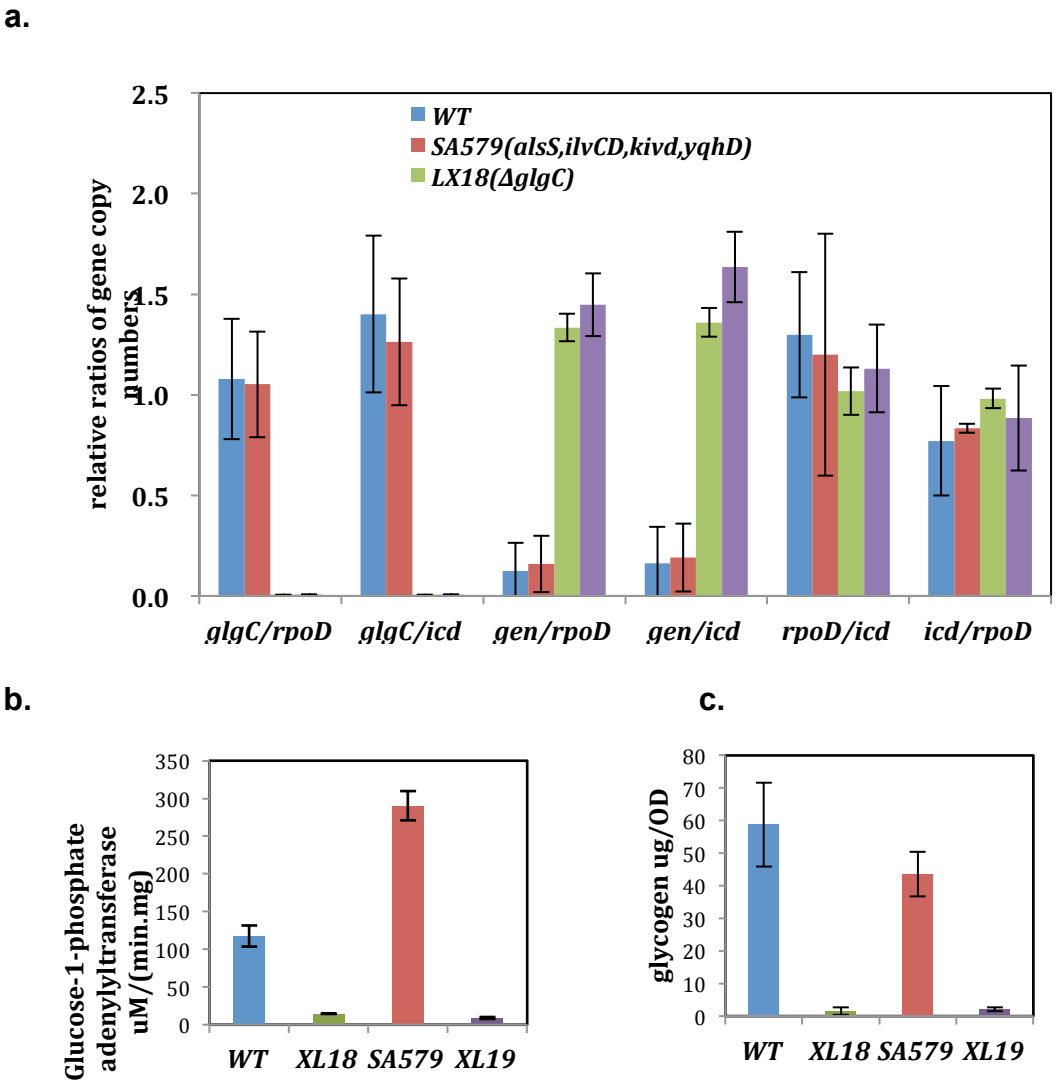

Figure 4- 2 Confirmation of *glgC* mutant strains.

(a) Quantitative PCR results of *glgC* mutant strains. The copy number of *glgC* and gentamicin(*gen*) gene were measured through quantitative PCR. The reference genes for *Synechococcus elongatus* PCC 7942 were *rpoD*, RNA polymerase sigma factor and *icd*, isocitrate dehydrogenase. The relative gene copy number ratio of *glgC*, *gen* were quantified in wild type strain (Blue), *SA579* (Red), *XL18* (Green) and *XL19* (Purple).

(b) (b) Glucose-1-phosphate adenylyltransferase activity. Enzyme activities were assayed in the crude extract of wild type strain (Blue), *SA579* (Red), *XL18* (Green) and *XL19* (Purple). The activities were normalized by total protein content.

(c) (c) Glycogen content measurement. Glycogen amount were assayed in 1ml (OD=1) cell culture of wild type strain (Blue), *SA579* (Red), *XL18* (Green) and *XL19* (Purple). Error bars indicate standard deviations from 3 replicates.

a

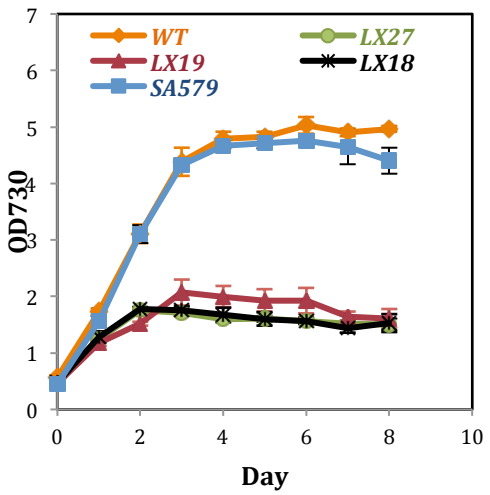
WT
LX27
LX19
LX18
SA579
OD730
Day
0
1
2
3
4
5
6
7
0
2
4
6
8
10

c

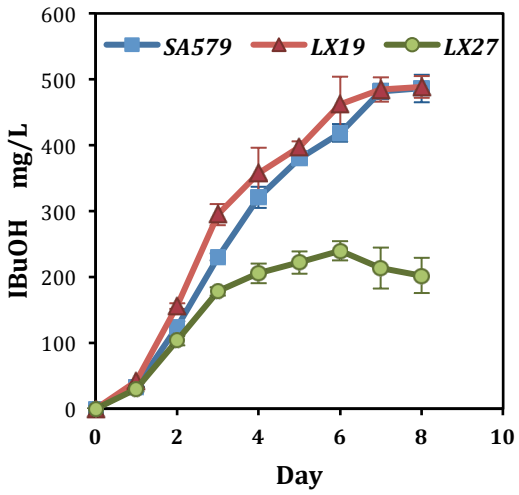
SA579
LX19
LX27
IBuOH mg/L
Day
0
100
200
300
400
500
600
0
2
4
6
8
10

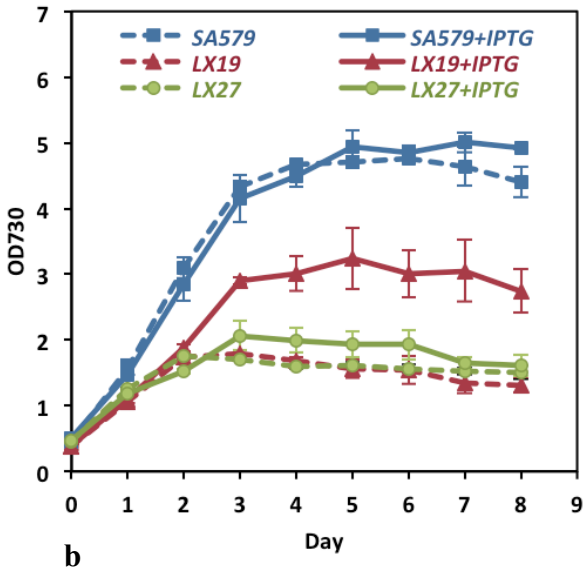

SA579(alsS,ilvCD,kivd,yqhD)

LX19(ΔglgC,alsS,ilvCD,kivd,yqhD)

LX27(ΔglgC,kivd,yqhD)

LX18(ΔglgC)

Figure 4-3 Induction effect of isobutanol pathway on glgC mutant strains under constant light conditions (150 µE $s^{-1}m^{-2}$).

(a) Growth rates comparison of uninduced cultures show the effect of *glgC* knockout in strains. (b) Induction of the isobutanol pathway with 1 mM IPTG (solid lines) partially rescued the growth retardation effect of *glgC* knockout in cultures without IPTG induction (dashed lines). (c) Isobutanol production in the induced cultures of *SA579, XL19, XL27*. The growth rescue effect correlated with the isobutanol production activity. Data a to c represent averages from 3 independent experiments. Error bars indicate standard deviations from 3 replicates.

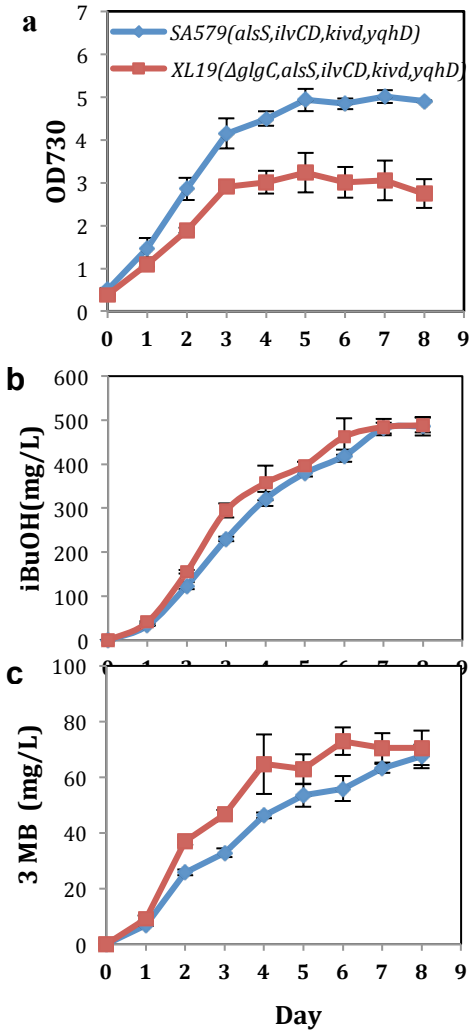

Figure 4-4 Effects of glycogen deficiency on productions.

a-c: *SA579* and *XL19* cultured under constant light (150 μE•m^{-2} •s^{-1}) with induction by 1mM IPTG when the cell OD reached 0.4-0.6. (a) Growth curve (b) Production of isobutanol (c) Production of 3-methyl 1-butanol Data a to c represent averages from 3 independent experiments. Error bars indicate standard deviations from 3 replicates.

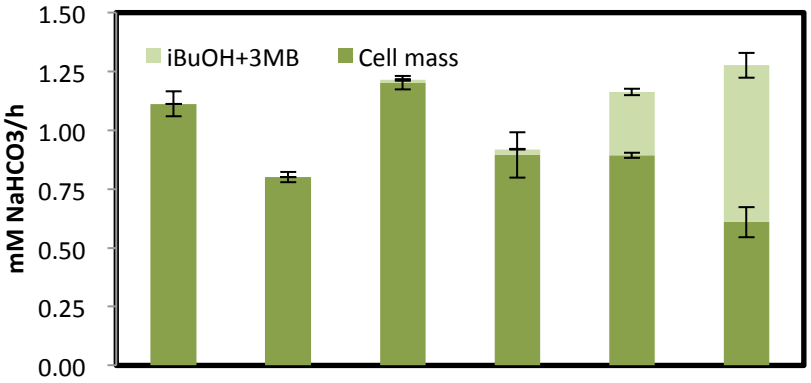

glgC	+	-	+	-	+	-
alsS,ilvCD,kivD,yqhD	-	-	+	+	+	+
IPTG	-	-	-	-	+	+
	WT	***XL18***	***SA579***	***XL19***	***SA579***	***XL19***

Figure 4-5 Carbon flux distribution between cell mass and alcohols of various mutants.

$NaH^{14}CO_3$ incorporation amount into biomass and fuel pathway (isobutanol and 3MB) were characterized among wild type and various *glgC* mutant strains. Cell pellet and supernatant were separated after incubation with $NaH^{14}CO_3$ and were measured for scintillation counting individually after treatment. +/- indicated the presence/absence of each gene or IPTG. Data represent averages from 3 independent experiments. Error bars indicate standard deviations from 3 replicates.

4.4 Tables

Type	Description	Reference
***Synechococcus elongatus* PCC 7942**		
Wild type		S.S Golden
XL18	Δ*glgC*	This work
SA579	*NSII:: alsS , ilvCD NSI:: kivD, yqhD, lacI*	(Atsumi et al. 2009)
XL19	Δ*glgC*, *NSII:: alsS , ilvCD NSI:: kivD, yqhD, lacI*	This work
XL27	Δ*glgC*, *NSI:: kivD, yqhD, lacI*	This work
plasmids		
pEL44	Gen^R ColE1 ori, contain recombination fragment of *glgC*	This work
pSA150	$Spec^{R,}$ NSI recombination sites, Ptrc::kivd,yqhD	(Atsumi et al. 2009)

Table 4-1 Strains and plasmids used in this research

	Log-Phase		Stationary phase			
	D1	D2	D3	D4	D5	D6
SA579	34.1	42.1	30.4	21.1	12.4	8.1
$(mg \cdot L^{-1} \cdot OD^{-1} \cdot d^{-1})$	±4.9	±4.2	±3.4	±3.5	±4.7	±4.3
XL19	55.8	76.9	58.1	21.0	14.1	19.7
$(mg \cdot L^{-1} \cdot OD^{-1} \cdot d^{-1})$	±0.7	±4.5	±7.3	±7.2	±16.8	±13.2
Increase (%)	63.7	82.7	91.4	0	13.9	144.3

Table 4-2 Improvement in per cell productivity of isobutanol in *glgC* mutant at different stages

Log phase and stationary phase daily isobutanol productivity on per OD basis were recorded and the improvement in *XL19* in per cell productivity was analyzed.

Errors indicate standard deviations from 3 replicates.

4.5 Supplementary Figures

a.

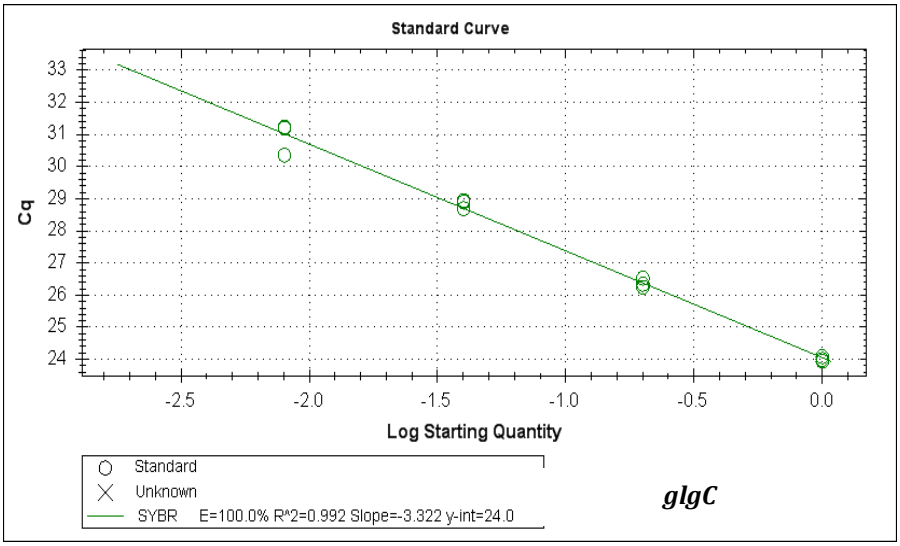

b.

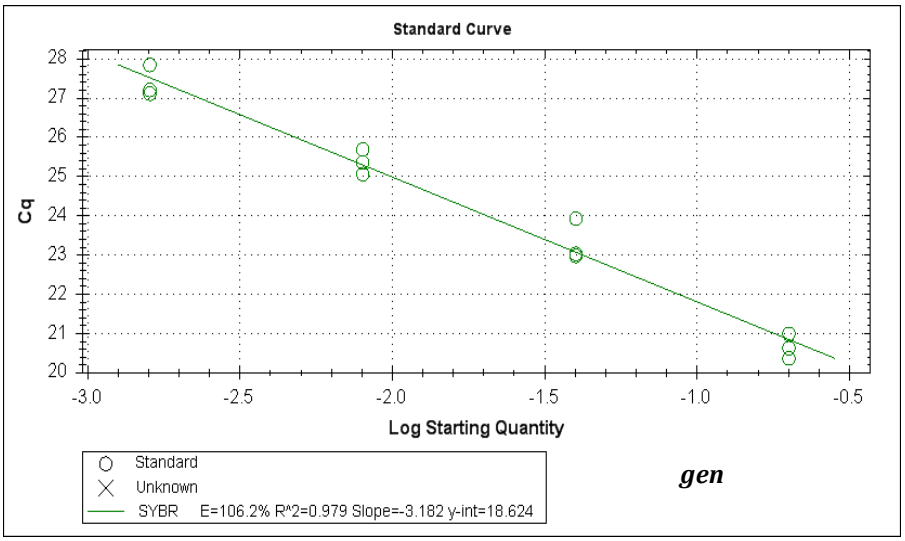

c.

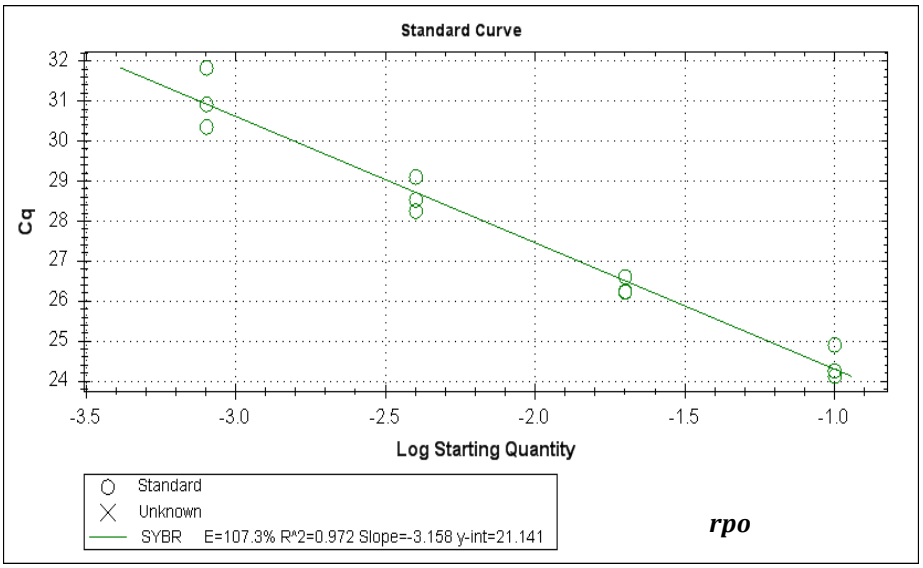

d.

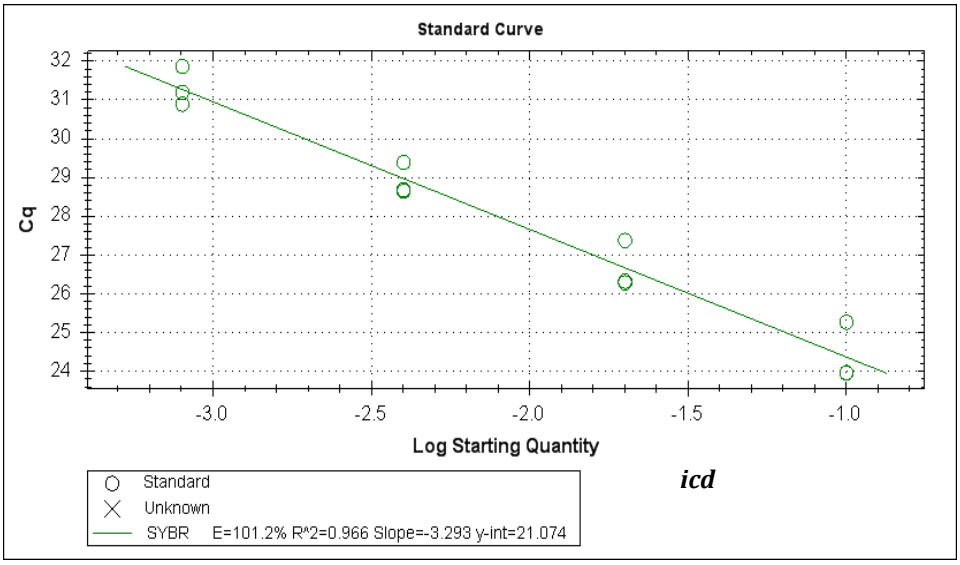

Figure S4-1 Quantification standard curves with Genomic DNA.

Quantification standard curves of *glgC* (a)*, gen* (b)*, rpoD* , reference gene 1 (c) and *icd* , reference gene 2 (d) were determined by serial dilution of genomic DNA to 0.1 ng/μL, 0.02 ng/μL, 0.004 ng/μL and 0.0008 ng/μL. Primer efficiency of those four pairs of primers all reached to 100%.

a.

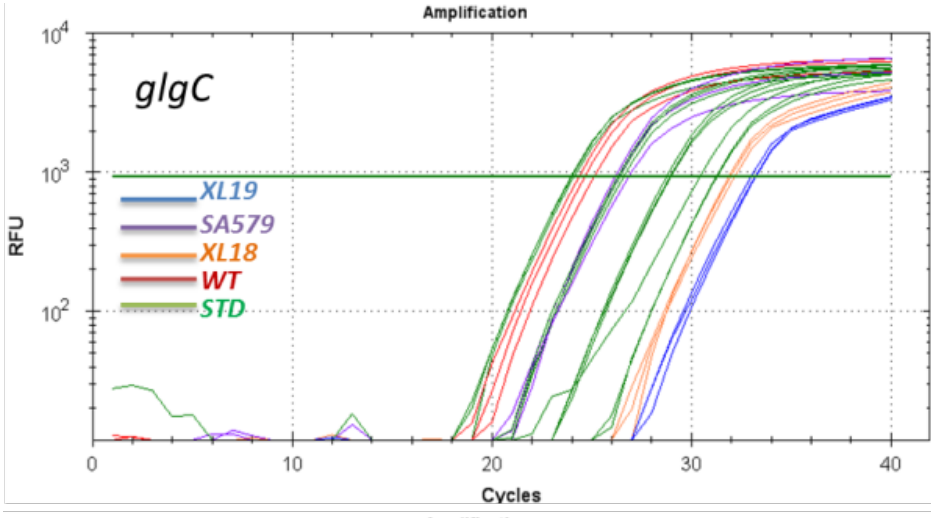
Amplification
glgC
XL19
SA579
XL18
WT
STD
RFU
Cycles

b.

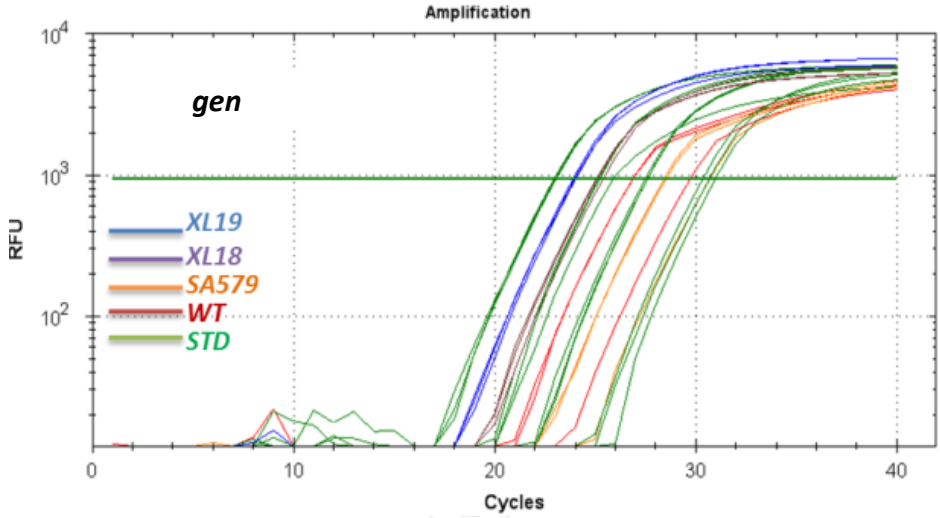
Amplification
gen
XL19
XL18
SA579
WT
STD
RFU
Cycles

c.

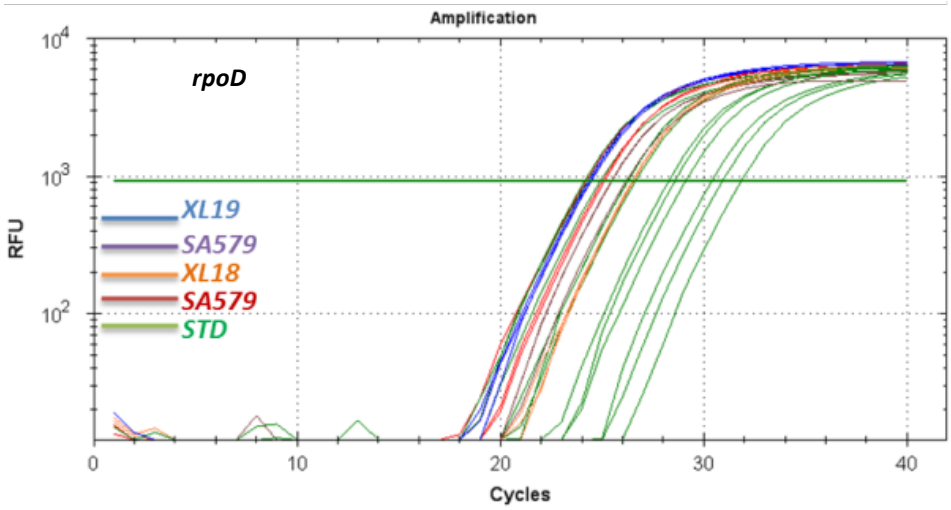
Amplification
rpoD
XL19
SA579
XL18
SA579
STD
RFU
Cycles

d.

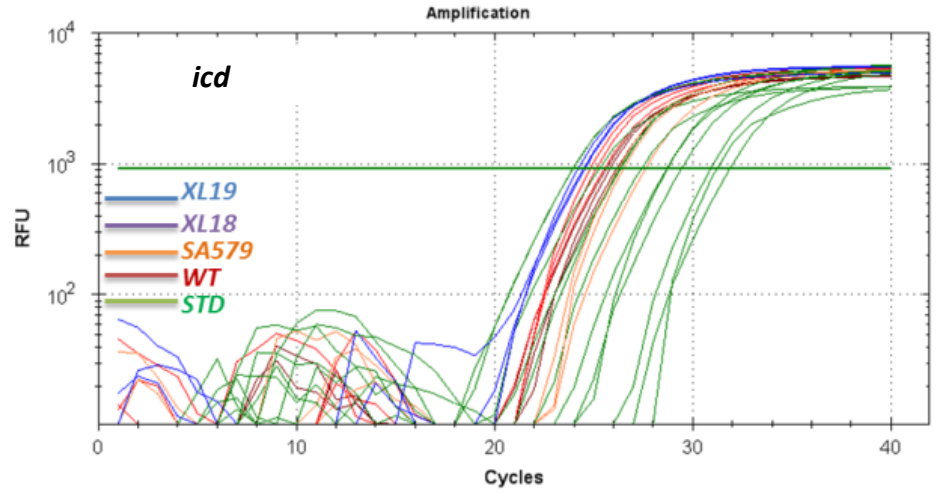
Amplification
icd
XL19
XL18
SA579
WT
STD
RFU
Cycles

e.

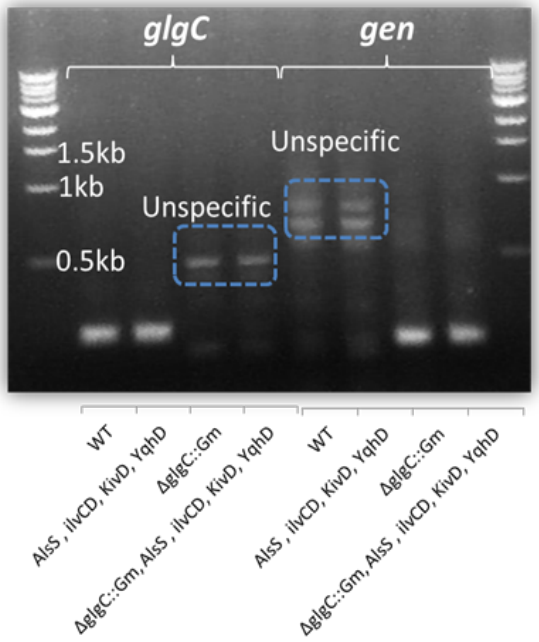

Figure S4-2 Quantification of amplified products.

Amplification plot of target genes : *glgC* (a), *gen* (b), *rpoD* , reference gene 1 (c) and *icd* , reference gene 2(d). The Ct value threshold was set at 10000 RFU (Relative Fluorescence Units) for all samples. The various strains were colour coded to show the (Ct) number individually. (e) Gel electrophoresis validation of amplified product. The presences of *glgC* and gen correct bands were confirmed by gel picture. Unspecific PCR product was detected on the gel in the amplification by *glgC* primers in XL18 and XL19and by the primers of gen in WT and SA579.

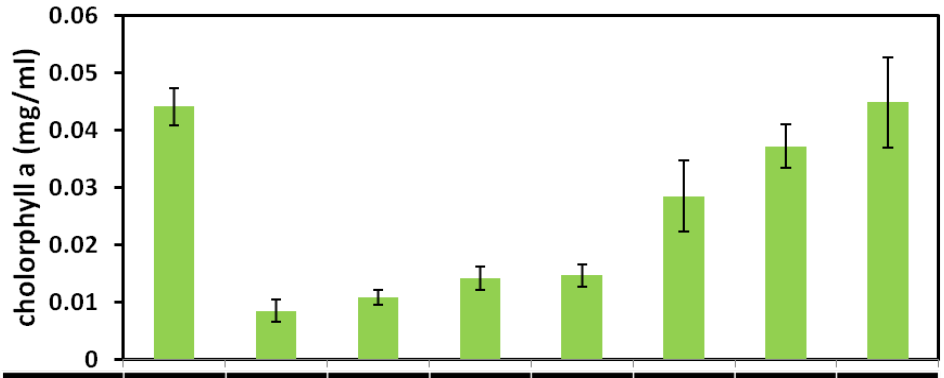

strain	WT	XL18	XL27	XL27	XL19	XL19	SA579	SA579
glycogen	+	-	-	-	-	-	+	+
iBuOH	-	-	-	+	-	+	-	+

Figure S4-3 Chlorophyll *a* contents in various strains.

Glycogen +/-: glgC gene present/knockout; iBuOH +/-: induction/no induction. WT, wild-type; SA579, alsS,ilvCD,kivd,yqhD; XL18, Δ glgC; XL19, Δ glgC, alsS,ilvCD,kivd,yqhD; XL27, Δ glgC, kivd, yqhD; Data represent averages from 3 independent experiments. Error bars indicate standard deviations from 3 replicates.

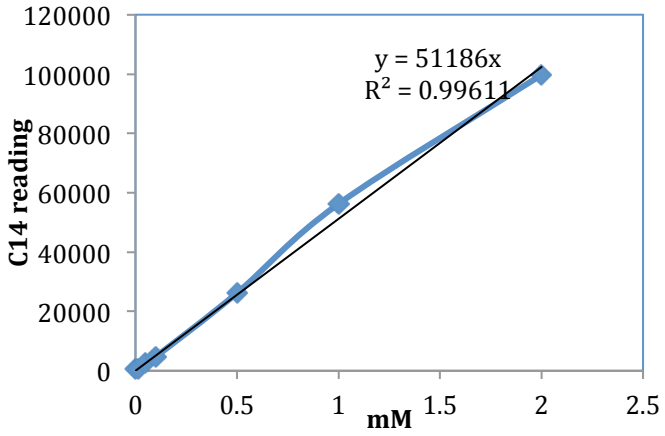

Figure S4-4 $NaH^{14}CO_3$ scintillation reading and bicarbonate amount conversion standard curve.

The standard curve was made by measuring the scintillation reading of 50 µl 20% NaH14CO3 at various final concentrations (0 mM, 0.01 mM, 0.05 mM, 0.1 mM, 0.5 mM, 1 mM, 2 mM) in the counter.

4.6 Supplementary Tables

	Cts											
	glgC			*gen*			*rpoD*			*icd*		
WT	25.09	24.3	24.58	26.84	26.83	29.66	25.02	25.1	24.18	25.12	24.81	25.5
SA579	26.27	26.82	26.14	28.45	28.36	30.62	26.51	26.44	26.5	26.46	26.21	27.57
XL18	32.12	31.94	31.83	23.94	23.86	24.01	24.42	24.36	24.28	24.19	24.44	24.51
XL19	33.18	32.97	33.15	25.03	25.08	25.32	25.42	25.44	26.17	25.81	25.6	26.15

Table S4- 1 C(t) determined by quantitative PCR

All samples were tested in triplicates.

$(V_{oleyl\ alcohol} : V_{medium})$ a	1:1	2:1	3:1	4:1
Cpm in oleyl alcohol	44837	789	1165	1024
Cpm in BG-11	487510	487510	487510	487510
Efficiency (%)	9	0.16	0.23	0.21

Table S4-2 Extraction efficiency test with non-incorporated $NaH^{14}CO_3$.

a. Oleyl alcohol was mixed with BG-11 medium dissolved with NaH14CO3 at different volume ratios.

Alcohol concentration in medium before extraction(mg/L)	Alcohols concentration in oleyl alcohols after extraction			
	Concentration(mg/L)		Efficiency(%) [a]	
	iBuOH	3MB	iBuOH	3MB
1000	287.5	324.0	28.8	32.4
500	139.0	156.5	27.8	31.3
200	55.2	59.7	27.6	29.9
100	27.4	30.2	27.4	30.2
50	12.8	15.6	25.6	31.2

Table S4-3 Isobutanol and 3-Melthy-1-Butanol (3MB) Extraction efficiency test.

a. Isobutanol and 3MB concentration in the extractant were measured in order to calculate the extraction efficiency.Efficiency was calculated through dividing the iBuOH and 3MB concentration in the extractant after extraction by the alcohol concentration in medium before extraction.

	Cell mass [a]	fuel [a]	Fuel :Cell mass
XL18	0.72[a]	ND	
SA579	1.08	0.006	
XL19	0.80	0.01	
SA579(Induced)	0.80	0.24	23:77
XL19(Induced)	0.54	0.60	52:48

Table S4-4 Normalized carbon flux distribution ratios among various mutants

a. The net incorporation rates were normalized by wild type NaH14CO3 biomass incorporation rate.

4.7 Reference

Arp WJ (1991) Effects of source-sink relations on photosynthetic acclimation to elevated CO2. Plant, Cell & Environment 14 (8):869-875. doi:10.1111/j.1365-3040.1991.tb01450.x

Atsumi S, Higashide W, Liao JC (2009) Direct photosynthetic recycling of carbon dioxide to isobutyraldehyde. Nat Biotech 27 (12):1177-1180.

Ballicora MA, Iglesias AA, Preiss J (2003) ADP-Glucose Pyrophosphorylase, a Regulatory Enzyme for Bacterial Glycogen Synthesis. Microbiology and Molecular Biology Reviews 67 (2):213-225. doi:10.1128/mmbr.67.2.213-225.2003

Carrieri D, Paddock T, Maness P-C, Seibert M, Yu J (2012) Photo-catalytic conversion of carbon dioxide to organic acids by a recombinant cyanobacterium incapable of glycogen storage. Energy & Environmental Science 5 (11):9457-9461

Dexter J, Fu P (2009) Metabolic engineering of cyanobacteria for ethanol production. Energy & Environmental Science 2 (8):857-864. doi:10.1039/b811937f

Ducat DC, Avelar-Rivas JA, Way JC, Silver PA (2012) Rerouting Carbon Flux To Enhance Photosynthetic Productivity. Applied and Environmental Microbiology 78 (8):2660-2668. doi:10.1128/aem.07901-11

Ducat DC, Sachdeva G, Silver PA (2011) Rewiring hydrogenase-dependent redox circuits in cyanobacteria. Proceedings of the National Academy of Sciences 108 (10):3941-3946. doi:10.1073/pnas.1016026108

Gibson DG, Young L, Chuang R-Y, Venter JC, Hutchison CA, Smith HO (2009) Enzymatic assembly of DNA molecules up to several hundred kilobases. Nat Meth 6 (5):343-345. doi:http://www.nature.com/nmeth/journal/v6/n5/suppinfo/nmeth.1318_S1.html

Gómez Casati DF, Aon MA, Iglesias AA (1999) Ultrasensitive glycogen synthesis in Cyanobacteria. FEBS letters 446 (1):117-121

Gründel M, Scheunemann R, Lockau W, Zilliges Y (2012) Impaired glycogen synthesis causes metabolic overflow reactions and affects stress responses in the Cyanobacterium Synechocystis sp. PCC 6803. Microbiology. doi:10.1099/mic.0.062950-0

Jacobsen J, Rosgaard L, Sakuragi Y, Frigaard N-U (2011) One-step plasmid construction for generation of knock-out mutants in cyanobacteria: studies of glycogen metabolism in <i>Synechococcus</i> sp. PCC 7002. Photosynthesis Research 107 (2):215-221. doi:10.1007/s11120-010-9613-1

Krapp A, Hofmann B, Schäfer C, Stitt M (1993) Regulation of the expression of rbcS and other photosynthetic genes by carbohydrates: a mechanism for the 'sink regulation' of photosynthesis? The Plant Journal 3 (6):817-828. doi:10.1111/j.1365-313X.1993.00817.x

Lan EI, Liao JC (2011) Metabolic engineering of cyanobacteria for 1-butanol production from carbon dioxide. Metabolic Engineering 13 (4):353-363.

Lan EI, Liao JC (2012) ATP drives direct photosynthetic production of 1-butanol in cyanobacteria. Proceedings of the National Academy of Sciences 109 (16):6018-6023. doi:10.1073/pnas.1200074109

Lan EI, Liao JC (2013) Microbial synthesis of n-butanol, isobutanol, and other higher alcohols from diverse resources. Bioresource Technology 135 (0):339-349. doi:http://dx.doi.org/10.1016/j.biortech.2012.09.104

Lee C, Kim J, Shin SG, Hwang S (2006) Absolute and relative QPCR quantification of plasmid copy number in Escherichia coli. Journal of Biotechnology 123 (3):273-280

Lindberg P, Park S, Melis A (2010) Engineering a platform for photosynthetic isoprene production in cyanobacteria, using Synechocystis as the model organism. Metabolic Engineering 12 (1):70-79. doi:http://dx.doi.org/10.1016/j.ymben.2009.10.001

Liu X, Sheng J, Curtiss III R (2011) Fatty acid production in genetically modified cyanobacteria. Proceedings of the National Academy of Sciences 108 (17):6899-6904. doi:10.1073/pnas.1103014108

Miao X, Wu Q, Wu G, Zhao N (2003a) Changes in photosynthesis and pigmentation in an <i>agp</i> deletion mutant of the cyanobacterium <i>Synechocystis</i> sp. Biotechnology Letters 25 (5):391-396. doi:10.1023/a:1022446330284

Miao X, Wu Q, Wu G, Zhao N (2003b) Sucrose accumulation in salt-stressed cells of agp gene deletion-mutant in cyanobacterium Synechocystis sp. PCC 6803. FEMS Microbiology Letters 218 (1):71-77. doi:10.1111/j.1574-6968.2003.tb11500.x

Ohnishi N, Mukherjee B, Tsujikawa T, Yanase M, Nakano H, Moroney JV, Fukuzawa H (2010) Expression of a Low CO2–Inducible Protein, LCI1, Increases Inorganic Carbon Uptake in the Green Alga Chlamydomonas reinhardtii. The Plant Cell Online. doi:10.1105/tpc.109.071811

Oliver JWK, Machado IMP, Yoneda H, Atsumi S (2013) Cyanobacterial conversion of carbon dioxide to 2,3-butanediol. Proceedings of the National Academy of Sciences 110 (4):1249-1254. doi:10.1073/pnas.1213024110

Preiss J, Romeo T (1989) Physiology, biochemistry and genetics of bacterial glycogen synthesis. Adv Microb Physiol 30:183-238

Shen CR, Liao JC (2012) Photosynthetic production of 2-methyl-1-butanol from CO2 in cyanobacterium Synechococcus elongatus PCC7942 and characterization of the native acetohydroxyacid synthase. Energy & Environmental Science 5 (11):9574-9583. doi:10.1039/c2ee23148d

Stal LJ, Moezelaar R (1997) Fermentation in cyanobacteria. FEMS Microbiology Reviews 21 (2):179-211. doi:http://dx.doi.org/10.1016/S0168-6445(97)00056-9

Suzuki E, Ohkawa H, Moriya K, Matsubara T, Nagaike Y, Iwasaki I, Fujiwara S, Tsuzuki M, Nakamura Y (2010) Carbohydrate Metabolism in Mutants of the Cyanobacterium Synechococcus elongatus PCC 7942 Defective in Glycogen Synthesis. Applied and Environmental Microbiology 76 (10):3153-3159. doi:10.1128/aem.00397-08

Tan X, Yao L, Gao Q, Wang W, Qi F, Lu X (2011) Photosynthesis driven conversion of carbon dioxide to fatty alcohols and hydrocarbons in cyanobacteria. Metabolic Engineering 13 (2):169-176. doi:http://dx.doi.org/10.1016/j.ymben.2011.01.001

Vonshak A, Chanawongse L, Bunnag B, Tanticharoen M (1996) Light acclimation and photoinhibition in threeSpirulina platensis (cyanobacteria) isolates. J Appl Phycol 8 (1):35-40. doi:10.1007/bf02186220

Zhou J, Zhang H, Zhang Y, Li Y, Ma Y (2012) Designing and creating a modularized synthetic pathway in cyanobacterium Synechocystis enables production of acetone from carbon dioxide. Metabolic Engineering 14 (4):394-400. doi:http://dx.doi.org/10.1016/j.ymben.2012.03.005